ADVANCED ELECTRONIC MATERIALS
www.advelectronicmat.de

# Ultrawide-Bandgap Semiconductors: Research Opportunities and Challenges

*J. Y. Tsao,* S. Chowdhury, M. A. Hollis,* D. Jena, N. M. Johnson, K. A. Jones, R. J. Kaplar,* S. Rajan, C. G. Van de Walle, E. Bellotti, C. L. Chua, R. Collazo, M. E. Coltrin, J. A. Cooper, K. R. Evans, S. Graham, T. A. Grotjohn, E. R. Heller, M. Higashiwaki, M. S. Islam, P. W. Juodawlkis, M. A. Khan, A. D. Koehler, J. H. Leach, U. K. Mishra, R. J. Nemanich, R. C. N. Pilawa-Podgurski, J. B. Shealy, Z. Sitar, M. J. Tadjer, A. F. Witulski, M. Wraback, and J. A. Simmons*

**Ultrawide-bandgap (UWBG) semiconductors, with bandgaps significantly wider than the 3.4 eV of GaN, represent an exciting and challenging new area of research in semiconductor materials, physics, devices, and applications. Because many figures-of-merit for device performance scale nonlinearly with bandgap, these semiconductors have long been known to have compelling potential advantages over their narrower-bandgap cousins in high-power and RF electronics, as well as in deep-UV optoelectronics, quantum information, and extreme-environment applications. Only recently, however, have the UWBG semiconductor materials, such as high Al-content AlGaN, diamond and $Ga_2O_3$, advanced in maturity to the point where realizing some of their tantalizing advantages is a relatively near-term possibility. In this article, the materials, physics, device and application research opportunities and challenges for advancing their state of the art are surveyed.**

Dr. J. Y. Tsao
Material, Physical, and Chemical Sciences Center
Sandia National Laboratories
PO Box 5800, Albuquerque, NM 87185-1421, USA
E-mail: jytsao@sandia.gov

Prof. S. Chowdhury
Electrical and Computer Engineering Department
University of California Davis
3133 Kemper Hall, Davis, CA 95616, USA

Dr. M. A. Hollis
Advanced Technology Division
MIT Lincoln Laboratory
244 Wood Street, Lexington, MA 02421-6426, USA
E-mail: hollis@ll.mit.edu

Prof. D. Jena
Electrical and Computer Engineering and Materials Science and Engineering Departments
Cornell University
326 Bard Hall, Ithaca, NY 14853, USA

Dr. N. M. Johnson, Dr. C. L. Chua
Electronic Materials and Devices Laboratory
PARC
3333 Coyote Hill Road, Palo Alto, CA 94303, USA

Dr. K. A. Jones
Sensors and Electron Devices Directorate
U.S. Army Research Laboratory
2800 Powder Mill Road, Delphi, MD 20783, USA

Dr. R. J. Kaplar
Material, Physical, and Chemical Sciences Center
Sandia National Laboratories
PO Box 5800, Albuquerque, NM 87185-1086, USA
E-mail: rjkapla@sandia.gov

Prof. S. Rajan
Electrical and Computer Engineering and Materials Science and Engineering Departments
Ohio State University
2015 Neil Avenue, 205 Dreese Laboratory, Columbus, OH 43210, USA

Prof. C. G. Van de Walle
Materials Department
University of California Santa Barbara
2510 Engineering II, Santa Barbara, CA 93106-5050, USA

Prof. E. Bellotti
Electrical and Computer Engineering Department
Boston University
8 St. Mary's Street Room 533, Boston, MA 02215, USA

Prof. R. Collazo
Materials Science and Engineering Department
North Carolina State University
911 Partners Way (EBI 219), Raleigh, NC 27695, USA

Dr. M. E. Coltrin
Material, Physical, and Chemical Sciences Center
Sandia National Laboratories
PO Box 5800, Albuquerque, NM 87185, USA

Prof. J. A. Cooper
Electrical and Computer Engineering Department
Purdue University
1205 West State Street, West Lafayette, IN 47906, USA

Dr. K. R. Evans, Dr. J. H. Leach
Kyma Technologies, Inc.
8829 Midway West Rd, Raleigh, NC 27617, USA

Prof. S. Graham
Mechanical Engineering Department
Georgia Institute of Technology
771 Ferst Drive, Atlanta, GA 30332, USA

**DOI: 10.1002/aelm.201600501**

 

## 1. Introduction

Modern semiconductor technologies are only 70 years old, but have already transformed human society. At the heart of the technologies are the physical characteristics of the

Prof. T. A. Grotjohn
Electrical and Computer Engineering Department
Michigan State University
2120 Engineering Building, East Lansing, MI 48824, USA

Dr. E. R. Heller
Materials and Manufacturing Directorate
Air Force Research Laboratory
3005 Hobson Way, WPAFB, OH 45433, USA

Dr. M. Higashiwaki
Green ICT Device Advanced Development Center
National Institute of Information and Communications Technology
4-2-1 Nukui-Kitamachi, Koganei, Tokyo 184-0015, Japan

Prof. M. S. Islam
Electrical and Computer Engineering Department
University of California at Davis
3139 Kemper Hall, Davis, CA 95616, USA

Dr. P. W. Juodawlkis
Quantum Information and Integrated Nanosystems Group
MIT Lincoln Laboratory
244 Wood Street, Lexington, MA 02421-6426, USA

Prof. M. A. Khan
Electrical Engineering Department
University of South Carolina
301 Main Street (Swearingen 3A26), Columbia, SC 29208, USA

Dr. A. D. Koehler, Dr. M. J. Tadjer
High Power Electronics Branch
Naval Research Laboratory
4555 Overlook Ave SW, Washington, DC 20375, USA

Prof. U. K. Mishra
Electrical and Computer Engineering Department
University of California Santa Barbara
2215C Engineering Science Building, Santa Barbara, CA 93106, USA

Prof. R. J. Nemanich
Physics Department
Arizona State University
PO Box 871504, Tempe, AZ 85287-1504, USA

Prof. R. C. N. Pilawa-Podgurski
Electrical and Computer Engineering
University of Illinois Urbana-Champaign
306 North Wright Street (4042 ECE), Urbana, Illinois 61801, USA

Dr. J. B. Shealy
Akoustis Technologies
9805-H Northcross Center Court, Huntersville, NC 28078, USA

Prof. Z. Sitar
Materials Science and Engineering Department
North Carolina State University
911 Partners Way (EBI 217), Raleigh, NC 27695, USA

Prof. A. F. Witulski
Electrical Engineering Department
Vanderbilt University
1025 16th Av. South, Ste. 200, Nashville, TN 37235-1553, USA

Dr. M. Wraback
Sensors and Electron Devices Directorate
U.S. Army Research Laboratory
2800 Powder Mill Road, Adelphi, MD 20783, USA

Dr. J. A. Simmons
Advanced Science and Technology Division
Sandia National Laboratories
PO Box 5800, Albuquerque, NM 87185-1421, USA

The ORCID identification number(s) for the author(s) of this article can be found under https://doi.org/10.1002/aelm.201600501.

**Jeffrey Y. Tsao** is currently a Distinguished Member of Technical Staff at Sandia National Laboratories. His Ph.D. is from Harvard University, under Professors Itamar Burak, Eli Yablonovitch and Nicolaas Bloembergen. From 1981 to 1991, he was research staff, first at MIT-Lincoln Laboratory then at Sandia, where he studied laser microchemistry and the materials science of strained heterostructures. From 1991 to 2001, he was manager of compound semiconductor materials research at Sandia, then VP of R&D at E2O Communications. Since 2001, he has played a "national community organizer" role, spearheading white papers which set national research strategies, including in solid-state lighting.

**Mark A. Hollis** received his Ph.D. from Cornell University in 1983 where he was in the renowned group of Prof. Lester Eastman. Dr. Hollis joined MIT Lincoln Laboratory where he co-supervised the fabrication of the first transistors ever to exceed an $f_{max}$ of 200 GHz (265 GHz attained). Since then Dr. Hollis has made a number of contributions across the fields of electronic devices, optoelectronics, and biotechnology, and today he co-leads work in advanced materials and devices for future-generation systems.

**Robert J. Kaplar** received his B.S. degree in Physics from Case Western Reserve University, Cleveland, OH, and his M.S. and Ph.D. degrees in Electrical Engineering from Ohio State University, Columbus. He subsequently joined Sandia National Laboratories, Albuquerque, NM, as a post-doctoral researcher, and is now a Principal Member of the Technical Staff at Sandia. His past work has included III-nitride optoelectronics and reliability physics, and he is currently focused on wide- and ultra-wide-bandgap III-nitride materials and devices for power applications.

semiconductor materials themselves: their fundamental electronic and optical properties that enable electrons, holes and photons to interact and control each other in a wide variety of device architectures and operating environments.

In this introductory Section 1, we give a short review of the history of the materials on which various semiconductor technologies are based, so as to place in a larger historical context the emerging ultrawide bandgap (UWBG) materials of interest to the larger article. Our review begins with the narrower bandgap materials Ge, Si and the III-As and III-P families and continues with the more recent wide bandgap materials InGaN/GaN and SiC. We then introduce the topic of this article, the emerging UWBG materials such as AlGaN/AlN, diamond and $Ga_2O_3$.

### 1.1. Ge, Si, and the "Conventional" III-Vs

For the first 40 years of semiconductor technology, through the late 1980s, the major semiconductor materials were Ge, Si and the "conventional" III-Vs.

The Ge- and Si-based technologies were spawned in 1947 by the demonstration of the first transistor.[1] The early devices were discrete and modest, but further development enabled the replacement of bulky, inefficient, and slow-turn-on vacuum tubes in applications that began with civilian radios and walkie-talkies but quickly expanded to police radios and later military communications satellites. Shortly thereafter, these devices were followed by integrated microelectronics, enabling the rise and spread of computer technology. By 2015, Si technology, dominated by Si complementary metal-oxide semiconductor (CMOS) architectures, had a direct economic impact measured by industry revenue of ≈US$330B per year,[2] and a far larger indirect impact on human society through its enabling of today's information economy.

The "conventional" III-Vs refer to the narrower-bandgap subset of compound semiconductors composed of elements from columns III and V of the periodic table. An example is GaAs, in which half the atoms are gallium and half are arsenic, arranged in alternating positions within the atomic lattice. These III-Vs, dominated by the III-P's and III-As's, have been of interest since the 1950s, when fundamental measurements showed not only that their electron mobilities were superior to those of Si and Ge, but also that their bandgaps were direct (implying stronger electron/hole/photon interactions, useful for optoelectronic devices), wider (implying higher breakdown voltages useful for electronic devices), and might be amenable to compositional modulation (or "engineerable" as in so-called "bandgap engineering").[3]

In electronics, the discovery[4] in the 1970s that the AlGaAs/GaAs heterojunction could give rise to a two-dimensional electron gas (2DEG) was pivotal, enabling the first high-electron-mobility transistors (HEMTs) in GaAs[5] and thin pseudomorphic strained InGaAs[6] channels. In the 1980s, these devices and their cousins, GaAs- and InGaAs-based heterojunction bipolar transistors (HBTs), quickly began setting records for unity-current-gain frequency ($f_T$) and output power above 10 GHz. In 1989, recognizing these benefits, the U.S. Defense Advanced Research Projects Agency (DARPA) launched its GaAs-based monolithic microwave integrated circuits (MIMIC) program.[7]

In optoelectronics, the invention[8] in the 1960s of the laser diode was just as pivotal. A long chain of progress led, among other devices, to the single-mode InP-based laser diodes that now power the broadband dense-wavelength-division-multiplexed (DWDM) optical fiber networks, and which in turn are the backbone of the modern Internet.

### 1.2. Wide-Bandgap InGaN: Optoelectronics

Until the late-1980s, semiconductor technology was limited to Ge, Si, and the "conventional" III-Vs, all having relatively narrow bandgaps of less than ≈2.3 eV. The wider bandgap semiconductors had proven extremely challenging to develop, despite their obvious potential advantages—light emission in the visible for optoelectronics and higher breakdown voltages for electronics.

In the late 1980s and early 1990s, a series of pivotal materials breakthroughs were made by Isamu Akasaki, Hiroshi Amano, and Shuji Nakamura, for which they were awarded the 2014 Nobel Prize in Physics.[9,10] Their breakthroughs, built upon the efforts of many earlier researchers, were completely unexpected: seemingly "magic" AlN and GaN buffer layers on sapphire that dramatically reduced dislocation densities; methods to activate p-type Mg doping of GaN; and a remarkable resilience of InGaN quantum well luminescence against structural defects.

These breakthroughs unleashed, beginning in the late 1990s, huge worldwide research efforts into InGaN-based light-emitting-diode (LED) technologies. The research benefitted from government support, particularly for longer-term "precompetitive" challenges whose science and technological components were closely intertwined. Key milestones include the establishment of the "Next Generation Lighting Initiative"[11] and Solid-State Lighting program[12] by the U.S. Department of Energy's (DOE's) Office of Building Technologies, as well as the Energy Frontier Research Centers[13] established by the DOE's Office of Science. The research also benefited from massive industrial support,[14] particularly for shorter-term challenges whose technological and use components were closely intertwined: for example, there is now a huge InGaN industrial ecosystem, anchored by a few very large InGaN LED chip companies such as Nichia, Samsung LED, Osram Opto Semiconductors, Lumileds, Seoul Semiconductor, Epistar and Cree.

At the time this is being written, in the late 2010s, InGaN has become the second most important semiconductor material after Si.[9] It is the basis for solid-state lighting (SSL), which is rapidly displacing conventional lighting and has the long-term potential for direct savings in world electricity consumption of 10% (equivalent to ≈US$100B per year)[14] as well as the emergence of new "smart and connected lighting" opportunities for enhanced human productivity.[15] Most importantly, SSL is driving the development of an infrastructure that spans substrates, epitaxy, processing, devices, packaging, and applications[16]—an infrastructure that can also be harnessed for other device architectures (electronics and optoelectronics) and materials (other wide-bandgap semiconductors).

### 1.3. Wide-Bandgap SiC and GaN: Electronics

While InGaN-based optoelectronics has been the main driver for the development of wide-bandgap (WBG) semiconductor materials, interest in electronics has also been high. Indeed, for electronics, some of the semiconductor material constraints that apply to optoelectronics are relaxed. Most importantly, bandgaps do not need to be direct, so SiC becomes a viable material; and light emission efficiency is not important, so GaN and AlGaN, not just InGaN, become workable materials. Of the two materials, SiC and GaN/AlGaN, SiC has the longer history.

Sustained investment in SiC electronics began in the late 1970s through the U.S. Department of Defense Office of Naval Research (program manager Max Yoder[17]), which catalyzed fundamental advances in SiC materials synthesis and quality, along with steady progress in a variety of device technologies. These included pn-junctions and Schottky diodes, metal–oxide-semiconductor and junction field-effect transistors (MOSFETs and JFETs) and bipolar junction transistors (BJTs). While Schottky diodes were the first devices to be commercialized in SiC (by Infineon in 2001), as of today all of the above device technologies have been commercialized in SiC.

Sometime thereafter, sustained investment in GaN electronics began, also through the U.S. Department of Defense Office of Naval Research.[17] That investment was driven in part by improvements in SiC material quality leading to the successful demonstration of SiC as a substrate for high quality epitaxial growth of GaN, and by the demonstration of high-quality GaN on sapphire substrates. Availability of epitaxial GaN techniques enabled the demonstration of the first AlGaN/GaN HEMT in 1993.[18] It quickly became recognized that GaN-based transistors had a significant power advantage over GaAs-based transistors, due to a much higher critical breakdown field and electron sheet density. Thus, beginning in the 2000s and accelerating in the 2010s, U.S. government investment in GaN electronics research deepened within the Department of Defense, especially by DARPA,[19] whose support enabled improved-reliability AlGaN/GaN HEMTs.[20] U.S. government investment also broadened to include the U.S. Department of Energy. Perhaps just as importantly, GaN-based electronics also began to take advantage of synergistic advances in InGaN optoelectronics and especially the huge InGaN manufacturing infrastructure driven by solid-state lighting.

All told, WBG SiC and GaN electronics are maturing rapidly, with a 2015 combined market size of ≈US$210M per year[21] and a significant ecosystem of small and large companies supplying devices for civilian and military applications. Recently, GaN RF/microwave HEMTs have been inserted into commercial cellular base stations. Significant future market growth is anticipated, particularly for power electronics applications in hybrid and electric vehicles, power supplies, and photovoltaic (PV) inverters.

### 1.4. Ultrawide-Bandgap Semiconductors: The Next Frontier

Even as the WBG semiconductor materials continue to mature, on the horizon are the ultrawide-bandgap (UWBG) semiconductor materials. These include AlGaN/AlN, diamond, $Ga_2O_3$ and cubic BN, and perhaps others not yet discovered. These materials have bandgaps significantly wider than the 3.4 eV of GaN—in the case of AlN as wide as ≈6.0 eV. Furthermore, because many of the figures-of-merit for device performance scale with increasing bandgap in a highly non-linear manner, these UWBG materials have the potential for far superior performance than conventional WBG materials have.

For example, in the simple case of a low-frequency unipolar vertical power switch, the widely used Baliga figure of merit (BFOM)[22] is defined as $V^2_{BR}/R_{ON\text{-}SP}$. Here, $V_{BR}$ is the breakdown voltage (the maximum voltage the switch can block when it is off), and $R_{ON\text{-}SP}$ is the specific on-resistance (the inverse of the conductance per unit area when the switch is on). The higher the BFOM, the higher the voltage the device can block when off and/or the higher its conductivity per unit area when on. Because both breakdown voltage and conductivity depend on background doping and depletion width, which in turn depend on the critical electric field, $E_{C,}$ at which avalanche breakdown occurs, the BFOM can be expressed in terms of that critical field: $¼\varepsilon\mu E_C^3$, where $\varepsilon$ is the electric permittivity and $\mu$ is the majority carrier mobility. The critical electric field, in turn, scales approximately as the square of the semiconductor bandgap, so the BFOM scales approximately as the sixth power of the semiconductor bandgap. In other words, moving from GaN to AlN gives an increase in bandgap by a factor of 1.8 ≈ 6.0 eV/3.4 eV, but a nonlinear increase in the BFOM of ≈ 34 ≈ $(1.8)^6$.

This nonlinear increase is illustrated in **Figure 1**, in which lines of constant BFOM are drawn on a log-log specific on-resistance versus breakdown voltage plot. The lines drawn correspond to various conventional, WBG and UWBG semiconductors; the lines corresponding to the UWBG semiconductors trend towards the higher performance lower-right region of the plot. Note that for high-frequency high-power applications, the Johnson figure of merit (JFOM),[23] which can be written

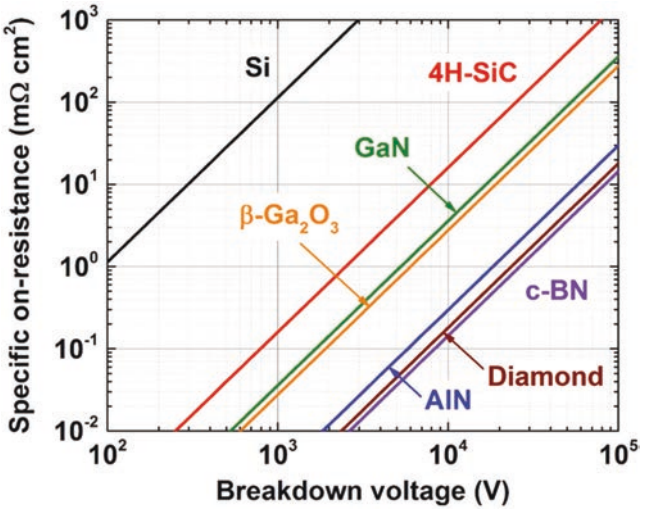


**Figure 1.** Contours of constant Baliga figure-of-merit (BFOM) for various conventional, WBG and UWBG semiconductors, drawn on a log-log specific on-resistance versus breakdown voltage plot. This is the figure-of-merit of interest for low-frequency unipolar vertical power switches; the lower right region represents higher BFOM, hence higher performance.

as $v_{sat}E_C/2\pi$, where $v_{sat}$ is the saturated carrier velocity, is more appropriate than the Baliga figure of merit. One finds for this figure of merit as well that UWBG semiconductors offer significantly higher performance, as discussed later in Section 4.

Despite such tremendous potential for revolutionary device performance improvement, UWBG semiconductors are immature. While some of the UWBG semiconductors have been a topic of research for a decade or two, only recently have there been demonstrations of devices, and even then only in a small number of laboratories around the world. Thus, the UWBG semiconductors currently find themselves at a stage of development similar to that of the WBG semiconductors GaN and SiC in the 1980s—emerging materials with many research challenges, but also with opportunities for orders-of-magnitude improvement in performance both for existing applications and for application domains heretofore considered impossible to address.

In recognition of both the challenges and opportunities, a nascent community of UWBG researchers held two recent workshops. The First Technical Exchange on Ultrawide-bandgap Semiconductors was held October 19–20, 2015 in Albuquerque, NM. The Second Technical Exchange on Ultrawide-bandgap Semiconductors: Research Opportunities and Directions was held April 24–25, 2016 in Arlington, VA, under Air Force Office of Scientific Research (AFOSR) and National Science Foundation (NSF) sponsorship.

This article articulates the research challenges and opportunities identified in that second workshop and fleshed out in subsequent months, with the hope that it will help serve in the short term as a research agenda for the community, and in the long term as a catalyzing agent for the realization of the potential of UWBG semiconductor technology.

The remainder of the article is organized in the following manner. Section 2 reviews the UWBG materials landscape and its research opportunities and challenges, organized by material family: AlGaN/AlN, diamond, $Ga_2O_3$, and others. Section 3 reviews the UWBG physics landscape and its research opportunities and challenges. Section 4 reviews the UWBG devices and applications landscape and its research opportunities and challenges. Throughout, we call out a set of especially important research opportunities and challenges, both scattered throughout the paper and compiled in summary in Section 5.

## 2. Materials

As mentioned in Section 1, it is only recently that control over UWBG materials synthesis and properties has advanced to the point where we can envision realizing some of their tantalizing advantages. A trio of materials has led the way—AlGaN/AlN, diamond, and $Ga_2O_3$—and these are the materials discussed in most detail in this Section 2. We emphasize, however, that the space of UWBG materials of potential future interest extends beyond these three, as will be touched on briefly in Section 2.4.

**Table 1.** Selected materials properties of WBG and UWBG semiconductors, including present-day states-of-the-art in key metrics of material quality and manipulability: substrate dislocation density, substrate diameter, and bulk p- and n-type doping levels. With respect to doping levels, by "good/moderate/poor/no" we mean relative to levels desirable for device technologies. More extensive sets of materials properties are given in Section 4.

| Material | WBG | | UWBG | | |
|---|---|---|---|---|---|
| | GaN | 4H-SiC | AlGaN/AlN | $\beta$-$Ga_2O_3$ | Diamond |
| Bandgap (eV) | 3.4 | 3.3 | Up to 6.0 | 4.9 | 5.5 |
| Thermal Conductivity (W $m^{-1}$ $K^{-1}$) | 253 | 370 | 253–319 | 11–27 | 2290–3450 |
| State-of-the-art substrate quality (dislocations per $cm^2$) | $\approx 10^4$ | $\approx 10^2$ | $\approx 10^4$ | $\approx 10^4$ | $\approx 10^5$ |
| State-of-the-art substrate diameter (inches) | 8 (on Si) | 8 | 2 | 4 | 1 |
| Demonstrated p-type dopability | Good | Good | Poor | No | Good |
| Demonstrated n-type dopability | Good | Good | Moderate | Good | Moderate |

Here, to put just this trio of materials in context, **Table 1** shows a few of their physical properties along with the states-of-the-art of three metrics important for device applications: the quality of their substrates as measured approximately by dislocations $cm^{-2}$ and substrate diameter; their ability to be p-doped; and their ability to be n-doped. Some devices can meet specific applications even without good values for all three metrics: for example, a unipolar majority-carrier field-effect transistor (FET) may have reasonable performance without high substrate quality and with only one type of doping. But the widest range of devices are enabled by good values for all three; perhaps the most prototypical examples are the bipolar junction transistor (BJT) and the laser diode (LD), each of which requires both types of doping as well as high substrate quality to minimize parasitic recombination of minority carriers.

One can see that each of the three UWBG materials presently has poor performance in their states-of-the-art in at least one of the three important metrics: AlN and $Ga_2O_3$ cannot (or can only poorly) be p-doped; and diamond has limited size or relatively poor quality substrates. One of our hopes with this article is to catalyze research that improves these metrics.

In the first three sub-sections of this Section 2, we discuss the three materials that are leading the way, and the research opportunities and challenges associated with advancing our control over their materials synthesis and properties. In the last two sub-sections of this Section 2, we discuss novel alternatives to these three materials, as well as a topic, doping, that cross-cuts all the UWBG materials.

### 2.1. AlGaN/AlN

The AlGaN alloys have exceptionally good fundamental physical properties. From an electronics perspective, they have (1) direct bandgaps spanning a wide range (3.4 to ≈6.0 eV), (2) high breakdown fields (>10 MV $cm^{-1}$ for AlN), (3) high electron mobility (bulk mobilities up to 1000 $cm^2$ $V^{-1}$ $s^{-1}$), (4) high saturation velocities (>$10^7$ cm $s^{-1}$), and (5) relative ease at being doped n-type with Si, which has a relatively small donor ionization energy up to ≈80–85% Al content.[24–32] From an optoelectronics perspective, these alloys offer direct access to emission

wavelengths shorter than about 365 nm, that is, into the UV-A, -B, and -C bands.

Moreover, AlGaN shares the same crystal structure as, and has overall material compatibility with, InGaN. Thus, it can readily take advantage of the huge global investment in the knowledge and manufacturing infrastructure associated with InGaN LEDs. Also, in common with InGaN, it is a ternary alloy, and thus can exploit the power of heterostructures and bandgap engineering just as have many other ternary alloys (AlGaAs, InGaAs, InGaP, etc.) in the III-V materials family. (Note that, though technically a ternary alloy, it is a so-called pseudo-binary alloy in that only the column III (Al,Ga) composition changes.)

However, the AlGaN alloys face three major challenges. The first challenge, control over doping, might be addressed in part by research approaches common to all the UWBG materials, and is discussed in Section 2.5. The second two challenges are addressed by research approaches more unique to AlGaN, and are discussed here. These are (1) the absence of readily available single-crystal substrates with the quality necessary for epitaxial growth; and (2) the immaturity of the scientific understanding required for control of heteroepitaxy on such substrates.

#### 2.1.1. Single-Crystal Substrates

The starting point of almost all mature semiconductor technologies is a high-quality substrate, lattice-matched or nearly lattice-matched to the active semiconductor material of interest that will be epitaxially grown upon it. InGaN optoelectronics technologies are unique in that they have succeeded despite their common use of non-lattice-matched foreign substrates (such as sapphire and SiC) and the resulting high ($\approx 10^8$ cm$^{-2}$) defect densities.[33,34] However, even these now-ubiquitous InGaN optoelectronics technologies improve markedly when they make use of low-defect-density single-crystal GaN substrates. We cannot discount the possibility that AlGaN technologies could be developed with similarly good performance on non-lattice-matched foreign substrates, despite high defect densities. But it is overwhelmingly more likely that a high-quality lattice-matched or nearly-lattice-matched substrate will be needed.[35–38] Two possible such substrates are being considered.

GaN substrates are the obvious possibility, as they are already being developed for InGaN optoelectronics and GaN power electronics technologies. However, high-quality epitaxial growth on GaN substrates is limited to lower-Al-content AlGaN suitable for WBG, not UWBG, applications (e.g., for lasers emitting at wavelengths longer than the middle of the UV-A band, about 365 nm). For higher Al-content AlGaN, the lattice mismatch between the epitaxial layers and the GaN substrate becomes increasingly large, and when strained epitaxial layers exceed their critical thickness, threading dislocations with some misfit component can be generated, which dramatically lowers device performance. Worse, AlGaN layers grown on GaN substrates are under tensile stress and are susceptible to forming extended cracks, which render the heterostructure useless. Indeed, this cracking is a common form of relaxation for the AlGaN alloys.[39]

AlN substrates are the more promising current possibility.[40,41] On such substrates, higher-Al-content AlGaN heterostructures can be grown with relatively lower strain. And, even if the residual strain becomes significant, the strain is compressive rather than tensile and so does not tend to cause extended cracks. AlN substrates for epitaxy have made much progress, with multiple commercial suppliers in existence, including HexaTech and Crystal IS. Such substrates are expensive and limited in availability, however, and these practical factors are currently restricting the rate of progress in the development of high-performance UWBG electronic and optoelectronic devices.

Moreover, it is insufficient for the substrates just to have high crystalline quality and be large in diameter. They must also have low lattice "bow." This is because heteroepitaxy is extremely sensitive to the atomic terrace and step structure of the growth surface (as discussed in the "Heteroepitaxy" subsection below). Ideally, a growth surface has a low (one to two tenths of a degree) offcut away from a specific crystallographic direction. This offcut promotes a bilayer step-flow growth mode that enables uniform alloy and dopant composition of the epitaxial layers.[42,43] If substrates have a significant lattice bow, the offcut of the growth surface will vary laterally, causing the bilayer step-flow growth mode to also vary laterally. In such a case, the alloy and dopant composition of the epitaxial layers will be non-uniform across the wafer.

To avoid this non-uniformity, the offcut deviation across a 5-cm wafer must be low, less than 0.1°.[42,43] From geometric considerations, the bow radius for a 5-cm wafer must be greater than 30 m; and for a 10-cm wafer must be greater than 60 m. These large bow radii are very difficult to achieve in practice. A key research opportunity/challenge, thus, is:

1. Materials: Large (>5 cm) diameter single-crystal AlN substrates with low (<$10^4$ cm$^{-2}$) dislocation densities and negligible bowing (radius of curvature >30 m).

A major obstacle to such AlN substrates is the extreme difficulty of growing AlN boules from a melt, which is the traditional approach to forming crystalline semiconductor boules free of dislocations, impurities, and bow. Except at very high pressures, AlN decomposes before it melts, so this method of substrate formation is not viable. Rather, alternative growth approaches are more actively being developed: for the III-nitrides, these are vapor-phase and solution-growth approaches. Because vertical epitaxy on a foreign substrate or on seed crystals leads to the bow mentioned above and illustrated in **Figure 2**, gradual crystal-size expansion of microscopic native seeds through iterative re-growth is preferred. However, since such expansion is slow, crystal size and production volumes remain low and wafer price is high. Note, though, that the approach to initial formation of the microscopic seeds does not need to be the same as that for lateral expansion to large areas or volumes. This raises the possibility of a mixed, or hybrid, approach. Indeed, very high quality homoepitaxial HVPE-grown GaN has recently been demonstrated using GaN seeds grown by the ammonothermal method.[44]

#### 2.1.2. Heteroepitaxy

To realize the potential of AlGaN/AlN-based devices, it is not sufficient to have access to high quality, negligibly-bowed

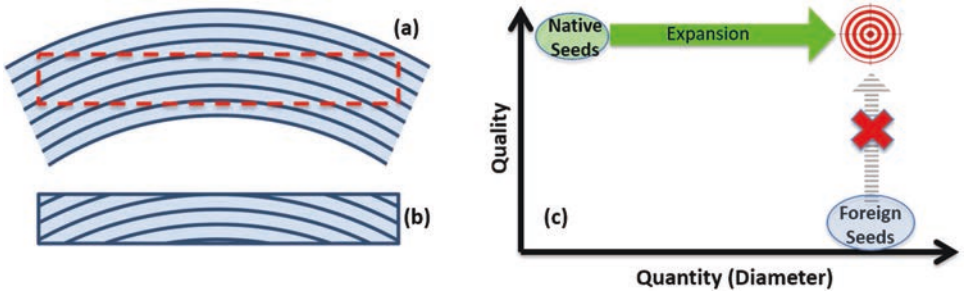


**Figure 2.** a) Schematic of a bowed substrate: initially grown by one-dimensional (vertical) epitaxy on either a lattice-mismatched or thermal-expansion-mismatched foreign substrate or seed; then released from that foreign substrate or seed by some chemical or physical process; upon which relaxation to its natural lattice constant takes place along with bowing. b) Even if that bowed substrate is polished flat, its lattice is still bowed, with the consequence that terrace widths decrease (step density increases) from the center to the edge of the wafer. c) An alternative approach might be growth on a native seed by iterative crystal expansion.

single-crystal AlN substrates. In addition, the growth of precision "bandgap engineered"[3] heterostructures on these substrates is also necessary, and this requires precise control over the evolution of the atomic terrace and step structure of the surface during growth.

The degree of control differs considerably from the case of InGaN heteroepitaxial growth on sapphire and other non-native substrates, where the surface kinetic growth mechanism is simple spiral growth mediated by screw dislocations that are present at a high density. Instead, for growth on low-dislocation-density native substrates, the surface kinetic growth mechanism is determined by an interplay (1) between the steps themselves (e.g., bilayer versus bunched steps), (2) between the adatoms and the steps (step-flow growth), and (3) between the adatoms themselves (nucleation on terraces). These three modes of interplay appear to be particularly difficult to control for AlGaN/AlN heteroepitaxy. For example, **Figure 3** shows a wide range of steady-state surface morphologies as a

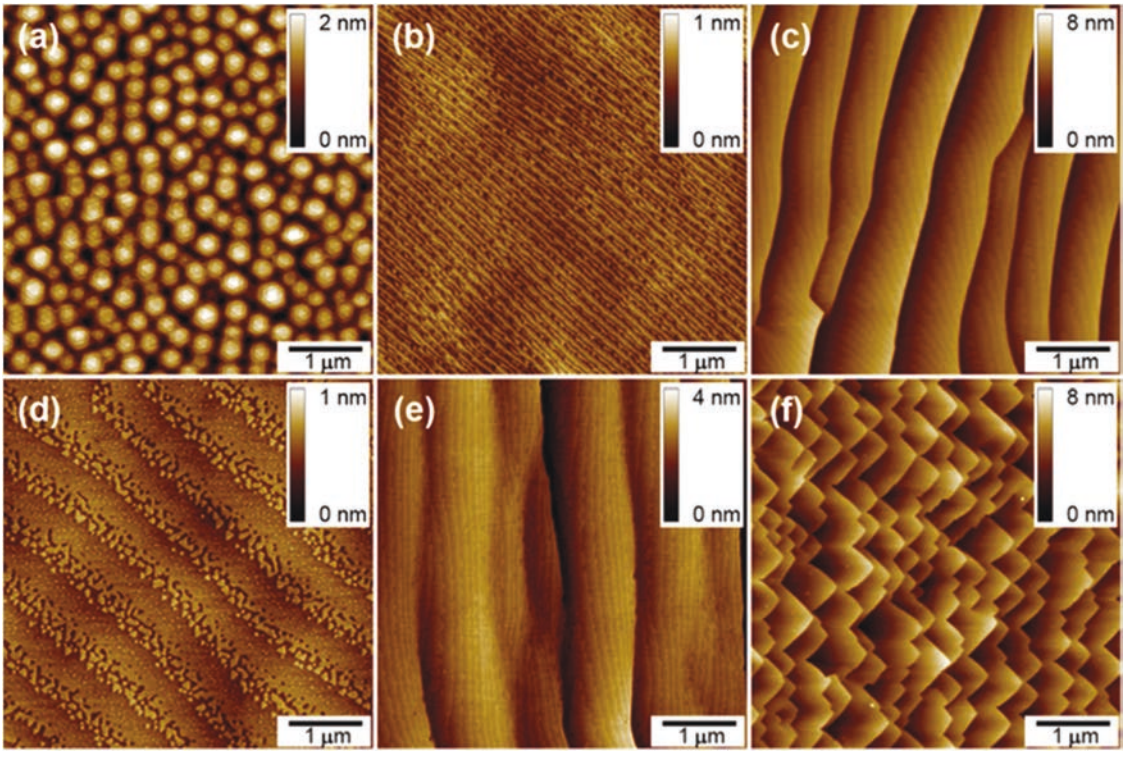


**Figure 3.** Atomic force microscopy (AFM) images of six distinct types of surface morphology observed for AlN homoepitaxial layers grown in the absence of dislocations. All were obtained under identical growth conditions but different out-of-plane offcuts. a) Growth on an on-c-axis AlN substrate with wide, atomically smooth terraces; due to large distances between steps, 2D nuclei formed on these surfaces and grew into epitaxial 3D islands. d) Growth on a surface with bilayer steps more densely spaced than in (a) but far apart enough that 2D nucleation on the terraces is still favorable. b) Growth on a surface with closely spaced bilayer steps (c/2) that yielded an RMS (root mean square) roughness of less than 50 pm. c,f) Step-bunched morphologies where the step heights are many times greater than the bilayer height; the difference between the straight and jagged step-bunch edges is due to the in-plane offcut direction. Finally, e) a meandering step morphology, which is a transitional stage between the bilayer and step-bunched morphologies. Reproduced with permission.[43] Copyright 2016, Elsevier.

function of terrace width (offcut angle) for the relatively simple homoepitaxial growth of AlN, all for the same nominal growth conditions.[42,43,45,46]

Moreover, since the surface kinetics of different adatom species of an alloy differ, the lateral compositional uniformity of ternary and quaternary alloys is directly related to the step structure. In particular, step-bunched surface morphology contains seemingly abrupt and undesirable lateral compositional gradients that are correlated with the differences in step density across such a surface. Therefore, in order to achieve a uniform composition in alloy films, controlling the surface morphology during alloy growth is critical.

To illustrate the challenge, **Figure 4** shows results from the growth of AlGaN films on two substrates with different offcut angles: one has a uniform composition, while the other shows phase separation into two different compositions. Since AlGaN forms a complete range of solid solutions without a miscibility gap, the observed apparent phase separation is believed to be related to surface kinetics. This kind of compositional inhomogeneity is highly detrimental to quantum well structures, as well as to carrier transport and breakdown fields that can be sustained across the structure.

Because the growth and morphology/composition co-evolution "phase space" is so crucial and so complicated, a key research opportunity/challenge is a predictive framework to guide the grower:

2. Materials: A predictive vapor-surface-film thermodynamic/kinetic framework for the atomic-scale co-evolution of morphology and composition during AlGaN heteroepitaxy.

Such a predictive framework would likely need to draw on a fundamental scientific understanding of the thermodynamics and kinetics of surfaces and adatoms. For example, what are the surface energies of the various crystallographic polar, non-polar, and semi-polar planes of interest? Accurately calculating the surface energies from first principles is challenging, requiring a precise depiction of the surface reconstruction under particular growth conditions, including the effects of the polar nature of the wurtzite crystal structure,[47] and of the vapor supersaturation. Vapor supersaturation, in turn, depends on a wide range of parameters—temperature, of course, but also V/III ratio, diluent gas, and total pressure.[48] A related question is that of the surface kinetics of (and interactions between) various growth species on these surfaces, which are currently mostly unknown.

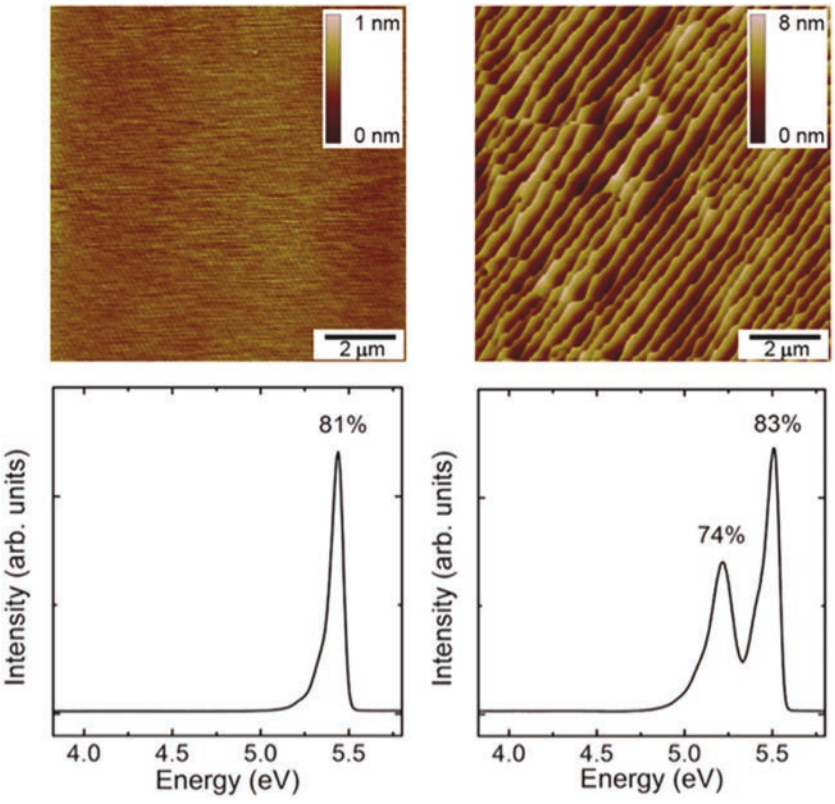


**Figure 4.** AFM images of surfaces after AlGaN growth (during the same run) on a low (upper left) and high (upper right) offcut (from c-axis) AlN native substrate. The sample on the left shows bilayer steps, while the sample on the right is step-bunched. Although high-resolution X-ray diffraction (HRXRD) did not show any noticeable difference in the crystalline quality between the two films, low-temperature photoluminescence (PL) revealed for the bilayer growth mode a single emission peak (lower left), whereas the step-bunched film showed two distinct peaks corresponding to two different AlGaN compositions (lower right). Reproduced with permission.[42] Copyright 2016, Elsevier.

### 2.2. Diamond

Diamond has extremely advantageous properties that enable UWBG applications such as high-power and high-frequency electronics, radiation detectors, electron emitters for ultra-high voltage vacuum switches and traveling wave tube cathodes, and thermionic emitters for energy conversion. Some of diamond's outstanding electronic properties include: a breakdown field of >10 MV $cm^{-1}$, high electron and hole mobilities >2000 $cm^2$ $V^{-1}$ $s^{-1}$, and saturated drift velocities as high as $2.3 \times 10^7$ cm $s^{-1}$ for electrons and $1.4 \times 10^7$ cm $s^{-1}$ for holes (see Section 4). Diamond also has the highest known thermal conductivity of any material, of particular importance because in so many power electronics and optoelectronics applications device operation is limited by heat removal. Some additional unique properties include: excellent electron emissivity on hydrogen terminated surfaces,[49,50] surface-transfer doping enabled by these hydrogen-terminated surfaces,[51] room-temperature UV exciton emission, and optical defect centers due to the nitrogen-vacancy (N-V) and silicon-vacancy (Si-V) complexes. These defect centers have been proposed, as discussed in Section 4.5, as a physical qubit platform for emergent quantum information systems.[52]

Unlike AlGaN/AlN, which can borrow from a considerable body of InGaN/GaN materials knowledge and manufacturing

infrastructure, diamond is more unique and cannot borrow, for example, from the even larger body of knowledge and manufacturing infrastructure of the material it is most similar to in crystal structure, Si. Nevertheless, two materials breakthroughs have stimulated much recent excitement over the diamond materials system.

The first breakthrough was the realization of single-crystal man-made substrates. Just as with AlGaN discussed above, the lack of large-area, low-defect-density, single-crystal diamond substrates has historically limited device concept demonstration. In the past few years, however, a number of approaches have been developed that enable both relatively low defect density ($<10^5$ cm$^{-2}$) substrates, as well as new synthesis strategies for larger substrates. Single-crystal diamond substrates with dimensions greater than $1 \times 1$ cm$^2$ can now be prepared by high-growth-rate chemical vapor deposition (CVD) on (100) crystal faces, and are commercially available.[108] On the horizon are a number of potential approaches to larger-area substrates that could approach 50 mm in diameter: lateral tiling of smaller substrates created through smart-cut-like extraction from small-size, high-pressure, high-temperature (HPHT) grown boules; homoepitaxial growth using an iridium nucleation layer; repeated CVD overgrowth on existing small-size HPHT grown boules; and higher pressure and temperature HPHT boule growth.[104–107] Given that the typical CVD growth temperature is relatively low (≈850 °C) and the cost of high-purity elemental material is low, it may even be projected that substrate costs will be substantially reduced in the future. Even if larger substrates ultimately prove difficult to develop, "Minimal Fab" strategies for manufacturing on 12 mm diameter substrates are also being considered as viable options.[109–111]

The second breakthrough is efficient doping. Doped diamond layers are generally prepared by gas-phase doping during plasma-enhanced CVD growth on single-crystal diamond substrates. In the past decade, substantial progress has been made in p-type doping with boron, and just in the past few years n-type doping with phosphorus has been demonstrated at a number of laboratories. While dopant levels are deep (0.3 eV for B and 0.57 eV for P), impurity concentrations greater than $10^{20}$ cm$^{-3}$ can be achieved, which provides low room-temperature resistivities through hopping conduction, and enables low-resistance electrical contacts. Moreover, as temperature increases, resistivity is reduced, making the performance of diamond devices potentially better at high operating temperatures, as well as potentially eliminating the thermal runaway often observed in other semiconductors at elevated temperature and/or high power operation.

With these two breakthroughs—the advent of substrates (albeit limited in diameter and availability, and at relatively high cost), and the demonstration of bipolar doping (albeit limited in achievable doping densities and resistivities)—there has been an explosion of diamond device studies. Unipolar Schottky diodes prepared with p-type diamond have demonstrated >5 kV breakdown voltage; bipolar pin diodes have demonstrated forward current densities greater than 500 A cm$^{-2}$ and breakdown voltages greater than 1000 V; and vertical bipolar junction transistors (BJTs) have been demonstrated on (100) and (111) substrates.[112] Both the bipolar pin diodes and BJT devices take advantage of the high electron and hole mobilities of diamond.

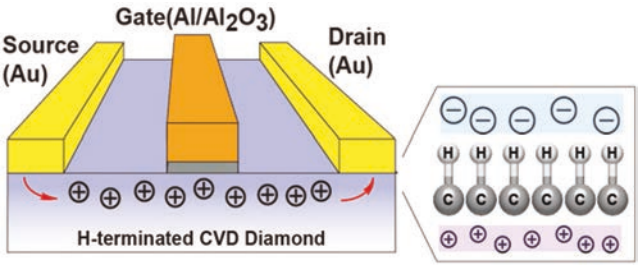


**Figure 5.** Right: Hydrogen termination of diamond lowers its ionization energy, driving electron transfer from the valence band at the surface into electronic states in adsorbates. Left: The resulting p-type surface conductivity, with holes confined to a subsurface layer of a few nanometers thickness, enables "surface-transfer-doped" field-effect transistors. Reproduced with permission.[51] Copyright 2014, Cambridge University Press.

Additional excitement has been generated by new approaches to controlling and exploiting surfaces, as well as excitonic and defect-center properties.

The key surface property of diamond—the low electron affinity of its hydrogen-terminated surface (H termination)—is often associated with electron emission. Indeed, diamond surfaces have demonstrated thermionic energy conversion, while pin diodes with H-terminated surfaces have shown efficient electron emission at room temperature and have been used in high voltage (≈10 kV) vacuum switches.[50] But the low electron affinity of diamond also enables surface doping on intrinsic diamond surfaces (similar to polarization doping in AlGaN/GaN). Early studies established that air adsorbates could lead to a two-dimensional hole gas (2DHG) with a sheet charge density in the $10^{14}$ cm$^{-2}$ range.[113] While these air-exposed surfaces are notably unstable, lateral metal–oxide-semiconductor field-effect-transistor (MOSFET) devices have now been fabricated with atomic-layer-deposited (ALD) dielectric layers, as illustrated in **Figure 5**. These have exhibited sheet charge densities greater than $10^{13}$ cm$^{-2}$, stability to ≈400 °C, and high-voltage and high-frequency operation.[51]

The key excitonic property of diamond is its high (80 meV) exciton binding energy. Because diamond, like Ge and Si, is an indirect-bandgap semiconductor, its light emission per se is unlikely to be very efficient; however, its large exciton binding energy has enabled room-temperature UV emission from pin diodes.[114]

The key defect-center property of diamond is its notable N-V and Si-V defect centers with their long spin-relaxation times. These defect centers show promise for use in quantum information and communication (single photon source) applications, and have now been incorporated in diamond devices in which applied voltages can change the charge state of the center.[115]

Diamond is now in an exciting "exploration" phase, in which the challenge is to build a toolkit of processes for controlling materials synthesis and properties. This would further build on and extend the substrate and doping breakthroughs mentioned above. A key research opportunity/challenge, thus, is:

3. Materials: A complete set of synthesis and processing tools for control of substrate diameter, defects, doping, carrier confinement, contacts, and heterostructures in diamond-based materials.

This toolkit would ideally address the full range of important materials challenges, including: (1) growth of larger-area diamond films on disparate substrates such as Si, or larger freestanding diamond plates; (2) reducing defect and impurity densities in substrates and epitaxial layers; (3) preparing stable dielectric interfaces that can sustain high-mobility 2D hole and electron channel conduction; (4) preparing low-resistance contacts to both p- and n-type diamond; and (5) formation of heterostructures (e.g., with c-BN) for high-mobility devices and III-V integration. As research progresses on all of these topics, new device concepts can be anticipated based on the outstanding, extreme, and unique properties of diamond materials.

### 2.3. $\beta$-$Ga_2O_3$

Of the UWBG materials currently of active interest, $\beta$-$Ga_2O_3$ is the newest and least mature. It is intriguing, however, because of (1) its fundamental materials properties, (2) the availability of affordable native substrates, and especially (3) the recent fabrication of a metal–semiconductor field-effect transistor (MESFET) with interesting properties.[62]

From an optoelectronics perspective, $Ga_2O_3$, like the other UWBG semiconductors, has a bandgap in the deep-ultraviolet (DUV) region. Thus, on the one hand, $Ga_2O_3$-based optoelectronic devices such as solar-blind DUV photodetectors are expected to be useful for a variety of applications (e.g., flame detectors). On the other hand, the complexity of optical processes in $\beta$-$Ga_2O_3$, as well as the inability to dope the material p-type, has so far prevented its application to bipolar devices such as light emitters.

From an electronics perspective, and in particular with respect to unipolar power device applications, $Ga_2O_3$ has some outstanding attributes. First, it has a bandgap wider than 4.5 eV, leading to a high breakdown electric field of $\approx$9 MV cm$^{-1}$.[62,116–119] Second, it displays good controllability of n-type conduction over a wide range of $n \approx 10^{15}$–$10^{19}$ cm$^{-3}$ through Si or Sn doping,[86,120,121] and an even more widely tunable resistivity spanning the range $\approx 10^{-3}$–$10^{12}$ $\Omega \cdot$cm. Third, as seen in Figure 1, its estimated Baliga figure of merit (BFOM) is higher than those of WBG SiC and GaN (despite its relatively lower mobility), though not as high as those of UWBG AlN, diamond, and c-BN. This has provided strong motivation for the development of $Ga_2O_3$ power devices.

From the perspective of device functionality beyond electronics or optoelectronics, other attractive applications for $Ga_2O_3$ include high-temperature signal processing, harsh-environment electronics, and wireless communication devices/circuits. With respect to harsh-environment operation, the inherent stability of $Ga_2O_3$ (as an oxide semiconductor) against oxidation and its wide bandgap are both important properties.

Perhaps the greatest advantage of $Ga_2O_3$ lies, as mentioned above, in the availability of affordable, high-quality, large native substrates, with the good material workability of $Ga_2O_3$ being an important feature for such economical mass substrate production. Today's 2″ $Ga_2O_3$ substrates are priced similarly to 2″ GaN substrates ($\approx$\$2K per substrate in low volume), though currently their delivered volume is much lower than that of GaN. Thus, should $Ga_2O_3$ devices begin to take off commercially, the market price of $Ga_2O_3$ is expected to drop, perhaps even approaching that of sapphire at high volumes. The situation for $Ga_2O_3$ is thus very different from that for UWBG AlGaN or diamond, whose progress has been hampered by a lack of such substrates. Indeed, the availability of $\beta$-$Ga_2O_3$ substrates has also spawned efforts to use them as substrates for III-nitride epitaxial growth, due to the hexagonal symmetry and the relatively small lattice mismatch of less than 5% between GaN and $Ga_2O_3$. In fact, high-power InGaN-based LEDs have already been demonstrated on $Ga_2O_3$ substrates—taking advantage of these substrates' high electrical conductivity and high optical transparency in the visible and UV ranges.[122]

At this point in time, $Ga_2O_3$ wafers can be fabricated in large volumes and at reasonable cost—with even lower costs possible should demand materialize. These wafers are fabricated from bulk single crystals synthesized by a variety of melt-growth techniques such as float-zone,[120,123] Czochralski,[124,125] vertical Bridgman,[126] and edge-defined film-fed growth (EFG) methods.[127–129]

To date, EFG has an advantage over the other melt-growth methods in producing such wafers. **Figure 6** displays a photograph of a 4-inch-diameter single-crystal $Ga_2O_3$ wafer produced from an EFG-grown bulk crystal. The EFG $Ga_2O_3$ wafers have exhibited very high crystal quality, with a full-width at half-maximum of the X-ray diffraction rocking curve as narrow as 17 arcsec and a dislocation density on the order of $\approx 10^3$–$10^4$ cm$^{-2}$. Commercial substrates now have full-width at half-maxima of 150 arcsec,[130] as well as in-plane Sn doping concentrations and resistivities ±20%, acceptable for practical vertical devices. Note that the growth direction of EFG $Ga_2O_3$ growth is [010], with arbitrary orientations around the [010] likely possible by optimizing growth conditions. This growth direction naturally gives (–201) wafer surface orientations; other orientations are possible

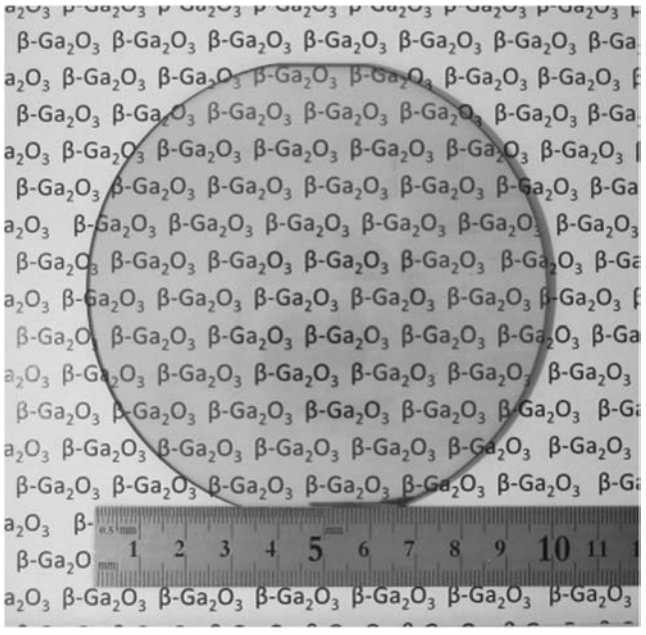


**Figure 6.** Photograph of transparent 4″-diameter single-crystal $Ga_2O_3$ wafer. Copyright Tamura Corporation via Masataka Higashiwaki, National Institute of Information and Communications Technology.

but with smaller diameters. Thus, other melt-growth methods may have advantages, depending on progress in device performance for these other wafer surface orientations.[131]

Two main drawbacks of $Ga_2O_3$ are often pointed out, however, in discussions about the material's power device potential.

First, in contrast to n-type material, there has been no report of successful p-type doping and thus of effective hole conduction in $Ga_2O_3$. Self-trapping of holes, which prohibits effective p-type conductivity due to the resultant low mobility, has been predicted by first-principles calculations.[132]

Second, $Ga_2O_3$ has poor thermal conductivity and therefore poor heat-dissipation capability. This low thermal conductivity is perhaps the single most serious potential weakness of $Ga_2O_3$ for power devices. The experimental thermal conductivity values of $Ga_2O_3$ fall in the range of ≈10–27 W $m^{-1}$ $K^{-1}$ at room temperature, which is one or two orders of magnitude lower than those of other UWBG semiconductors.[91]

The first drawback, the absence of p-type doping, and the difficulty of doping in general in the UWBG semiconductors, is discussed in Section 2.5. The second drawback, however, represents a separate, but key, research opportunity/challenge:

4. Materials: Novel synthesis, processing, and architectural routes for circumventing the low thermal conductivity of $Ga_2O_3$.

Among these routes might be those based on thin-film separation methods or nanomembranes,[133] which enable exploitation of the favorable electronic and optoelectronic properties of $Ga_2O_3$ in conjunction with the thermal conductance properties of other materials such as poly-diamond or Cu. It might also be possible to grow $Ga_2O_3$ directly on high thermal conductivity substrates such as SiC and diamond (single crystal and polycrystalline). Additional opportunities include polymorph control (since $Ga_2O_3$ can be stable in multiple phases), and the development of heterostructures, potentially with $Al_2O_3$ or $In_2O_3$.[134]

### 2.4. Other UWBG Materials

While AlGaN/AlN, diamond, and $Ga_2O_3$ are the UWBG materials that have generated the most interest in recent years, all UWBG materials are relatively immature, and many others are worthy of exploration. For example, $MgGa_2O_4$,[135] $Al_2O_3$, II-IV-N materials such as $ZnSiN_2$ and $MgSiN_2$,[136] and possibly various 2D materials, are all of interest.

Of special interest, though, is BN. Of its $sp^2$-bonded hexagonal structures (hexagonal (h-BN),[137] rhombohedral (r-BN),[138] and turbostratic (t-BN)[139]), the wide bandgap of h-BN and the ability to synthesize single layers make it especially attractive for two-dimensional electronics or as an interlayer for heteroepitaxy. In its $sp^3$-bonded structure, BN can occur in multiple polymorphs, including zinc blende cubic (c-BN).[140,141]

In its wurtzite structure, wz-BN can potentially be alloyed with AlN or GaN to achieve wider band gaps. Though BN does not naturally occur in the wurtzite structure,[142] for low concentrations of B, BGaN and BAlN alloys may maintain the wurtzite structure of GaN and AlN (although recent work has demonstrated the formation by MOCVD growth of a cubic phase of BGaN for low (≈1%) B composition).[143] BN thus might serve as a natural extension of the nitride family of semiconductors that consists of InN, GaN, and AlN. Among the interesting applications of BAlN alloys are as hetero-barriers for BAlN/AlN majority-carrier structures, and as quantum barriers for AlN quantum wells (e.g., BAlN/AlN/BAlN), potentially enabling optoelectronics in the ultra-deep-UV range.

In its cubic structure,[144] c-BN is isoelectronic with diamond. Doping is obtained with Si and Be for n-type and p-type characters, respectively. c-BN has a bandgap of 6.4 eV and is predicted to have a breakdown field greater than 15 MV $cm^{-1}$. It has the second-highest thermal conductivity of all materials (theoretically ≈2145 W $m^{-1}$ $K^{-1}$ for isotopically pure material)[94] and a small (1.4%) lattice mismatch with diamond that may enable, with the c-BN acting as an intermediary layer, integration of diamond with other III-V semiconductors.

Cubic BN faces challenges, however, particularly with regard to synthesis. Like carbon and as mentioned above, BN also possesses $sp^2$-bonded phases. And, just like graphite versus diamond, the hexagonal phase of BN is more stable than the cubic phase and any growth process needs to avoid forming $sp^2$-bonded regions.

c-BN films have been synthesized using several techniques including pulsed laser deposition,[145] ion-beam-assisted deposition,[146] e-beam evaporation,[147] various types of plasma-assisted chemical vapor deposition,[148,149] and physical vapor deposition.[150] In general, it is believed that the nucleation of c-BN requires energetic bombardment of the growing surface with charged or neutral ions, regardless of the synthesis approach. Degree of ion bombardment, strain, concentration of impurities (notably H), growth temperature, and issues related to adhesion to the substrate are all important factors that will determine the overall crystal structure and crystal quality in the c-BN films. A detailed discussion of the various approaches, along with extensive material characterization and analysis was reviewed by Samantaray and Singh.[151]

Because of these c-BN materials challenges, except for an early promising demonstration of a UV emitter,[152] progress toward realizing device technologies has been slow. A recent review of these efforts has been given by Zhang.[144]

A key research opportunity/challenge thus encompasses both the novel and much less explored UWBG materials, such as the various BN materials:

5. Materials: Exploration of novel UWBG materials (beyond AlN/AlGaN, diamond, and $\beta$-$Ga_2O_3$), including h-BN for 2D devices, wz-BN as an AlGaInN-alloying heterostructure-enabling material, and c-BN as a heterostructure with diamond and as a stand-alone material.

### 2.5. Doping

Since the birth of semiconductors, controlled shallow donor and acceptor doping has been the singular necessary step that transforms a semiconductor material from scientific curiosity to technological relevance. Though much progress has been made, breakthroughs similar to Mg acceptor p-type doping of GaN have not yet been achieved even for the most mature of the UWBG semiconductors: AlN, diamond, and $Ga_2O_3$. This is

in part due to the presence of three obstacles not present in the traditional narrower gap semiconductors.

The first is the fact that most dopant ionization energies increase with bandgap. As ionization energy increases, the fraction of carriers that are thermodynamically "activated" from bound to free states decreases, making it difficult to achieve the UWBG free carrier concentrations at room temperature necessary for many devices.

Second, the wide bandgaps of UWBG materials can make them prone to self-trapping of carriers. In particular, the localized nature of valence-band states derived from elements of the first row of the periodic table (notably oxygen) can lead to formation of small hole polarons, in which a hole is self-trapped due to lattice distortions.[132] Even if suitable shallow acceptors could be identified, this tendency for carrier localization will suppress mobility.

Third, there is a prevalent tendency of dopants in UWBG semiconductors to undergo compensation via impurities, native defects, or defect complexes. This tendency is illustrated in **Figure 7** for n-type doping of AlGaN by Si. As Si concentration increases, free carrier concentrations initially increase, but then reach a maximum and decrease—a signature of compensation, where vacancies and their complexes determine the net free-carrier density. Such compensation is universal to all UWBG semiconductors, not just AlGaN, since in general the formation energies of compensating defects decrease with increasing bandgap.

While the first and second obstacles are inextricably linked to fundamental materials properties, the third can benefit from materials engineering and merits closer inspection. Consider compensation by point defects. The equilibrium concentration of point defects is determined by the defect free energy of formation, which in turn depends on the atomic and electronic chemical potentials. Traditional synthesis approaches typically control defect concentration by changing the atomic chemical potentials via control of growth conditions (species supersaturation) and temperature. The electronic chemical potential, or Fermi level, is controlled through the addition of impurity dopants with shallow defect states in the host material. Increasing the concentration of these impurities leads to a commensurate change in the Fermi level as extrinsic carriers are added to the system. Although this holds true for all materials, the sizeable energy gap in UWBG materials leads to a significant change in the electronic chemical potential of compensating defects (ionized donors or acceptors for p- and n-type dopants, respectively). Unfortunately, charge neutrality can then be caused by having roughly equal concentrations of dopant impurities and compensating defects, effectively pinning the Fermi level far from the band edges and thwarting efforts to tailor conductivity.

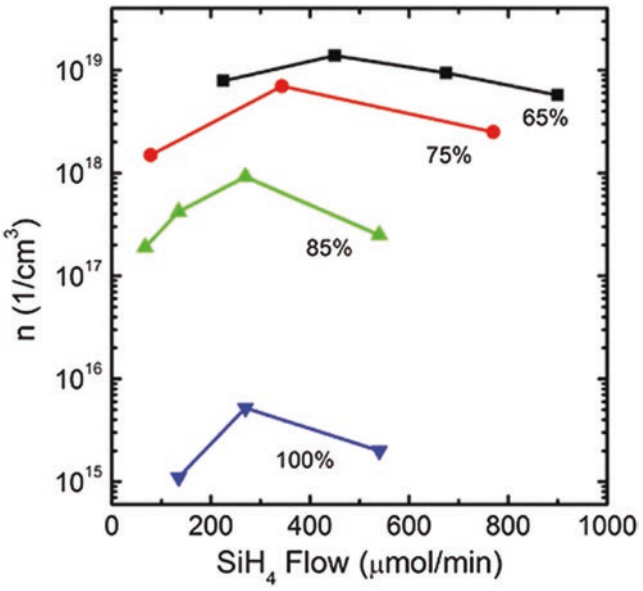


**Figure 7.** Room-temperature carrier concentration as a function of silicon doping for AlGaN alloys with various Al percentages. As Si doping increases, free carrier concentrations initially increase, but then reach a maximum and decrease—a signature of compensation.

Managing and achieving low compensation in UWBG materials is thus challenging, though mandatory in order to supply devices with needed free carriers. Novel synthesis approaches coupled with advanced characterization may be necessary. For example, might new synthesis approaches be possible, such as maintaining non-equilibrium growth conditions, which would prevent the crystal from generating compensating defects? Moreover, because the synthesis phase space is so large, new theory for the relationship between synthesis and dopant properties must be developed to provide critical experimental guidance. Here, we call special attention to the development and exploitation of such theory in a research opportunity/challenge:

6. Materials: A first-principles theory of doping in UWBG semiconductors in conjunction with new synthesis and doping approaches (e.g., based on broken symmetries at surfaces and hetero-interfaces) that enables improved understanding and control of conventional doping methods.

Indeed, first-principles theory has contributed a framework for understanding and studying doping and compensation, and has already addressed a number of important problems.[153,154] Additional developments will be necessary, for instance to address non-equilibrium situations, to more rigorously calculate free energies, and to analyze self-trapping.

In addition to the overarching research opportunity/challenge for a solution to doping that cuts across all the UWBG semiconductors, we now briefly mention here research opportunities/challenges that are specific to particular UWBG semiconductors and devices.

For AlGaN/AlN, which possesses spontaneous and piezoelectric polarization, new strategies that exploit broken crystal symmetries, such as polarization-induced doping, can potentially extend traditional chemical substitutional doping and offer significant opportunities for heterostructure engineering. Modulation doping may be useful for generating confined carriers at heterointerfaces. However, the heterostructure compositions and band offsets over which such modulation doping can be effective will remain limited due to the deep-level defects in the wider-bandgap layers. Utilization of quasi-electric fields in graded bandgap layers could aid in ionizing dopants.

For diamond, which does not have the luxury of polarization doping, other strategies may be possible.

For example, a high surface conductivity can be achieved with surface transfer doping due to surface adsorbates.[51] This process, illustrated in Figure 5 and discussed in more detail in Section 2.2, can lead to a two-dimensional hole gas (2DHG) with hole densities above $10^{14}$ $cm^{-2}$. The surface transfer doping is related to surface states, surface adsorbates and defects in the dielectric layer. The details of the interaction are an active area of research.

Or, for example, an additional approach to fabricating a pnp BJT in diamond using bulk doping might be to use B doping for the emitter and collector, and heavy B doping ($\approx 10^{20}$ $cm^{-3}$) for the emitter and collector Ohmic contacts. Such highly doped contact regions exhibit hopping conduction, which provides low-resistance contacts without "classical" doping (i.e., holes excited to the valence band where they can freely conduct). Doping the base with a P concentration of $10^{19}$ $cm^{-3}$ is thought to be the optimum value since the donor ionization is light.[112] A low-contact-resistance Ohmic contact to the base can be made by regrowing a thin contact layer doped to $>10^{20}$ $cm^{-3}$ with P, although this increases the cost and complexity of the device.

For $Ga_2O_3$, there are a number of interesting doping questions. Can stoichiometric $Ga_2O_3$ be routinely grown? Is the donor depth of the preferred n-type dopant (Sn) acceptably shallow, and can it routinely be inserted in the $Sn^{+4}$ state as opposed to the $Sn^{+2}$ state? Is its seemingly low measured mobility of 153 $cm^2$ $V^{-1}$ $s^{-1}$[155] the maximum value, and if so, is that sufficient? Can 2DEGs be created using heterostructures with oxides based on other group-III metals like Al and In?

For cubic BN, among the doping challenges are the following. Although not as deep as in diamond, at least one donor (Si) and two acceptor (Be and Mg) levels are >200 meV deep.[144] As mentioned in Section 2.4, control of chemical stoichiometry during synthesis can be difficult, and this is critical because boron vacancies act as acceptors and nitrogen vacancies act as donors. Also as mentioned in Section 2.4, BN has many different phases, making it challenging to retain the cubic structure during thermal removal of damage created by implanted dopants.

## 3. Physics

As discussed in Section 2, tantalizing progress is being made in UWBG materials synthesis and properties. Progress is now to the point where devices are being fabricated and tested, enabling the physics underlying device performance to be probed and explored. Because UWBG devices' raison d'etre is to operate in new domains beyond those possible for conventional WBG or narrower-gap devices, our understanding of the solid-state physics underlying their operation is critical for advancement of the technology.

Perhaps the most important way in which this emerging UWBG device frontier depends on advances in our physics understanding will be in the very high electric fields at which the devices will operate. These high fields will drive physical phenomena much farther from equilibrium than in devices based on conventional semiconductor materials. Just as in other physical domains, probing regimes that have never before been accessed can be anticipated to lead to the discovery of new phenomena. Fundamental concepts—in carrier dynamics and transport, doping and impurity scattering, electron–phonon coupling, photon emission and absorption, photoelectron emission, interface electronic band structure, and thermal conduction—may all undergo significant reexamination and refinement.

In addition, the interaction of electrons in UWBG semiconductors with high-energy photons (exceeding ≈4 eV) and high-energy phonons (e.g., ≈0.16 eV in diamond) may lead to novel effects not seen in traditional semiconductors, including internal photoemission (since the photon energy is larger than the electron affinity) and robust superconductivity. Ultimately, we anticipate that this new solid-state physics understanding will enable a new generation of device designs with unprecedented levels of performance.

In this Section 3, we articulate some of the research opportunities and challenges associated with exploration of these new physical domains, collectively captured with the following overarching research opportunity/challenge:

7. Physics: Exploration of extreme high-field and non-equilibrium physics regimes opened up by UWBG semiconductors—regimes that will likely lead to re-evaluation of standard models for the fundamental properties of, and interactions between, the various carriers of energy (electrons, holes, phonons and photons).

In the following three subsections, we identify more specific research challenges and opportunities regarding electronic transport, carrier confinement, and thermal transport.

### 3.1. Electronic Transport

Among the most important of electronic properties are the transport of electrons and holes in response to internal and externally applied electric fields. This area of physics is rich, governed by a wide range of carrier relaxation processes, all interacting in three different electric-field regimes (i) when electric fields are low and carrier velocities are linear in field, (ii) when electric fields are high and carrier velocities saturate, and (iii) when electric fields are so high that "breakdown" by avalanche multiplication occurs.

In this Section 3.1, we discuss what is known and not known about the physics of electronic transport in UWBG materials in these three different electric field regimes. The broad research opportunity concerning transport is:

8. Physics: A comprehensive understanding of the carrier and lattice dynamics underlying electron and hole transport—at low and high fields and in the breakdown regime—across the range of polar and non-polar UWBG semiconductors.

#### *3.1.1. Low-Field Transport*

With respect to the most basic transport property, low-field carrier mobility, there are uncertainties with respect to all of the UWBG semiconductors.

In the III-N's, transport in the least explored BN (both the hexagonal and cubic forms) materials remains largely

unexplored. But uncertainties exist even for the relatively more mature III-N's. Indeed, the III-N's, taken to include the ternary, quaternary, or quinary (B,Al,Ga,In)N alloys, represent a rich yet untilled field for transport studies, both experimental and theoretical.

Experimentally, room-temperature electron mobilities in excess of ≈1000 $cm^2\ V^{-1}\ s^{-1}$ can be achieved in very lightly doped bulk GaN, and hole mobilities of ≈24 $cm^2\ V^{-1}\ s^{-1}$ can be attained in Mg-doped GaN samples.[29,65,74] The corresponding numbers are not yet clearly known in UWBG AlN, however, primarily because control over doping levels has not yet reached the level of maturity it has in GaN. For degenerate electron populations for which electron transport is not limited by impurity scattering (such as two-dimensional electron gases), the mobility in AlGaN is primarily limited by alloy and phonon scattering. In this case, the electron mobility drops significantly as the alloy composition is varied from GaN towards AlGaN, or AlN to AlGaN, and for mole fractions of Al or Ga larger than ≈10%, the electron mobility is dominated mainly by alloy scattering. As reported by Bajaj et al, electron mobilities can be factors of 2× or 3× lower than in GaN, based on conventional models.[156] Electron mobilities in doped AlGaN layers approach hundreds of $cm^2\ V^{-1}\ s^{-1}$, and are slightly higher in polarization-induced 2DEGs.[54,66,157]

Theoretically, electron and hole transport properties are likely to require fundamentally new concepts and approaches, because of the highly mismatched electronic properties of the binary constituents. For example, consider the AlInN material system. The ≈6 eV energy bandgap of AlN is ≈10× the ≈0.6 eV bandgap of InN. Electronic states in narrower-gap AlGaAs or InGaAs ternaries can sometimes be treated as "averages" in the virtual crystal sense. They probably cannot be considered averages in that same sense for AlGaN, BGaN or the other UWBG III-N ternaries, however, because of the very large scattering potentials. Coupled with the randomly varying polarization fields, low-field transport in UWBG ternaries is likely to be much more complicated than in narrower-gap ternaries.

Uncertainties in transport are even more pronounced in the relatively less mature $\beta$-$Ga_2O_3$ and diamond semiconductors.

In bulk $\beta$-$Ga_2O_3$, transport has recently begun to be explored—in particular, electron transport in material n-doped by Si and Sn, which form shallow donor states. Measured electron mobilities are in the 100–200 $cm^2\ V^{-1}\ s^{-1}$ range at room temperature, up to about 500 $cm^2\ V^{-1}\ s^{-1}$ in the 100–200 K range for low-doped bulk material,[158,159] and up to even 5000 $cm^2\ V^{-1}\ s^{-1}$ at 80 K in high-quality HVPE-grown epitaxial layers.[160] As illustrated in **Figure 8**, mobility in $Ga_2O_3$ appears to be limited by optical phonon scattering at high temperature and ionized impurity scattering at low temperature.[161] Hole transport has not yet been explored, since, as mentioned in Section 2.3, acceptor p-type doping is a severe challenge in this material system. It can be anticipated that the combination of a very heavy valence band effective mass and a strong Fröhlich interaction will lead to formation of polarons with very low conductivity.[162]

In $\beta$-$Ga_2O_3$-based alloys and heterostructures, transport is completely unexplored. 2D electron gases in heterostructures are yet to be created in this material system, though this is expected to happen as the material matures. Ternary alloys of

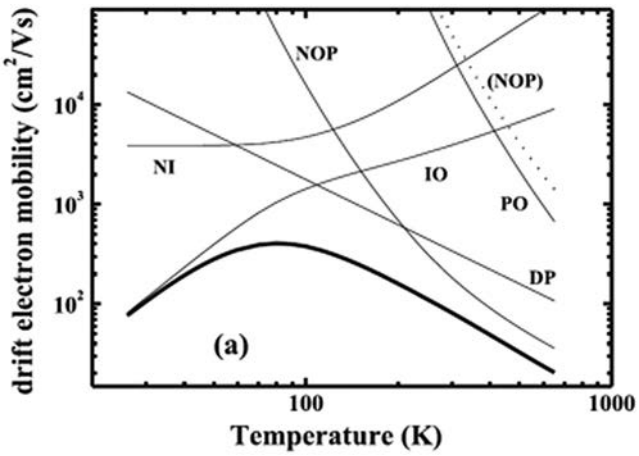


**Figure 8.** Temperature dependence of the drift mobilities calculated for $Ga_2O_3$.[161,163] IO and NI indicate ionized and neutral impurity scattering; DP, NOP and PO indicate non-polar acoustic, non-polar optical and polar optical phonon scattering; the dotted line (NOP) represents the single NOP mobility. The bold solid line is the total drift mobility for all scattering mechanisms. Reproduced with permission.[161] Copyright 2016, IOP Publishing.

$\beta$–$(Al_xGa_{1-x})_2O_3/Ga_2O_3$ have been reported;[164] however, in that study surface roughness arising from step bunching prevented carriers from forming a high mobility two-dimensional electron gas (2DEG). Nevertheless, first-principles calculations[134,165] have indicated that $\beta$–$(Ga_{1-x}In_x)_2O_3$ can be stable for low concentrations of In, thus potentially enabling heterostructure devices using In-containing instead of Al-containing barrier layers.

In diamond, room-temperature electron and hole mobilities of ≈2000 $cm^2\ V^{-1}\ s^{-1}$ are often reported, while electron mobilities above 4000 $cm^2\ V^{-1}\ s^{-1}$ have been claimed from observations of high-purity samples.[72] Moreover, cyclotron resonance measurements on ultra-pure substrates have shown low-temperature mobilities $>10^6$ $cm^2\ V^{-1}\ s^{-1}$ and extrapolated room temperature values that exceed 5000 $cm^2\ V^{-1}\ s^{-1}$ for holes and 7000 $cm^2\ V^{-1}\ s^{-1}$ for electrons.[73] As highly crystalline diamond materials continue to become more available, low-field-transport measurements will perhaps probe regimes dominated by diamond's exceptionally high threshold for phonon scattering, and explore the extremes of properties that follow from C residing at the top of the periodic table and possessing the most covalent of all bonds.

### *3.1.2. High-Field Transport*

At high electric fields, electrons lose energy by optical phonon emission. This process governs the saturation of carrier velocities in steady state (DC, or direct current) transport, and velocity overshoot in non-equilibrium situations. In addition, an understanding of high-field ballistic transport in UWBG materials could spur their heterogeneous integration in applications for which a thin, wide bandgap material is required.

For polar UWBG semiconductors such as the nitrides, electron–phonon coupling is exceptionally strong, and drives a very high phonon-emission rate. This, combined with the

large mass difference between N and Ga, leads to a large gap in the phonon density of states between the acoustic and optical branches.[166–171] Such analysis typically implies an electron-density-dependent saturation velocity in the materials. These high-field transport properties have been investigated experimentally in WBG GaN, but not yet in UWBG AlGaN.[91,172] Saturation velocities of the order $10^7$ cm $s^{-1}$ are measured at electric fields above 0.1 MV $cm^{-1}$ in GaN. High-field carrier saturation in the oxides and diamond are expected to follow similar trends since the effective mass is similar to that of GaN.

Improved understanding of transport physics would be of great benefit in the quest for high voltage (>20 kV) and RF ultrawide-bandgap devices, beginning with first-principles calculations and experimental verification of the high-field saturation velocities, impact ionization, and their dependences on carrier density and temperature. An example of an initial comprehensive analysis of scattering mechanisms in $Ga_2O_3$, performed by Parisini and Fornari,[161] was discussed above and illustrated in Figure 8. A similar comprehensive analysis at high fields would be illuminating.

#### *3.1.3. Breakdown*

The principal promise of UWBG semiconductors lies in the high breakdown fields they can sustain. While critical breakdown fields in GaN have been measured[59,60] to be in excess of ≈4 MV $cm^{-1}$, those in AlN, BN, $Ga_2O_3$, and diamond are yet to be accurately determined. While the fields sustainable in these UWBG materials are expected to far exceed those in GaN and SiC, the physical mechanisms responsible for breakdown will likely involve new physics, for the following reason.

Because the bandgaps of most UWBG materials are larger than the electron affinity, breakdown mechanisms such as the onset of the avalanche process by impact ionization require carriers in the conduction band to have a kinetic energy larger than the electron affinity. This implies the carrier momentarily spends time in vacuum states before causing impact ionization. This sort of physics is new and unique to UWBG semiconductors, and would have intriguing consequences for device design and operation.

In this area of avalanche breakdown, a key research opportunity/challenge is thus:

9. Physics: New theoretical descriptions and models of high-energy carrier transport and avalanche breakdown in UWBG materials, coupled with experimental verification.

### 3.2. Carrier Confinement

As with devices based on narrow-bandgap semiconductors, those based on UWBG semiconductors will benefit greatly from their ability to confine carriers (electrons and holes)—either for simple passivation or for engineering the active region (e.g., FET gate dielectrics).

For the highly desirable normally-off power devices discussed later in Section 4.2, gate insulators would enable carrier confinement and hence the normally-off MOSFET-like devices that are commonplace in narrow-gap Si, and that have been demonstrated in WBG SiC and GaN.[173] Towards that end, materials such as $Al_2O_3$ (itself an UWBG semiconductor in its crystalline form), $SiO_2$, and $Si_3N_4$ have been used in conventional AlGaN/GaN power HEMTs to limit gate leakage in normally-off, gate-recessed structures (in these structures the gate dielectric is deposited on the AlGaN barrier layer).[174] Also, $Al_2O_3$ deposited on AlGaN has been shown to affect HEMT properties such as 2DEG density and mobility.[175,176] More exotic dielectrics such as MgCaO, a crystalline material that can be lattice-matched to InAlN and AlGaN over a range of compositions, have also shown promise.[177,178]

In general, the wider the bandgap of the semiconductor, the more difficult is the carrier confinement. For thin semiconductors where quantum confinement and bandgap widening occurs, this is extremely important. Indeed, the WBG and UWBG semiconductors have recently sprung a few surprises in the limit of extreme thinness: 2D GaN and quasi-2D $Ga_2O_3$ have been fabricated by sublimation or mechanical exfoliation, respectively,[133,179] potentially enabling significant increases in energy gap as fewer monolayers of material are isolated (e.g., 5.28 eV for 2D GaN). These ultrawide bandgaps, comparable even to the 5–6 eV of h-BN, will likely motivate research in advanced techniques for layer-by-layer epitaxial growth of both WBG and UWBG semiconductors.

Indeed, it is rather remarkable from a fundamental physics standpoint that these ultrathin (≈0.9 monolayers) GaN quantum wells and ultrasmall (≈0.56 nm) GaN quantum dots, by sheer quantum confinement between AlN barrier layers, can push bandgaps up to 5 eV or more.[180,181] This is even higher than what is claimed for a 2D version of GaN, and is enabled by the very large band offsets offered by UWBG semiconductor heterostructures, able to confine severely quantized states within the wells. This sort of engineering of quantized states also expands the scope of bandgap-engineered physics and devices, and offers unique opportunities in ultra-fast tunneling and inter-sub-band devices, possibly in the 1.55 μm regime of importance for free-space and optical-fiber communications.

Despite these tantalizing advances, challenges to carrier confinement abound. As the bandgap of the semiconductor increases, the number of suitable semiconductors or insulators with large enough band offsets available for carrier confinement decreases. As illustrated in **Figure 9**, the UWBG semiconductors have conduction bands that trend towards the vacuum level. There are few dielectric layers with a predicted band alignment that will confine electrons in AlN, BN or diamond. In contrast, there are a number of dielectric layers that will confine holes, with $Al_2O_3$ and $SiO_2$ having shown good results for diamond. New UWBG materials such as $AlF_3$ could also be considered for gate dielectric or passivation applications. The most fundamental obstacle is that any dielectric with a large bandgap will tend to have a low dielectric constant—and vice versa. This problem restricts the possibility of the high-k dielectrics desirable for realizing high-performance UWBG MOSFETs in the future, and is an extremely important research opportunity/challenge.

Note, however, that it is not sufficient for the band offsets of the confining semiconductor or insulator to be theoretically large enough to enable confinement. From a practical point of view, both the confining layer and the interface between the

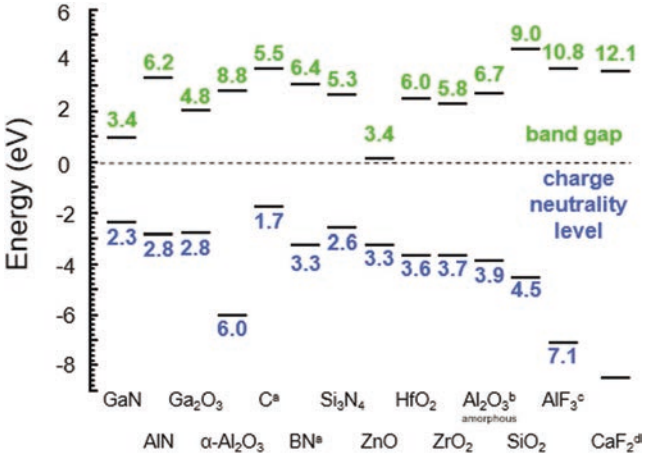


**Figure 9.** Schematic of band alignment of WBG and UWBG semiconductors (left side) and possible passivating dielectric materials (right side). The alignments are based on calculated charge neutrality levels or from experimental reports. The energy zero in the schematic is the charge neutrality level. The numbers above each conduction band minimum (CBM) line represent the bandgap, and the numbers below each valence band maximum (VBM) line represent the position of the charge neutrality level relative to the VBM. References: (a) Monch;[182] (b) Fonseca, Liu and Robertson;[183] (c) König, Scholz, Zahn and Ebest;[184] and (d) Izumi, Hirai, Tsutsui and Sokolov.[163] Adapted with permission.[185] Copyright 2006, AIP Publishing.

active semiconductor and the confining layer must be relatively defect free. The absence of defects would enable gate dielectrics to exhibit minimal hysteresis when subjected to IV sweeps of opposite polarity, and also to have good reliability (especially threshold voltage stability). The presence of defects, in contrast, leads to charge trapping either at the insulator–semiconductor interface or within the dielectric itself; thus, bulk and interface state density must be minimized. For example, SiC/$SiO_2$ MOSFETs have suffered from poor channel mobility and threshold voltage stability, due primarily to issues with defects at the SiC/$SiO_2$ interface.[186]

Similar issues are expected for the UWBG semiconductors; indeed, the issues are expected to be more severe, both for epitaxial and non-epitaxial insulators. For confinement by epitaxial insulators, trapping effects associated with gate insulators have been documented numerous times for power HEMTs based on the epitaxially "simplest" AlGaN/GaN interface, and are at present a significant area of study in the reliability physics community.[187] For confinement by non-epitaxial insulators, the prime example is the Si/$SiO_2$ interface. However, $SiO_2$ cannot be thermally grown with as high-quality an oxide on non-Si-containing materials as it can be on Si or SiC. This is a potentially rich area of materials science and device physics, as researchers search for the thus-far elusive semiconductor/insulator system that displays the astounding robustness of the Si/$SiO_2$ interface. Note that Figure 9 includes $Al_2O_3$ in both crystalline and amorphous forms, with the interesting possibility that $Al_2O_3$ could be both a dielectric (amorphous form) and an UWBG semiconductor (crystalline form).[188]

In general, surface states are likely present in all UWBG materials, and there have been studies that have explored their role in interface band structure and defect formation. For dielectric–nitride interfaces, near-interface states are sometimes termed border traps, and appear to be influenced by polarization fields.[189] Polarization fields, in turn, can potentially be manipulated, both to influence the interface and/or border states, and to enhance confinement.

In this area of carrier confinement, key research opportunities/challenges are:

10. Physics: Exploration of the physics of carrier confinement under extreme conditions (e.g., ultrathin heterostructures whose confinement requires UWBG semiconductors).
11. Physics: High-k, ultrawide-bandgap dielectrics with low-interface-state-density interfaces to UWBG semiconductors.

### 3.3. Thermal Transport

The performance of many semiconductor devices is limited by heat removal. This is expected to be all the more critical for UWBG semiconductor devices, which will be driven "harder" (at higher current densities) than their narrower-gap cousins. Further, to fabricate devices with the desired electronic properties, UWBG devices may make use of a number of materials and device building blocks: binary, ternary, and quaternary compounds; tailored doping; interfaces between dissimilar materials; and UWBG materials that exhibit the highest thermal conductivity of all crystals (e.g. diamond, BN) as well as UWBG materials that exhibit among the lowest (e.g., $Ga_2O_3$). The result will be a complex set of internal impedances to heat conduction and removal, in some cases limiting device performance. As one simple example, **Figure 10** shows how the creation of alloy semiconductors from the SiGe[190] and AlGaN[191] material systems results in thermal conductivities far lower than those of their end-point materials—Si and Ge, or AlN and GaN, respectively—due to increased alloy scattering of phonons.

With these challenges comes opportunity, however. Are there architectures that can exploit this large range of properties as well as the wide variety of ways in which those properties can be

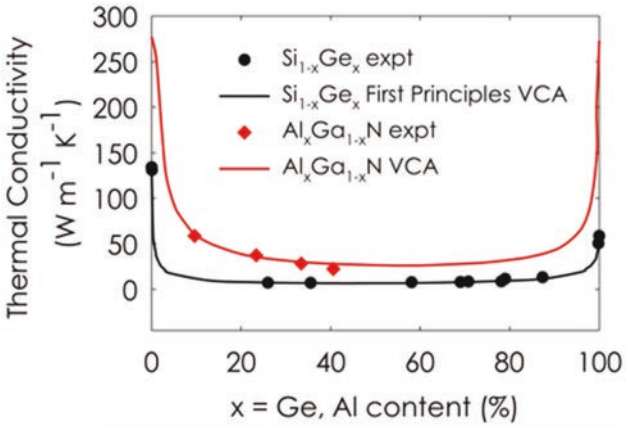


**Figure 10.** Thermal conductivity of SiGe and AlGaN alloys as functions of Ge and Al content. The plot shows experimental data as well as predictions of the virtual crystal model (VCA) which shows the strong dependence on alloy composition.

integrated into a device? If so, can one manipulate thermal properties to nearly the same level of precision as electrical properties, and ultimately tailor both in the device design and modeling process?

We are far from having in hand such methods for co-design of both thermal and electrical properties, however. At present, detailed models exist for electrical transport including full-band Monte Carlo down to continuum-scale hydrodynamic codes. However, most of these models treat thermal transport very simply, neglecting important interface and non-continuum effects, and even at a continuum level do not take into account the interplay between electrical and thermal responses at the relevant spatial and time scales.

Moreover, it will be necessary to develop a more sophisticated theoretical and experimental understanding of thermal transport in these materials and device architectures.

Our theoretical understanding of thermal transport in the UWBG semiconductors is relatively immature: the framework of the phonon gas model, which has been used to correlate thermal conductivity of semiconductor alloys, has not shown sufficient predictive capability to determine which UWBG materials will have large or small thermal conductivities. Recently, though, a molecular dynamics framework (the Green–Kubo modal analysis, or GKMA method) has shown a remarkable ability to predict the thermal conductivity of crystals and alloys.[192] A key research opportunity is thus to apply this and other atomistic modeling approaches to better understand the phonon and vibrational-mode physics in UWBG materials and at their interfaces. One practical example is as follows: current efforts to use CVD diamond to remove heat from nitride devices appear to be limited by the quality of the interface between GaN and diamond.[193] Understanding such interfaces will become important as device designers begin to transfer and bond low-thermal-conductivity devices to higher-thermal-conductivity substrates.

Our experimental understanding of UWBG materials is also relatively immature. For example, while the thermal conductivity of $Ga_2O_3$ is known to be in the vicinity of 27 W $m^{-1}$ $K^{-1}$ at room temperature,[91] very little is known about doped materials and ternary systems made with $Ga_2O_3$. Moreover, because it will not always be feasible to fabricate special structures designed solely for the measurement of thermal properties, there is a need to develop thermal metrology approaches that can extract the spatial and temporal distribution of the thermal gradients in working UWBG devices. Indeed, over the past decade a number of techniques have been developed to measure the thermal response in GaN RF and power devices, improving the accuracy over that obtained using IR thermography.[194–199] The most prominent of these methods is Raman spectroscopy—a thermal metrology method that has been used to measure vertical temperature gradients inside UV-C LEDs and AlGaN/GaN HEMTs.[200] More recently, methods based on transient Raman spectroscopy and transient thermoreflectance have enabled measurements of the thermal response in AlGaN/GaN HEMTs with a time resolution <100 ns and temperature resolution less than several degrees.[201,202] Such techniques can yield real-time, in-situ data on specific heat, thermal conductivity, and thermal boundary resistance—all of which are parameters needed for accurate electro-thermal modeling of devices under transient operation.

Overall, these new space- and time-resolved thermal metrology methods are expected to yield critical information on temperature rise and other thermal phenomena for both power and RF devices, and will help to refine electro-thermal models of UWBG devices with experimental data that is on the same time-scale and spatial resolution as the simulation techniques. Going forward, however, it will be important to better understand the accuracy and limits of these new techniques.

Thus, in this area of thermal transport, a key research opportunity/challenge is:

12. Physics: New techniques for monitoring space- and time-varying temperature profiles, and for modeling and co-designing devices for combined electrical and thermal performance.

## 4. Devices and Applications

The ultimate goal of UWBG semiconductors is to enable devices that improve, even revolutionize, applications, including new applications that do not yet exist. The ability to handle large amounts of power is certainly one common theme for UWBG applications, but there are many other themes. In this Section 4, we review the landscape of known UWBG devices and applications, and articulate some of the key device-level research opportunities and challenges that might enable them. However, we emphasize that we survey only the known applications—with the understanding that the new technology capabilities represented by UWBG semiconductors will surely create applications that do not yet exist.

We organize this Section 4 in the following way. In Section 4.1, we provide a much more comprehensive version of the summary of materials properties in Table 1 at the beginning of Section 2. In Section 4.2, we review high-power electronics technology, in which high voltages and/or high currents are switched. In Section 4.3, we review RF power/switching technologies, in which the intent is to transmit and receive RF power at high frequencies for long-distance communication or imaging. In Section 4.4, we review deep-UV optoelectronic technologies relevant to a variety of applications. In Section 4.5, we review quantum information applications. In Section 4.6, we review a particularly important cross-cutting feature of all UWBG technologies—their robustness and thus ability to operate in extreme environments, including high-radiation environments. Finally, in Section 4.7, we discuss device processing, modeling/calibration, and packaging.

### 4.1. Materials/Device Types and Properties

As an aid to navigating the UWBG materials and device landscape, in this Section 4.1 we summarize the results of a comprehensive survey and analysis of the room-temperature materials properties most relevant to electronic applications. Our intent is to provide the most current and accurate properties available at the time of writing. It was necessitated in part by the fact that many material properties in common use (even for GaN) were determined by measurements performed decades ago on material that was highly defective by today's standards.

The results of the survey and analysis are summarized in **Table 2** and discussed below. We consider first the materials/device

**Table 2.** Material/device properties for electronic applications. Columns A–H represent various WBG and UWBG semiconductors, as well as particular device types of special interest. Rows 1–8 represent parameters that characterize fundamental physical properties of the materials. Rows 9a–9c represent the current states-of-the-art for various non-fundamental properties of the materials, on which the maturity assessment in row 9 is based. The format used in many of the boxes is: Measured number/Theoretical number; Year [ref.]/Year [ref.].

| Parameter at 27 °C | (A) GaN (for reference) | (B) $Al_xGa_{1-x}N$ | (C) AlN | (D) Example AlGaN/GaN HEMT[53] | (E) $\beta$-$Ga_2O_3$ | (F) Cubic BN | (G) Diamond | (H) Diamond MOS |
|---|---|---|---|---|---|---|---|---|
| (1) Bandgap (eV) | 3.4[29] | Interpolation[54] | 6.0[55] | Multiple | 4.9[56] | 6.4[57] | 5.5[58] | Multiple |
| (2) Projected bulk $E_C$ (MV cm$^{-1}$ at doping = $10^{16}$ cm$^{-3}$) | 4.9[59,60] (measured baseline) | Varies non-uniformly by composition[61] | 15.4[60] | 2.6 (reported) | 10.3[60] | 17.5[60] | 13.0[60] | Depends on insulator |
| (3) Sheet carrier density $n_s$ (cm$^{-2}$) | Various (see Doping below) | Various (see Doping below) | Low at 300 K | $1.2 \times 10^{13}$ | $1.5 \times 10^{13}$/TBD 2012[62]/– | Various (see Doping below) | Various (see Doping below) | $4 \times 10^{13}/1.7 \times 10^{14}$ 2012[63]/2013[64] |
| (4) Electron drift mobility (cm$^2$ V$^{-1}$ s$^{-1}$) | 1000[29,65–67] | Interpolation | 426/300 (experimental number is Hall mobility) 2006[68]/1994[66] | 1200 (Hall mobility) | 180/171 (Hall mobility) 2012,2015[70,86]/2017[71] | 825/TBD (Hall mobility) 2003[69]/– | 4500/7300 2002[72]/2014[73] | TBD |
| (5) Hole drift mobility (cm$^2$ V$^{-1}$ s$^{-1}$) | 24 (Hall mobility at $7 \times 10^{16}$ cm$^{-3}$ hole density)[74] | Various | – | – | – | 500/TBD (Hall mobility) 1998[75]/– | 3800/5300 2002[72]/2014[73] | 340 to 47/TBD (over $2 \times 10^{17}$ to $6 \times 10^{19}$ cm$^{-3}$ hole density) 2016[76]/– (corrected for Hall factor in diamond)[58] |
| (6) Saturated carrier velocity $\nu_{sat}$ ($10^7$ cm/s): | | | | | | | | |
| $e^-$: electrons | 1.4[77] | Various | 1.3[77] | 2.8; velocity overshoot due to short gate[77] | –/1.1 @ $10^{18}$ cm$^{-3}$ –/2015[78] | – | 1.9/2.3 2006[79]/1975[80] | TBD/TBD |
| $h^+$: holes | – | – | – | – | – | – | 1.4/1.1 2006[79]/1981[82] | ≈ 0.94/TBD 2008[81]/– |
| (7) Relative permittivity | 10.4 for E//c axis; 9.5 for E ⊥ c axis[83,84] | Interpolation | 9.76, E//c axis[85] (corrected for fringing fields); NR ⊥ c axis | – | 10[86] | 7.1[87] | 5.7[58] | Depends on insulator |
| (8) Thermal conductivity $\sigma_{thermal}$ (W m$^{-1}$ K$^{-1}$) | 253[88] | Interpolation | 285/319 both 1987[89] | <370[90] (on 4H-SiC) | 11 to 27/16 to 22 2015[91]/2015[92] | 768/940 (natural isotopic ratio) –/2145 (isotopically pure) 1983[93]/2013[94] | 2270/2290 (natural isotopic ratio) 3300/3450 (pure $^{12}$C) 1992–3[95,96]/2013[94] | 2270/2290 (natural isotopic ratio) 3300/3450 (pure $^{12}$C) 1992–3[95,96]/2013[94] |

**Table 2.** Continued.

| Parameter at 27 °C | (A) GaN (for reference) | (B) $Al_xGa_{1-x}N$ | (C) AlN | (D) Example AlGaN/GaN HEMT[53] | (E) $\beta$-$Ga_2O_3$ | (F) Cubic BN | (G) Diamond | (H) Diamond MOS |
|---|---|---|---|---|---|---|---|---|
| (9) Maturity assessment | Mature for GaN HEMTs; Immature for vertical GaN devices | Immature | Immature | Mature | Immature | Immature | Immature | Immature |
| (9a) Doping (p & n); or polarization-induced; or surface-transfer | Both n & p (Si & Mg)[29,54] | n (Si) below 80–85% Al; p (Mg deep)[54,97]; polarization doping[355,356] | Possible S donor[97]; no good acceptor | Polarization-induced 2DEG | n type (Sn, Si, Ge donors)[357]; no known acceptor | n type (S donor); deep acceptors[98] | Light to medium p type for $N_A$ < mid-$10^{19}$ $cm^{-3}$; Heavy for $N_D$, $N_A$ > mid-$10^{19}$ $cm^{-3}$[99–101] | Surface-transfer doping[63,64,76,81] |
| (9b) Dual use/low cost or low volume/high cost | Dual use/low cost | Dual use/low cost? | Low volume/high cost? | Mid to low volume/Mid to high cost? | Dual use/low cost? | Low volume/high cost? | Low volume/high cost? | Low volume/high cost? |
| (9c) Substrate size/availability | 50-mm GaN substrates available; GaN layers on 150-mm SiC and 200-mm Si available | Uses common substrates for GaN | 2016: 25 mm<br>2017: 50 mm[102] | On 75-mm SiC | 2016: 50 mm 2017: 100 mm[103] | Few-mm size HPHT crystals | 2016: 15 & 25 mm.[104,105] 7 × 20 mm; Larger diamond on Si[106,107]<br>2018: 38 mm.[105] | 2016: 15 & 25 mm.[104,105] 7 × 20 mm; Larger diamond on Si[106,107]<br>2018: 38 mm.[105] |

types (the columns in Table 2), then the materials/device properties (the rows in Table 2). We discuss both properties that are more fundamental as well as those that are less fundamental (e.g., doping levels) but are evolving in time as the technology for materials synthesis and control advances. Finally, based on the current state-of-the-art values for their properties, we give an informal assessment of the maturity level of the various materials.

#### 4.1.1. Materials/Device Types (Table 2 Columns)

The columns in Table 2 are organized by materials/devices.

The first column (A) for WBG GaN is given for comparison with the later columns for UWBG materials.

The third materials column (C) is for AlN, which, together with GaN, brackets the variable-composition alloy $Al_xGa_{1-x}N$ (column B). For parameters such as bandgap, as well as some others, interpolation between the endpoint values for GaN and AlN (with appropriate bowing parameter) can be used to estimate the desired value for a given composition of $Al_xGa_{1-x}N$.

The fourth materials column (D) lists the parameters for a state-of-the-art AlGaN/GaN HEMT having a GaN channel, again to provide a baseline reference for comparison with the UWBG materials. The mobility of the 2DEG listed for this device is 1200 $cm^2$ $V^{-1}$ $s^{-1}$,[53] but GaN-based HEMTs having a different barrier structure have shown 2DEG mobilities as high as 2200 $cm^2$ $V^{-1}$ $s^{-1}$.[203]

The fifth through seventh materials columns (E)–(G) are for $\beta$-$Ga_2O_3$, cubic BN, and diamond, respectively.

The eighth (and last) materials column (H) reports some of the work in diamond metal–oxide-semiconductor (MOS) systems, where surface-transfer doping via hydrogen termination is used to form a 2D hole gas (2DHG) just under the surface, and then the surface is passivated with a gate insulator such as $Al_2O_3$.

#### 4.1.2. Materials/Device Properties (Table 2 Rows)

The rows in Table 2 are organized by materials/device properties.

The first materials/device properties row lists bandgaps, as generally accepted by the community for some time, with the exception of AlN whose "historical" bandgap of 6.2 eV (based on older absorption measurements) was redefined more accurately in 2010 to ≈6.0 eV using high-resolution photoluminescence.[55] $Ga_2O_3$ has both a direct and an indirect bandgap with nearly identical values,[56] and cubic BN and diamond both have indirect gaps.

The second materials/device properties row reports projected bulk values of the critical electric field ($E_C$) at avalanche breakdown for each UWBG material starting with AlN (the HEMT column is a measured result). The projection uses the experimentally derived $E_C$ for GaN[59] as the baseline (corrected for the updated values of mobility and permittivity in the table), as this is the highest known $E_C$ for any GaN or SiC diode. These projections follow the method described in detail in Hollis and Kaplar,[60] and, to ensure a level playing field for all materials,

 

assume a non-punched-through p+/n diode having an ionized donor concentration of $10^{16}$ cm$^{-3}$ in the n-region.

The third materials/device properties row reports sheet carrier density ($n_s$): the 2D sheet density for electron or hole gases and the doping × thickness product for the $Ga_2O_3$ device (a doped-channel metal-semiconductor FET, i.e. MESFET). Most GaN HEMTs achieve sheet densities just above $1 \times 10^{13}$ cm$^{-2}$, which have been approximately matched by the $Ga_2O_3$ MESFET and a high-breakdown $Ga_2O_3$ MOSFET.[204] Further, a recent developmental $AlN/Al_{0.85}Ga_{0.15}N$ HEMT has demonstrated $n_s = 6 \times 10^{12}$ cm$^{-2}$.[157] All of these devices are exceeded by about 3× or more in this category by the surface-transfer-doped diamond MOSFETs reported in the last column, many of which have shown credible high-frequency performance.[81,205]

The fourth materials/device properties row reports electron drift mobility, where the best-known values for low-doped materials are given. The value for GaN represents the bulk value at a donor concentration of ≈$10^{16}$ cm$^{-3}$, which differs markedly from Hall mobilities as high as 2200 cm$^2$ V$^{-1}$ s$^{-1}$[206] reported for 2DEGs formed in regions that have a similar background donor level. This apparent discrepancy is due to the complexity of the Hall factor in GaN (which enables conversion of a Hall mobility to a drift mobility) as a function of different types of carrier scattering mechanisms,[67,207] as well as a reduction in density of scattering states as bulk transport is confined to 2D transport. It should also be mentioned that two studies that derived the drift mobility for GaN using fits to *I–V* characteristics report higher values for the bulk mobility: 1200 (obtained by extrapolating to a doping level of $10^{16}$ cm$^{-3}$ in Fig. 14 of Kizilyalli, et al.[208]), and 1470 for an electron concentration of $2 \times 10^{15}$ cm$^{-3}$ in highly compensated material.[74] As *I–V* fits generally have more assumptions and uncertainties than direct Hall measurements, we chose to use the Hall-derived bulk drift mobility of 1000 to extract the critical field for GaN in row 2; since the critical field varies as the cube root of mobility in such calculations, the differences are not large. Finally, in several instances in the table the reported mobilities are Hall mobilities, as the Hall conversion factor is unknown for those materials.

The fifth materials/device properties row reports hole drift mobilities. Note that the mobilities are not really of significance except in BN and diamond: for diamond a bipolar transistor has been demonstrated leveraging the parity in electron and hole mobilities.[112] Note also that, to date, diamond MOS work has mostly focused on 2D hole gases induced using H-termination; the reported mobilities for these 2DHGs are substantially below the measured bulk values for low-doped material. The reasons for this may involve hole scattering due to surface roughness, surface charges (Coulombic), lattice defects, and even phonons in the insulator, and requires further investigation. A similar effect is seen in Si MOSFETs where the channel electron mobility is limited to <600 cm$^2$ V$^{-1}$ s$^{-1}$ while the bulk value for low-doped material is >1400 cm$^2$ V$^{-1}$ s$^{-1}$.[209] As discussed in Sections 2.2 and 2.4, the growth of a high-quality c-BN/diamond heterostructure could in principle mitigate this mobility reduction and produce very-high-mobility transistors.

The sixth materials/device properties row reports saturated carrier velocities for both electrons and holes, where available. Values are typically in the 1–2 × $10^7$ cm s$^{-1}$ range for all materials except for the AlN/GaN HEMT, which benefits from velocity overshoot with a very short gate. Some developers of diamond MOSFETs do not report their intrinsic unity-current-gain frequency ($f_T$) values de-embedded from parasitic pad capacitances, and in these cases the $v_{sat}$ value for the diamond p-MOSFET was estimated by making the common assumption that half of the capacitance in the reported extrinsic $f_T$ is parasitic.

The seventh materials/device properties row reports relative permittivity. Surprisingly for GaN there are at least five different sets of permittivity values in common use, and an important outcome of this study has been to establish the best values for GaN and AlN based on our thorough literature search and on recent measurements of AlN by the U.S. Naval Research Laboratory. As indicated in the table, the accurate permittivity values for GaN, AlGaN, and AlN depend on the alignment of the electric field with respect to crystal orientation, which is expected, given their highly anisotropic crystal structure.

The eighth materials/device properties row reports bulk thermal conductivities. Cubic BN and diamond are the dramatic standouts, especially if grown in an isotopically pure form, which greatly minimizes scattering of the acoustic phonons that transfer the majority of the thermal energy. It should be noted that if a thin device layer is grown on a disparate substrate, the thermal conductivity of that layer can be substantially less than the bulk value listed due to phonon scattering at the interface(s); for example, a 2-μm GaN HEMT channel layer grown on a SiC substrate exhibits a lower effective thermal conductivity of about 140 W m$^{-1}$ K$^{-1}$ at 300 K.[210] It should also be noted that the thermal conductivity of $\beta$-$Ga_2O_3$ is quite anisotropic, as given in the references.

#### 4.1.3. Maturity Assessments

The last few rows, 9 and 9a–9c, of Table 2 comprise a materials maturity assessment across the categories of doping, volume/cost, and substrate size/availability, with an overall assessment of "Mature" or "Immature." For the row 9a doping category, there are three general methods for inducing carriers in the various materials: (1) traditional doping using donors or acceptors, ideally with shallow enough activation energies to produce sufficient carriers at room temperature, (2) polarization-induced 2DEGs, and (3) surface-transfer doping as described in Sections 2.2 and 2.5.[63,64,76,81] For the row 9b volume/cost category, we assess whether a given material system has a broad commercial market (dual use/low-cost) or only specialized or government markets (low-volume/high-cost), recognizing the leverage that large commercial markets (such as LED lighting for WBG InGaN) can bring to a material system.

In the following, we discuss maturity assessments for each material system in turn.

GaN and AlGaN: This system has greatly benefitted from the large worldwide investment in LED lighting—layers of GaN and its AlGaN alloys are readily available on large SiC and Si

substrates, and the technology for doping GaN both n and p type using Si and Mg is well established. AlGaN can be doped with Si up to an Al fraction of ≈80–85%, but doping with Mg is more difficult even for low Al fractions because it rapidly becomes a deep acceptor.[54] Both GaN and most of the AlGaN range is judged as dual-use/low-cost due to availability of large-area substrates and relative ease of doping, at least for n type up to ≈80–85% Al fraction. But the AlGaN alloys are judged as immature since high-quality growth and spurious oxygen incorporation become increasingly problematic for higher Al fractions.

AlN: The growth of boules of AlN has been demonstrated by multiple developers, as mentioned in Section 2.1. The available size of substrates cut from them is still limited, but is expected to increase with time as shown in the table. Doping of AlN is still in its infancy, with no known acceptors available and sulfur postulated as the only likely shallow donor.[97] For the next several years, bulk AlN is judged as an immature, low-volume/high-cost technology, at least until substrate sizes become larger and optoelectronic and/or electronic markets adopt AlN as a substrate.

AlGaN/GaN HEMT: The representative AlGaN/GaN HEMT in the next column is judged mature, because the MBE and MOCVD growth technology for such devices is established and similar devices (with lower Al fraction) have been fielded in electronic markets over the past several years. This general technology is judged mid-to-low-volume/mid-to-high-cost, as these devices tend to serve specialty and government markets, where the volumes are dramatically smaller (and epitaxial costs are higher) than for large markets such as LED lighting.

$Ga_2O_3$: $Ga_2O_3$ is judged immature as it is still in the early phase of its research and development cycle. It has available donors (Sn, Si, Ge),[357] but no acceptors. Possibly its greatest advantage is the availability of reasonably-sized substrates, thanks to the growth technologies described in Section 2.3. It is judged as a possible candidate for dual-use/low-cost as it is the most transparent conductor known and this, combined with the available substrate sizes, could enable penetration into the high-volume LED markets. Indeed, LEDs have already been demonstrated on it. As discussed earlier, its greatest challenges appear to be low thermal conductivity and low mobility.

c-BN: c-BN is the least mature materials technology in this table, with substrates of c-BN now produced only by the high-pressure, high-temperature (HPHT) method that historically has produced most industrial diamonds. There is an available shallow donor, but the known acceptors are deep. This technology will remain a low-volume/high-cost one for some time until methods for producing larger substrates are established or until methods for growing epitaxial c-BN on dissimilar substrates are developed.

Diamond: Doping for p-type bulk diamond is accomplished using boron as an acceptor which, though fairly deep at 0.36 eV, has about 1% activation at room temperature. For n-type, phosphorus is used, which is deeper (0.57 eV) and has a lower activated fraction of only $\approx 10^{-5}$ at 300 K. Both dopants can be incorporated into the diamond lattice at well over $10^{20}$ $cm^{-3}$ concentration, and for doping levels above mid-$10^{19}$ $cm^{-3}$ the conduction mechanism for both changes to low-resistivity hopping conduction which is advantageous for Ohmic contacts.

Diamond MOS: For the diamond MOS structures, doping is accomplished via a surface-transfer mechanism as described earlier, which can generate two-dimensional hole gases (2DHGs) with densities $>10^{14}$ $cm^{-2}$ at room temperature. Progress is being made by several developers worldwide toward larger diamond substrates as indicated. Figure 1 in Schreck[106] even shows a 2-micron-thick diamond film grown on an Ir film on a 100-mm Si wafer. While the presence of the conducting Ir film probably inhibits the use of such a diamond film for electronic applications, this group has recently shown a separated free-standing thicker diamond layer that is 92 mm in its largest lateral dimension, which could open the door to low-cost diamond electronics using such layers grown on inexpensive Si wafers and then separated. Until this occurs, though, we judge diamond to be a low-volume/high-cost technology with an overall rating of immature.

### 4.2. High-Power Electronics (HPE)

Perhaps the UWBG technology with the widest application space is high-power electronics (HPE). High-power electronics feed all those applications that require power switching—standing off high voltages when the switch is off, while conducting high currents when the switch is on. Such applications will only become increasingly important in the future, as electricity—the most flexible and dispatchable power form—continues to become more important in our increasingly "smart" and sustainable energy economy. It could also enable radically new military technologies, such as electric armor.

Indeed, en route to the potential impact of UWBG technology, conventional WBG technology is already advancing power electronics in a critical and impactful way. Led by GaN-on-Si and bulk SiC, it is competing to be the next viable alternative to silicon, even as silicon itself continues to evolve towards higher performance (with advances in superjunction MOSFETs, IGBTs, and other devices).

In particular, WBG technology presents the tantalizing possibility that losses in power switching can be reduced to a level at which thermal dissipation and heat sinks no longer determine sub-system and system design. Such an achievement would thereby reduce waste and cost, while enhancing personal mobility in grid-disconnected end uses. In this case, the conversation becomes less about performance/cost of the device and more about the performance/cost of the system the device enables.

For example, with their wider energy gap, WBG semiconductors can be doped more heavily for a given breakdown voltage, reducing conduction and switching losses and dramatically increasing the efficiency of power converters. Even if the efficiency change appears to be small, the system impact can be large: replacing a 96%-efficient Si-based power converter with a 98%-efficient WBG-based power converter decreases waste heat by half. Furthermore, WBG devices can in principle operate at higher temperatures (with the caveat that the thermal limit of the device might be set not by the semiconductor material but

by nearby non-semiconductor materials used for contacts, gate insulators, wire-bonding, die attachment, packaging, etc.).

For higher voltages (breakdown voltages $V_{BR} \geq 1200$ V), SiC vertical devices are at present preferred because very thick drift layers (tens of μm or more) can be grown homoepitaxially and controllably doped at low concentration (in the $10^{14}$ cm$^{-3}$ range). In addition, present-day SiC vertical device processing technologies (e.g., selective-area doping via ion implantation) are more advanced than are GaN device processing technologies.

For lower voltages (breakdown voltages $V_{BR} < 650$ V), GaN devices are increasingly preferred. These GaN devices at present differ considerably from traditional power devices: because of today's processing-technology limitations (whose research opportunities/challenges are discussed in Section 4.7), they are lateral (HEMTs) rather than vertical devices; hence they can be viewed as relatives of RF GaN devices. They are fast (switching frequencies >1 MHz) due to their lack of pn junctions and low input and output capacitances, but their lateral geometry makes electric-field management challenging and limits the achievable device breakdown voltage. They are also very efficient, due to their extremely low on-resistance ($R_{ON}$) enabled by a two-dimensional electron gas (2DEG) with a large electron concentration ($n_S \approx 10^{13}$ cm$^{-2}$) at the AlGaN/GaN hetero-interface and a high electron mobility of ≈1700–2000 cm$^2$ V$^{-1}$ s$^{-1}$, which is at least 20× larger than the channel mobility for SiC MOSFETs.

Even as WBG devices based on SiC and GaN technology become more mature, we can anticipate the subsequent development of UWBG devices with the potential to extend further the electrical and thermal system performance envelope, for both higher and lower voltage applications. This is illustrated by the Baliga/unipolar figures-of-merit (BFOMs) plotted in Figure 1 in Section 1, and also by **Table 3**, which shows the underlying materials properties and sixth power dependence on bandgap that enables the very high FOMs for the UWBG semiconductors.

In the remainder of this Section 4.2, we discuss three aspects of high-power electronics.

The first two aspects are the potential of particular device opportunities and challenges associated with the continuous and pulsed power applications illustrated in **Figure 11**. This figure presents a broad view of the present and future application spaces for WBG and UWBG materials, mapped by power and frequency for continuous-power applications, and by power, frequency, and voltage for pulsed-power applications. In particular, some of the highest power and voltage applications in pulsed power (e.g. vehicle survivability, i.e. electric armor) may require UWBG semiconductors, as opposed to today's WBG materials.

The third aspect are the opportunities and challenges that the high switching speeds of UWBG devices bring to the passive components that surround the active devices.

#### *4.2.1. Continuous Power*

By continuous power, we mean applications in which electrical power is routed, switched, or converted across all of its full range of voltages, currents, frequencies (AC/AC, DC/DC, AC/DC, DC/AC) and phases. Such conversion may be associated with a stationary application such as the modern electrical grid and the appliances connected to it; a small-scale mobile application such as an electric vehicle; or larger-scale mobile "micro-grids" such as those present on all- or mostly-electric aircraft and ships. For all of these applications (and especially for mobile applications), size, weight and power (SWaP) are important and can be favorably impacted by UWBG semiconductors.

For example, it has been suggested that neighborhood power transformer stations, currently school-bus-sized behemoths with a mass of 4500 kg or more, might be replaced with suitcase-sized switched power converters with a mass of only 450 kg (a "sub-station in a suitcase"; quote attributed to former US Department of Energy (DOE) Secretary Steve Chu). SWaP improvements of a similar magnitude are anticipated for voltage converters, where DC and/or AC voltages are converted from one level to another for use within an electronic system, and which are core components in aircraft, spacecraft, solar photovoltaic installations, electric vehicles, and military systems such as all-electric warships.

**Table 3.** Baliga figures of merit (BFOMs) for the UWBG semiconductors. Mobility values for Si and SiC are taken from Baliga's 2008 book. Permittivities and mobilities for GaN, AlN, $Ga_2O_3$, and BN are taken from UWBG Materials-Properties Table 2. Mobility values for AlN, $Ga_2O_3$, and BN are estimates only, as there is no information to our knowledge about how mobility and Hall factor vary with doping for those materials. Mobility for diamond is taken from Landstrass' measurement.[211]

| Material | Relative permittivity | Electron drift mobility at $N_D = 10^{16}$ cm$^{-3}$ (cm$^2$ V$^{-1}$ s$^{-1}$) | $E_C$ at $N_D = 10^{16}$ cm$^{-3}$ (MV cm$^{-1}$) | Thermal conductivity (W m$^{-1}$ K$^{-1}$) | BFOM = $¼\varepsilon\mu E_C^3$ ($10^6$ V$^2$ Ω$^{-1}$ cm$^{-2}$) |
|---|---|---|---|---|---|
| Si | 11.9[212] | 1240[90] | 0.3[90] | 145[212] | 8.8 |
| 4H-SiC | 9.7[90] | 980[90] | 3.1[213] | 370[90] | 6270 |
| GaN | 10.4//c axis | 1000 | 4.9 | 253 | 27 900 |
| AlN | 9.76//c axis | 426 est. | 15.4 | 319 | 336 000 |
| $\beta$-$Ga_2O_3$ | 10.0 | 150 est.[71] | 10.3 | 27 | 36 300 |
| c-BN | 7.1 | 825 est. | 17.5 | 940/2145 natural/isotop. pure | 695 000 |
| Diamond | 5.7 | 2000[211] | 13.0 | 2290/3450 natural/isotop. pure | 554 000 |

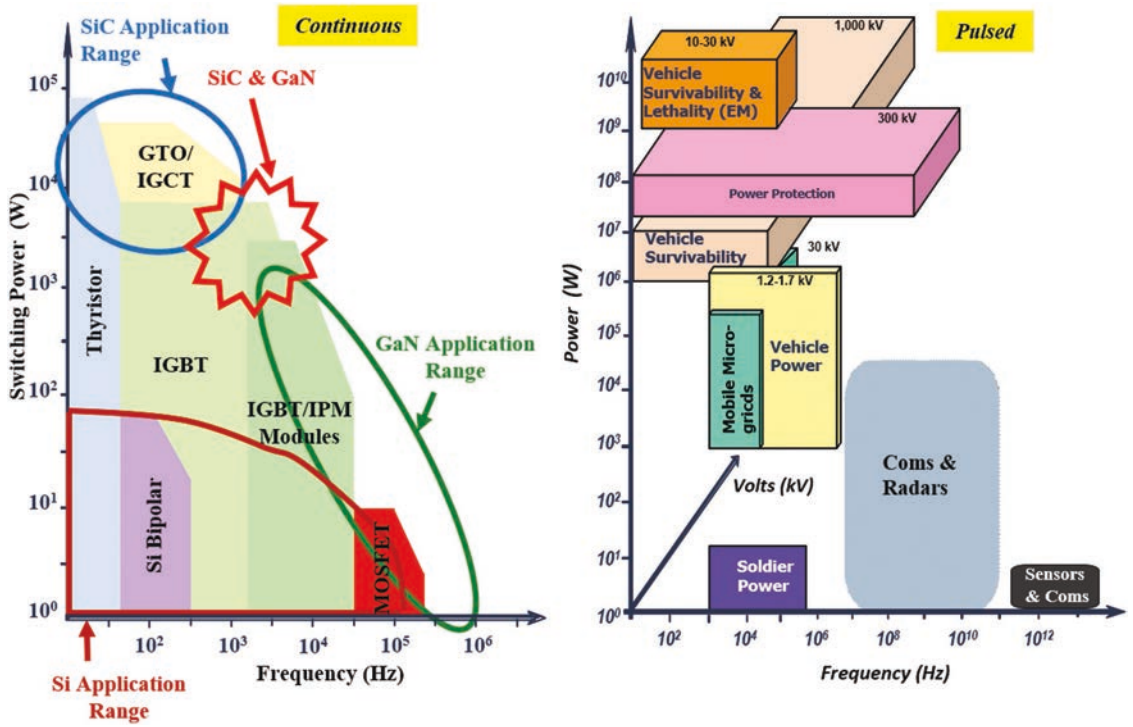


**Figure 11.** Left: Map of current device families used in continuous power switching applications, organized by switching frequency and switching power. GTO = gate turn-off; IGCT = insulated-gate commutated thyristor; IGBT = insulated-gate bipolar transistor; IPM = intelligent power module; MOSFET = metal–oxide-semiconductor field-effect transistor. The regimes in which Si, SiC and GaN operate (or are anticipated to operate) are indicated. The regimes in which the UWBG semiconductors are anticipated to operate are not shown, but would extend these considerably. Right: Map of applications for pulsed power devices, organized by switching frequency and power.

In general, for UWBG materials to have impact on these applications, vertical device structures[90,214,215] similar to those utilized today for Si and SiC will need to be developed. While lateral UWBG devices such as HEMTs or MESFETs may be quite useful for high-frequency switching applications (and preliminary devices of this type have been realized in the AlGaN[157] and $(AlGa)_2O_3$[216] systems), lateral devices will likely be less useful for very high-voltage (defined somewhat arbitrarily as >5 kV) applications. However, practical realization of vertical device architectures in UWBG materials (and even in GaN) will require development of new processing technologies, as discussed in Section 4.7.

Amongst vertical devices there are several classes: two- and three-terminal devices, each of which can be either unipolar or bipolar.

Two-terminal diodes are the simplest vertical device. Of these, pin (p-type/intrinsic/n-type) and Schottky diodes are the simplest, though not ideal. While pin diodes offer high blocking voltages, their forward turn-on voltages are roughly equal to the bandgap, which results in significant power loss. While Schottky diodes circumvent the forward voltage turn-on problem, they suffer from higher leakage currents due to various forms of carrier transport over or through the Schottky barrier. And, since their peak electric field is closer to the surface than in a pn junction, and the dissimilar surfaces may create interface states that can be electrically active, they also are more susceptible to premature breakdown.

Instead, a more ideal diode would be the so-called junction-barrier Schottky (JBS) or merged pin-Schottky (MPS) diode. In these hybrid devices the pn junction blocks the high reverse voltage, but the Schottky barrier governs forward-bias transport; in the MPS diode the pn junction also contributes to the forward surge current. Moreover, the JBS/MPS diode can be a test vehicle for developing various important and more-advanced processing steps in UWBG materials: it is the simplest device that requires selective-area doping (in the core of the device, not just for edge termination), a prerequisite and hence a stepping-stone for the more advanced three-terminal vertical power devices we discuss next.

Three-terminal devices are more complex, but also are a more powerful class of vertical device, and here we emphasize that for power applications it is challenging but highly desirable that these devices be normally-off. This is for safety and stability reasons: if a transient or voltage surge occurs while the power converter is powered off, it is important that no current travels through the inactive converter to reach equipment down the line. Thus, a high degree of electrical isolation should be present when the power converter is off, requiring that the power transistors themselves be off when no gate bias is applied. Thus, a key research opportunity/challenge here is:

13. Devices: Normally-off vertical power switches that combine ultra-high breakdown voltage with ultra-low on-resistance.

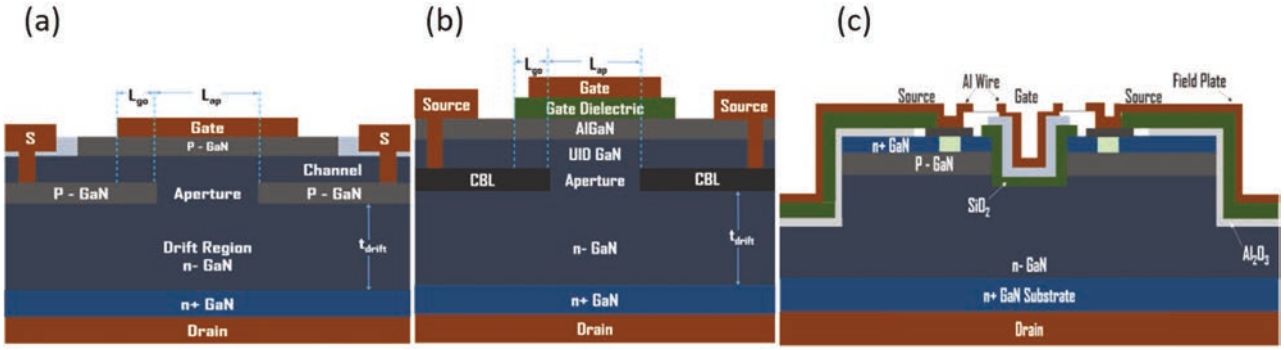


**Figure 12.** (a) and (b) illustrate two varieties of CAVET: in (a) the lateral channel is defined by a GaN pn homojunction, and is thus JFET-like, whereas in (b) the lateral channel is defined by an AlGaN/GaN heterojunction, and is thus HEMT-like. Both feature a current aperture linking the channel to the vertical drift region, characteristic of a CAVET. (c) illustrates a vertical trench MOSFET in GaN. CBL = current blocking layer; UID = unintentionally doped, S = source.

Among the three-terminal devices, unipolar devices are the simplest and most likely to be realized first in any UWBG material. In most cases, such unipolar devices will be based on electrons, due to their higher mobility. They include device types such as junction field-effect transistors (JFETs), current-aperture vertical electron transistors (CAVETs), and metal–oxide-semiconductor field effect transistors (MOSFETs), as illustrated in **Figure 12**.

The vertical JFET (not shown) is the simplest of these, and has been demonstrated in WBG GaN (but not yet in UWBG semiconductors) by several groups. However, the JFET is in most cases a normally-on device, which as noted above is undesirable. Its operating characteristics are also in large part determined by horizontal geometries that depend on more-difficult-to-control lithography, as opposed to vertical geometries that depend on easier-to-control epitaxy.

The CAVET[217] shown in Figure 12a is a variant of the JFET in which the gate junction is a horizontal rather than a vertical layer, hence with its critical dimension determined epitaxially. Another variant of the CAVET is shown in Figure 12b: in this case, the device has an AlGaN/GaN high mobility 2D electron gas (2DEG) channel for high conductivity. In both cases, the high electric field is confined to the vertical drift layer, which is coupled to the channel by the current aperture. Similar devices can be realized with all-AlGaN or $Ga_2O_3$, with appropriate current blocking techniques, to access higher operating voltages.[217–220] However, the CAVET suffers from its own problems; for example, it requires a number of etch-and-regrowth steps which to date have resulted in buried pn junctions with excessive leakage current, due to traps introduced at the etched surfaces. Nonetheless, normally-off devices may be easier to realize in a CAVET than in a vertical JFET, again due to the precise doping and layer thickness control afforded by epitaxy as opposed to lithography and implantation.

Finally, the MOSFET is highly desirable because it is a normally-off device and has several possible variants, including the D-MOSFET and trench MOSFET (the latter is shown in Figure 12c, and is also known as a U- or V-MOSFET, depending upon the profile of the trench). The research challenge required to achieve this, however, is fundamental: the development of a high-quality, high-reliability gate oxide (or other gate insulator). The outstanding $Si/SiO_2$ system that Si technology has so greatly benefited from (with a remarkably low density of electronic traps at the interface) has proven to be the exception amongst semiconductor-insulator systems. Even the thermal oxide grown on SiC has, despite many years of research, suffered from numerous problems such as high interface state density, low channel mobility, and threshold voltage instability. As discussed in Section 3.2, the formation of stable, high-quality gate insulators on UWBG materials is no doubt one of the chief areas in which research is needed.

Among the three-terminal devices, bipolar devices are more complex, but follow a long tradition. Today's very-high-power devices based on Si such as IGBTs and thyristors are bipolar devices. In WBG SiC, IGBTs have been reported, and in WBG GaN, the most prevalent vertical device today is the pn-junction-based pin diode (albeit a two-terminal, not a three-terminal, device). This is actually a "quasi-bipolar" device, because the hole lifetime in its homoepitaxial GaN is extremely short (single-digit ns[208]) and the corresponding hole diffusion length (a few μm, compared to a drift region thickness of several tens of μm) is similarly very short. The result is a drift current dominated by electrons, without the "conductivity modulation" that occurs when a drift region is flooded with minority carriers at a concentration much higher than the background doping. Due to these transport properties, it is not clear whether bipolar vertical switches in WBG GaN, much less in UWBG semiconductors, are achievable or even advantageous: the short diffusion length may preclude coupling of adjacent junctions in an IGBT or thyristor (note, however, that III-N heterojunction bipolar transistors, HBTs, have been reported[221]). A final challenge is that bipolar devices require doping of both polarities, which as discussed in Section 2.5 is very challenging for UWBG materials.

#### *4.2.2. Pulsed Power*

Pulsed-power sources are designed to deliver a specified amount of energy to a load in a very short period of time, thus resulting in very high peak power for the duration of the pulse. The pulse may be repeated at a given frequency (often termed the "repetition rate"); the average power delivered over the period of repetition is typically much lower than the

peak power. Pulsed power is of interest for a variety of applications, including electromagnetic railguns, electric reactive armor, pulsed microwave sources, directed energy weapons, high-power pulsed lasers, and fusion energy, to name a few. Desired characteristics are high peak power, high repetition rate, and low system size and weight.

A prototypical pulsed-power source is the Marx generator. This circuit consists of N capacitors initially connected in parallel and charged to a voltage $V_0$ by a power supply. In the simplest manifestation of the circuit the charging occurs through a resistive network, but in practical circuits any of a number of more efficient charging networks may be utilized. The circuit also contains switches that link the high side of each capacitor to the low side of the capacitor in the next stage. When the circuit is charged, both the capacitors and the switches each have a voltage $V_0$ across them. The first switch is then closed, and the switches in the following stages close in quick succession, resulting in a fast voltage pulse of magnitude $NV_0$ across the load; this results in a current through the load and hence a fast pulse of very high peak power.

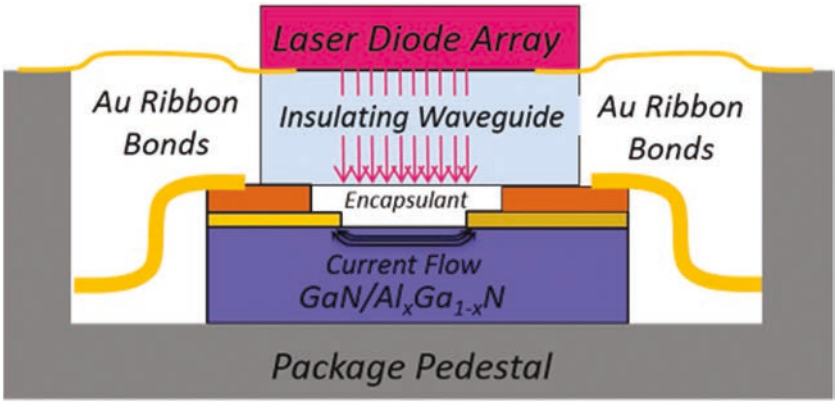


**Figure 13.** Schematic of a lateral photo-conductive semiconductor switch (PCSS), including its optical triggering array.

Traditionally, gas-discharge switches have been used in such circuits. Gas-discharge switches have several desirable characteristics, including nanosecond rise-times, high-voltage hold-off, effectively zero leakage current, and radiation hardness. Unfortunately, gas-discharge switches also require gas turn-over between "shots" whenever a shot produces enough current to ablate the electrode metal. This process severely limits the repetition rate of the system and also limits the switch lifetime.

More recently, high-voltage semiconductor devices have been investigated.[222,223] However, extremely high pulsed-power applications stretch the boundaries of what is possible with semiconductors: GaN and SiC switches are limited to handling $\approx 10^5$ W, but electric armor would require them to handle $\approx 10^6$ W. Thus, for applications of semiconductor switches, there is a strong motivation to use UWBG semiconductors, for two important reasons.

First, their blocking voltages should approach those of gas-discharge switches. Since the breakdown voltage of a semiconductor depletion region scales as $E_C^2$,[224] and $E_c$ scales as the 2nd power of $E_G$,[225] $V_{BR}$ of a semiconductor switch scales as the 4th power of $E_G$. Thus, UWBG devices have outstanding potential to achieve a very high blocking voltage, which in turn reduces the number of stages N required in the Marx generator to achieve a desired output voltage, drastically reducing system size and weight. Other desirable properties of UWBG materials discussed elsewhere in this report, including low intrinsic carrier density, robust radiation resistance, and good thermal stability, will also contribute to the robustness of switches used in a pulsed-power environment.

Second, being a semiconductor switch, an UWBG device contains no gas to be fouled, hence no moving parts are needed to accomplish gas turn-over between shots. Thus, UWBG-based systems are likely to achieve better repetition rates compared to gas-discharge-based systems for pulsed power applications. In addition to improved repetition rates, replacing gas-discharge switches with UWBG switches will likely improve the reliability of the switches, since the electrode metal ablation failure mechanism is eliminated. Further, system reliability and cost are expected to improve due to simplified triggering and reduced part count. Additionally, as UWBG materials are implemented in pulsed-power circuits, the capacitors' charge rate may be improved by replacing the charging resistors with active converters.

One candidate semiconductor switch for pulsed-power applications is the photo-conductive semiconductor switch (PCSS). This switch, which can be built in either a vertical or lateral configuration (a schematic of a lateral PCSS is shown in **Figure 13**), is essentially a very thick (hundreds of μm, which might be fabricated from a bulk wafer, instead of an epitaxial layer) semi-insulating drift region. This drift region blocks very high voltage, and is triggered into a conducting mode by an incident light pulse. In the "high-gain" mode the incident light not only generates photo-carriers but also initiates an avalanche process, which results in very high current density for a brief period. The PCSS is thus a nearly perfect semiconductor analogue of the gas-discharge switch. Such high-gain PCSS's in GaAs are capable of blocking 40 kV and passing 350 A.[226]

PCSS's based on UWBG semiconductors should bring additional advantages (PCSS's have been demonstrated in GaN,[227] but to our knowledge not yet in any UWBG material). First and foremost, blocking voltages and currents that are orders of magnitude larger should be possible. Second, the same factors that give rise to fast turn-on and turn-off transients for UWBG switches for continuous power applications also apply to pulsed-power systems,[225] allowing for very short pulses with fast rise and fall times (nanoseconds) and hence very high values of peak power. Third, there is also a system-level side benefit to the use of UWBG semiconductors in the continuous power applications discussed above: in many cases the size and weight of the overall pulsed power system is important, and can be minimized if the power supply (which is a continuous-power converter) for the Marx generator itself uses UWBG semiconductors.

A promising Research Opportunity/Challenge is thus:

14. Devices: Photoconductive UWBG-semiconductor switches for pulsed-power applications.

#### 4.2.3. Passive Elements

In any of the power electronics applications discussed in Section 3.1, the active devices are accompanied by passive elements such as capacitors and inductors for local storage of charge or current. In essentially all cases, these passive elements occupy more volume and weight than the active devices, and in some cases they are the limiting factor in the overall performance of the system. For example, inductive coils play a central role in power circuits that convert one AC waveform or voltage into another AC waveform or voltage, and their properties have major implications on power converter system performance and size. Thus, there are research opportunities and challenges for passives in UWBG-enabled high-power electronics—in both the continuous- and pulsed-power applications discussed earlier in this Section 4.2.

In continuous-power applications, as noted above, UWBG semiconductors enable power switches to operate at higher frequencies (>1 MHz)[228] than those made from conventional silicon. The resulting higher frequency AC waveforms enable proportionally smaller passive elements to be used in these power switches. The smaller size of the passive elements then opens up the possibility of increased integration, enabling systems where passives are batch micro-fabricated on-chip along with the active elements. Moreover, on-chip integration of passives is not only enabled by the higher switching frequencies, but also in turn enables yet faster switching, by minimizing parasitic coupling between components that would otherwise suffer too-high losses via the electromagnetic radiation that is enhanced at higher frequencies.[228]

There is thus opportunity for UWBG-semiconductor-based power converters in which the passives are miniaturized and integrated on-chip with the active elements. One example is the micro-fabrication of inductors on GaN for a dc-boost converter.[229] Another example is illustrated in **Figure 14**, where an array of high Q-factor on-chip inductors was micro-fabricated on a Si CMOS wafer to form low-phase-noise oscillator circuits.[230] The coils were fabricated with a micro-machining technology to form 3D out-of-plane structures with improved Q-factors. Similar approaches to integrating low-loss passives with UWBG semiconductors could significantly advance power converter capabilities. Ultimately, the smaller footprint, lower weight, and higher-temperature operation enabled by UWBG semiconductors will yield system-wide benefits for power converters and significantly impact applications in aerospace, transportation, and military systems.

In pulsed-power (as well as in more extreme switched continuous-power) applications, not only is there a similar need and opportunity for SWaP improvement via miniaturization and integration of passive elements, there is also need and opportunity for improvement in the performance of the passive elements themselves, both capacitors and inductors, so that they keep pace with the potential system improvements enabled by UWBG semiconductors. A major challenge is ensuring that the passives maintain good performance at the higher switching frequencies of the UWBG active devices.

For capacitors—the primary electrical energy storage component—not only is high capacitance usually desired, but high efficiency and hence low parasitic loss is also essential. The parasitic losses can be thought of as stemming from the inductive and resistive components of the equivalent circuit of a capacitor. The series inductance component must be minimized, because otherwise large current transients ($di/dt$) lead to significant voltage drops. The parallel resistive component must also be minimized, as it represents a dielectric loss leading to heating that reduces capacitor lifetime. Minimizing these parasitic inductive and resistive components, as well as enabling reliability at high temperature, may require new dielectric materials.

For inductors—the magnetic passive component—high inductance is usually desired. However, since inductance scales with size, inductances are size, weight and power limited. There is a need for magnetic cores with high resistivity (to decrease eddy current losses), high saturation polarization (to increase energy density allowing smaller inductor size) and small saturation polarization frequency-roll-off (allowing operation at high frequencies). There is thus an opportunity to realize further miniaturization of magnetic components, especially when monolithically integrated, by introducing new materials, such as hexaferrites, to function as magnetic cores.[231] Thick (multi-hundred micron), high-quality hexaferrites, if they could be realized, would enable on-chip inductors to be

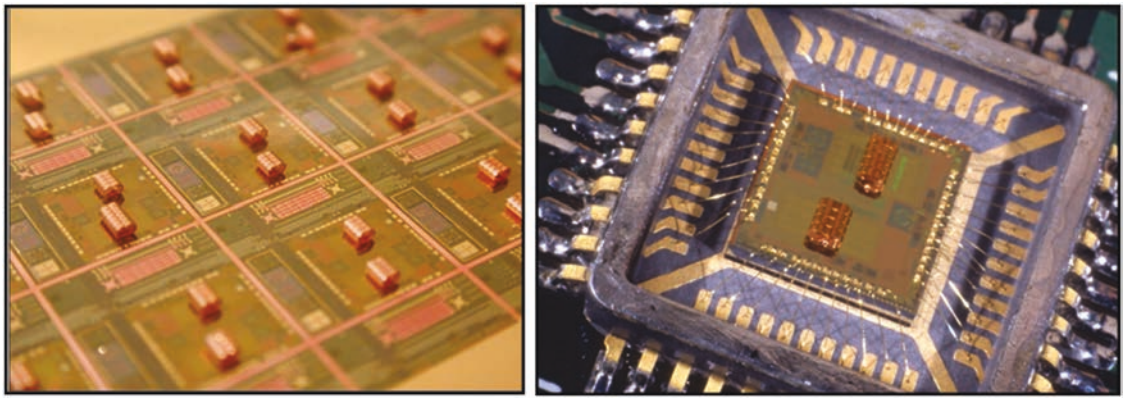

**Figure 14.** Left: Si oscillator circuit wafer with integrated high-Q-factor out-of-plane coils. Right: Oscillator chips after die singulation and packaging.

made significantly smaller. Other materials that may have good properties at higher frequencies include FeN and emerging Fe-based nanocomposites.

15. Devices: New dielectric and magnetic materials and architectures that enable high-frequency ultra-compact integrated passive elements, which in turn enable system performance not limited by performance of those passive elements.

### 4.3. Radio-Frequency (RF) and Microwave Electronics

UWBG semiconductors have the potential to impact high-frequency technologies as well, in particular technologies for generating, switching and receiving high-power RF and microwave signals. Here, we discuss four different ways they might have impact. First, they can serve as either sources or amplifiers of high-power RF signals, most often feeding an antenna. Second, they can serve as a fast switch that connects or disconnects an RF source and receiver to or from an antenna. Third, they can serve as resonant filters for processing RF signals. Fourth, they can serve as the basis for new vacuum electronics architectures, of interest for microwave power and thermionic energy conversion.

#### *4.3.1. RF Source Power*

Radio-frequency power transistors are required for electronic systems that transmit signals into air or space, with applications ranging from communications to imaging to sensing. For all of these applications, a high output power is usually desired as it improves signal/noise ratio. In addition, the efficiency of power usage (often defined as radiated power out/prime power in) is generally important for all systems, because the non-radiated power is lost as heat which must be removed to avoid overheating the system. Additionally, a system with low efficiency requires excessive prime power that, for systems that use batteries, shortens battery life.

Transistors based on Si, GaAs, and more recently GaN have been the workhorses to date for these power applications,[232] but a consideration of the fundamental materials properties from Table 2 for $Ga_2O_3$, high Al-content AlGaN, AlN, BN, and diamond shows that these UWBG materials offer even greater promise for RF applications.

First, power output is proportional to the product of the maximum usable voltage across the output of the device times the maximum allowed current through the device, and both the voltage and current are governed by material properties. The maximum voltage is determined by the critical electric field ($E_C$) for the material in the given device geometry and doping concentration; and the maximum current is determined by the carrier sheet density ($n_s$) and the saturation velocity ($v_{sat}$) of the electrons or holes.

A higher-breakdown-field material offers two possible advantages for high-frequency transistors. First, for a given drift-region length and $f_T$, a higher breakdown material will support a higher output voltage and therefore more output power. Alternatively, if output voltage is held fixed, the drift region length can be reduced, which leads to a smaller delay and therefore higher power gain at a given frequency. At a given supply voltage, highly-scaled ultrawide-bandgap transistors could therefore provide gain at much higher frequencies than GaN transistors. This gain can be used not just to increase the power-added efficiency at the signal frequency, but also to realize new switched-mode amplifier designs that can go beyond the efficiency limits of class A/B amplifiers.

**Table 4.** Johnson figures of merit (JFOMs) for UWBG semiconductors, calculated from underlying properties taken from UWBG Material/Device Properties Table 2.

| Material | $v_{sat}$ ($10^7$ cm $s^{-1}$) | $E_C$ at $N_D = 10^{16}$ $cm^{-3}$ (MV $cm^{-1}$) | Thermal conductivity (W $m^{-1}$ $K^{-1}$) | JFOM ($10^{12}$ V $s^{-1}$) |
|---|---|---|---|---|
| Si | 1.0 | 0.3 | 145 | 0.48 |
| GaN | 1.4 | 4.9 | 253 | 11.0 |
| AlN | 1.3 | 15.4 | 319 | 31.9 |
| $\beta$-$Ga_2O_3$ | 1.1 | 10.3 | 27 | 18.0 |
| c-BN | unknown | 17.5 | 940/2145 Natural/Isotop. pure | – |
| Diamond | 2.3 (e–) 1.4 (h+) | 13.0 | 2290/3450 Natural/Isotop. pure | 47.6 (e–) 29.0 (h+) |

Since power transistors typically generate heat in their active region that must be removed to avoid exceeding a maximum junction temperature for reliable operation, the thermal conductivity is an additional material parameter that is important. As mentioned in the Introduction, the Johnson figure of merit (JFOM) is often used to compare the promise of materials for RF power, and is given in **Table 4** together with thermal conductivity as key indicators of the potential of the respective UWBG materials for RF power, with Si and GaN given for comparison. It should be noted that existing GaN-based devices already face challenges with heat removal at high power levels and have used diamond layers for heatsinking.[233–237] Devices made of AlGaN, AlN, and especially $Ga_2O_3$ will likely also need to be bonded to diamond heatsink layers for thermal management. Materials such as c-BN and diamond that offer not only high potential power capability but high thermal conductivity in the same material could be especially advantageous for next-generation RF power devices. Therefore, a key research opportunity/challenge is:

16. Devices: Thermally managed UWBG RF transistors that generate higher output powers and power densities than present Si-, III-V-, SiC-, and GaN-based devices.

The higher power densities may be realized via higher voltages and/or higher current densities. Both lateral (FET) and vertical (bipolar or FET) designs may be viable here.

#### *4.3.2. RF Switching*

In all RF transmitter/receiver architectures there needs to be some means for preventing the high-power output signal from leaking into the receiver input and burning it out. Traditionally, ferrite circulators have been used, but they are bulky and heavy

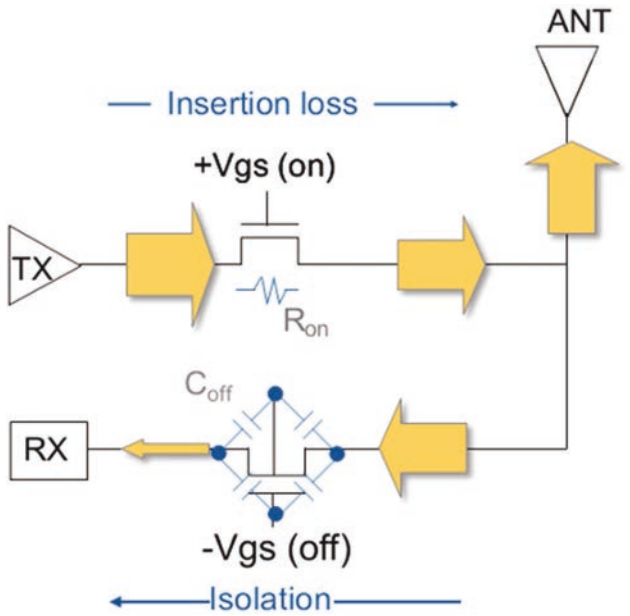


**Figure 15.** Illustration of FETs used as RF switches to separate transmitted and received signals in a modern transceiver. Figure courtesy of Randy Wolf, Global Foundries.

and have been increasingly replaced by FETs used as switches to isolate the receiver, as shown in **Figure 15**.

Similar to the high-frequency power-switching application discussed in 4.2, these devices need a low on-resistance for low RF insertion loss when in the "on" state, and a high-voltage-blocking/low-signal-leakage capability (isolation) when in the "off" state. The relevant figure of merit is $(R_{on}C_{off})^{-1}$, where $R_{on}$ and $C_{off}$ are the on and off-state resistance and capacitance, since minimizing $R_{on}$ minimizes the insertion loss and minimizing $C_{off}$ minimizes the RF feedthrough and switching time.

As UWBG transistors are developed and integrated into power transmitters (the 'TX' in Figure 15), their higher output power and voltage will require that the lower transistor switch in Figure 15 be made from the same or similar materials to hold off the higher voltage generated by the transmitter in order to prevent it from burning out the receiver input (the 'RX'). Therefore, RF switch development must track the advances in RF power-transistor development in the UWBG materials, and the switches can typically either use the same material as their power-device counterpart but with a slightly different design for higher voltage-standoff margin, or use a higher-bandgap alloy (or material) in a similar design. $R_{on}$ is minimized by using materials having high mobility, and $C_{off}$ is minimized by using lower permittivity materials that also yield a small device area as discussed previously in Sections 1 and 4.2. Traditionally, with Si-, GaAs-, and GaN-based switches, the on/off isolation ratio only needed to be ≈30 dB or slightly better to prevent burnout of the receiver, but with the higher potential voltages and output powers of future UWBG transistors, this specification will likely need to be raised by many dB, which presents additional challenges in the design of the switching devices and circuits. Thus, another key research opportunity/challenge is:

17. Devices: High-voltage, low-capacitance, low-on-resistance UWBG RF switches having the ability to stand off voltages higher than those generated by UWBG power transistors.

#### *4.3.3. Electromechanical Filters*

Electromechanical filters consist of transducers that convert an electrical signal to mechanical motion, which is then passed through a vibrating mechanical system, and then transduced back into electrical energy at the output.

Such filters are widely used in commercial applications: high-performance RF filters based upon physical-vapor-deposited PVD-AlN resonators, such as the film bulk acoustic resonator (FBAR)[238] and the solidly mounted resonator (SMR),[239] are the dominant technology currently utilized in 4G/LTE (4$^{th}$ generation long-term evolution) communication systems. This is due to their small footprint, high Q-factor, high operating frequency, and relatively good power handling.[240–243]

Due to the size and rapidly evolving requirements of the commercial smartphone market, filters used in commercial wireless devices have become lower cost and more compact, and possess improved filter response. This has led to greater overlap in both the requirements and characteristics of filters between commercial smartphones and military Department of Defense (DoD) systems. For instance, all commercial smartphone filters are thin-film-based resonators and are therefore compact and light. In addition, 4G networks and as-yet undefined 5G and internet of things (IoT) future wireless standards have begun to use mm-wave frequencies that overlap with traditional DoD radar bands, ranging from L through Ka bands. Besides decreased size and weight and higher center frequency, the impetus to improve insertion loss and rejection characteristics is also common to both commercial and DoD systems.

Note though, that despite the increasing convergence between DoD and commercial piezoelectric filter characteristics, the requirements of DoD systems do in fact extend beyond the capability of current commercial filter devices in two important aspects: power handling and bandwidth.

With respect to power level, commercial surface acoustic wave (SAW) or bulk acoustic wave (BAW) resonator-based filters are typically limited to low power (<2 W), while many DoD applications such as radar and military communication require a combination of decade (10×) wide bandwidth, medium to high power (few W to 100s of W) and low filter loss (<1 dB) at high power. Due to these requirements, many DoD applications cannot use currently available SAW- or BAW-based filters. Instead, they implement the filtering function using either: discrete L and C elements (including varactor-diode-based implementations); transmission-line-based elements; or cavity-, waveguide-, ceramic-, or dielectric resonant oscillator- (DRO) based filters. Each of these approaches has disadvantages in either size or weight, or is forced to make a trade-off between performance versus size and weight.

With respect to bandwidth, cellular communication formats generally possess narrow signal bandwidths (typically <5% fractional bandwidth). This aspect is well-suited to the capabilities of filters built using existing thin-film resonators, which use either BAW or SAW vibration modes. However, as formats

move beyond the historical 2.5G and 3G frequency bands and into the higher frequency 4G/LTE bands, requirements become more challenging due to larger fractional bandwidth requirements.[244] Because the bandwidth of an RF filter is primarily fixed by the electromechanical coupling efficiency of the resonator, and since the electromechanical coupling efficiency in turn depends on the piezoelectric constant of the material used to facilitate the conversion of electrical to acoustic energy during operation, increasing the piezoelectric constant is of great interest.

In the incumbent poly-crystalline PVD-AlN-based resonator technology, the relatively low effective electromechanical coupling coefficient, $k_{eff}^2$ (e.g. 6–7%), can be attributed to the low piezoelectric constant, $e_{33}$, of the PVD-AlN thin-film itself. Recent studies have demonstrated that the piezoelectric coefficient of PVD-AlN films can be increased by alloying with scandium (Sc),[245,246] or by co-doping of AlN using Mg-Zr or Mg-Hf.[247] However, the process of doping PVD-AlN has other drawbacks that degrade the Q-factor of the resonator.

A particularly promising alternative approach to improving piezoelectric constants is to move beyond polycrystalline materials and to explore crystallographically oriented single-crystal undoped $Al_xGa_{1-x}N$ films synthesized via metal-organic chemical vapor deposition (MOCVD). While early work has been published on AlGaN films for acoustic resonators, those results may have been limited by the fabrication processes[248–250] or material quality.[251] Recently, simulations of AlN acoustic resonators using undoped PVD AlN and undoped MOCVD-AlN predicted significant benefits of using highly oriented, single-crystal AlN films with high $e_{33}$.[252] Further, recent results on single-crystal MOCVD-AlGaN piezoelectric films on silicon substrates were demonstrated as a preliminary stepping-stone to MOCVD-AlN.[253] Thus, a key research opportunity in this area is:

18. Devices: Single-crystal AlGaN and AlN electromechanical RF filters with very high bandwidth and power-handling capability, small size and weight, and potential for monolithic integration with AlGaN electronics.

Some of the performance and reliability advantages of such single crystal III-N resonator technology for resonator and filter applications are illustrated in **Figure 16**a. Potential specific research directions follow from these potential advantages. These research directions include direct materials characterization to understand the piezoelectric, acoustic and thermal material properties of the single-crystal materials. By building and characterizing resonators and filters fabricated from single-crystal materials, the proposed advantages of single-crystal-based resonators and filters can be explored with respect to improved filter bandwidth, improved filter power handling, improved filter ruggedness and survivability and higher frequencies of operation.

Moreover, with the III-N materials, resonator $k_{eff}^2$ can be tailored by varying Al composition, as shown in Figure 16b. The ability to tailor resonator $k_{eff}^2$ allows optimal realization of filters with widely varying bandwidths, thus mitigating the design trade-offs inherent when fixed resonator $k_{eff}^2$ is utilized to design filters with widely varying bandwidth. In recent work, resonators with a $k_{eff}^2$ of 4.44% and Q of 1277 using 40% $Al_xGa_{1-x}N$ films on <111> Si have been fabricated.[253]

Finally, we mention that in the long-term, the ability to use single-crystal AlGaN or AlN in RF MEMs also brings the possibility of integrating this high-performance crystalline piezoelectric material directly with RF electronics. This, in turn, would open up new possibilities for integrated RF switches, filters, MIMs, and optomechanics.

#### *4.3.4. Vacuum Electronics*

Vacuum electronics technology is still the most efficient technology for generation of very high microwave power, with applications ranging from the cavity magnetrons that generate power for kitchen microwave ovens, to the traveling-wave tubes (TWTs) that serve as amplifiers in radars and satellite transponders.[254] Vacuum electron emission is also a key element of thermionic energy conversion (TEC). While TEC is not a power electronics technology, it is discussed in this section due to its dependence on low work function surfaces.

The ways in which UWBG semiconductors could make impact on vacuum electronics technology include three general areas, outlined below.

*Power Electronics*: A first way that UWBG semiconductors could make an impact is in the high-power and RF electronics, discussed throughout Sections 4.2 and 4.3, necessary to drive the vacuum electronics. Improvements in these electronics will result in improved system-level reliability, size, weight and power, as well as enable new concepts such as microwave power modules.

*Electron Emitters*: A second way that UWBG semiconductors could make an impact is as electron-emitting cathodes for the vacuum electronics device itself. Indeed, the electron-emitting cathode is the heart of vacuum electronics, and replacement of thermionic emission hot cathodes with field emission cold cathodes has been a longstanding goal for the vacuum electronics community for decades. Improved lifetime and efficiency are the key motivators, but rapid turn-on and pulsed operation enabled by near-ambient temperature operation are also motivators. As an example, direct vacuum electron emission has been established from forward-biased diamond-based pin diodes; these devices could be employed in very high voltage (>10 kV) switches or TWT cathode designs (**Figure 17**).[49,255]

Interest in using UWBG semiconductors for electron emission can be traced to early measurements of efficient electron emission from diamond surfaces stimulated by above-bandgap light.[256] The measurements were related to a negative electron affinity (NEA) of the hydrogen-terminated surface, and could be described by theoretical analysis of the dipole due to the C—H bonding.[257]

Since then, there have been many studies of electron field emission from various forms of diamond, both thin-film and single-crystal. For thin films, while hydrogen termination seems to lead to an improvement of the effect, many results have been related to defects and the presence of $sp^2$-bonded regions in the films. These structures have been used for field-emission cathodes and diodes. For single crystals, there have been a number of reports of diodes that show electron emission from hydrogen-terminated surfaces where the surface included the interfaces of the pin junction. The early work by

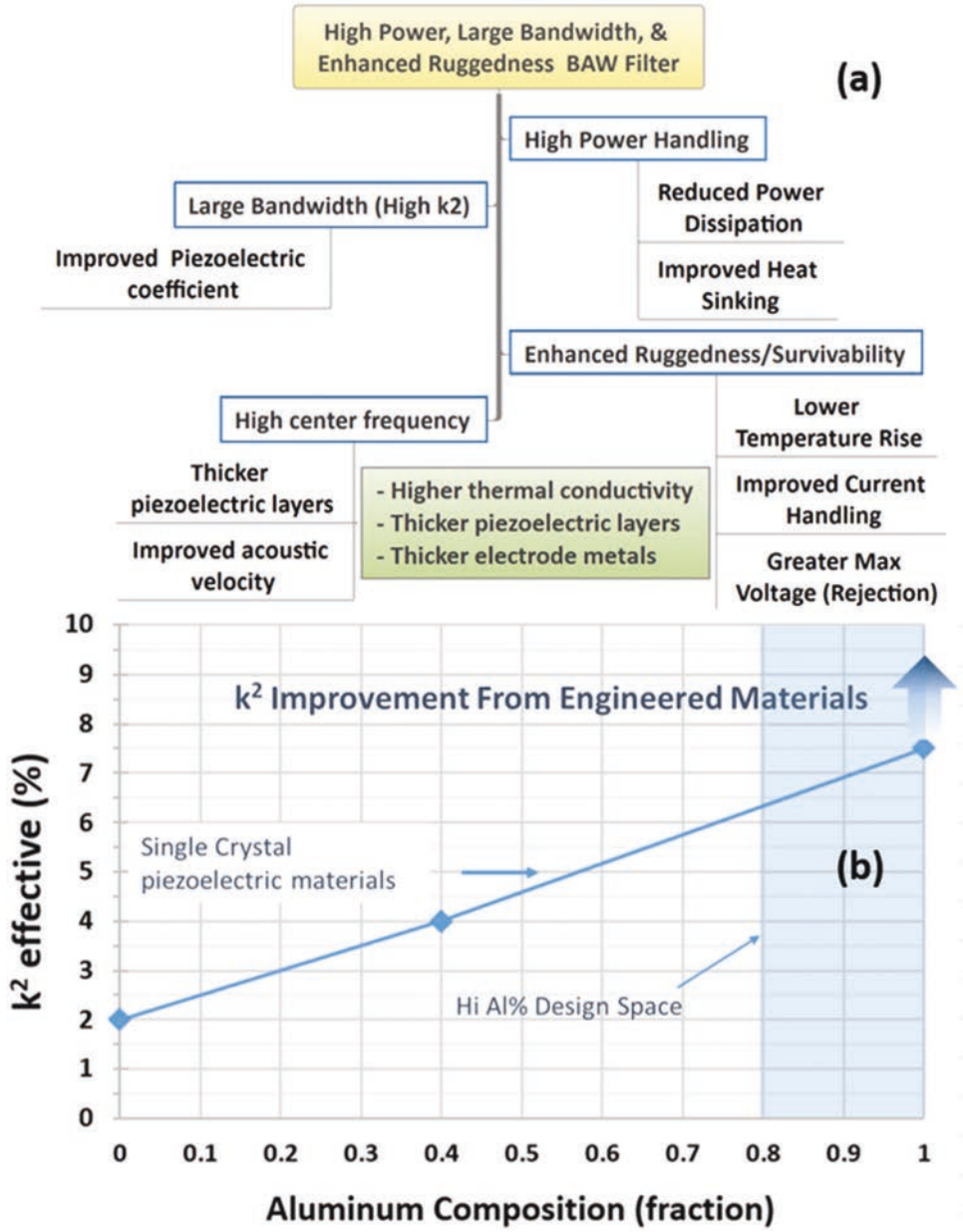


**Figure 16.** a) Advantages of single-crystal electromechanical resonators for high power, large bandwidth, extreme ruggedness and survivability, and high center frequency. b): $k^2_{eff}$ as a function of Al composition, highlighting increased bandwidth and design.

Geis and co-workers employed[258] a carbon-implanted layer to inject electrons into the junction that was fabricated on a p-type base layer. With the development of in-situ phosphorus doping, diamond pin diode structures have been fabricated that display electron emission from hydrogen-terminated NEA surfaces. Reports have shown emission efficiencies that approach 2.5% of the diode current, similar to the efficiency of thermionic cathodes.[49,50]

There is also interest in other UWBG materials for electron emission. A negative electron affinity has been found for hydrogen-terminated c-BN,[259] and ammonia-exposed surfaces of AlN have shown an electron affinity of less than 1 eV.[260] The AlN surfaces are particularly sensitive to exposure to oxygen, which increases the electron affinity. Research is yet to establish whether structures fabricated from c-BN or AlN could achieve electron emission, and to date electron emission diodes have not been reported for these materials.

*Electron Collectors for Thermionic Energy Conversion*: A third way that UWBG semiconductors could impact vacuum electronics is as low-work-function collector surfaces in thermionic energy conversion (TEC) devices. In these devices a low-work-function surface is heated such that it emits electrons, which transit a vacuum gap to a low-work-function collector surface. A direct analysis of the energy-conversion efficiency suggests that a collector work function of 0.5 eV could lead to a TEC with performance that would be similar to a thermoelectric energy

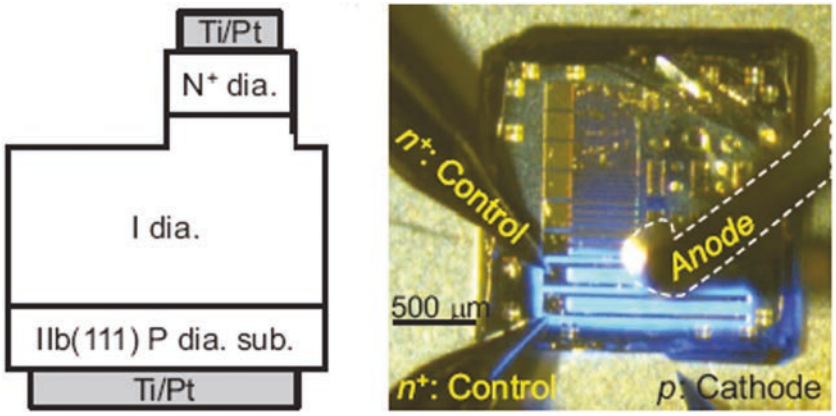


**Figure 17.** Left: Cross-section schematic of an electron-emission diamond diode. Right: Image of fabricated electron-emission diode (on-state) and measurement probes. The electroluminescence originates from defects and was only observed at forward bias. Reproduced with permission.[49] Copyright 2013, John Wiley and Sons.

conversion device with a thermoelectric figure-of-merit (ZT) of nearly 10.

There has been a search for low-work-function surfaces that could be anticipated from NEA surfaces of UWBG materials. Several studies of H-terminated nitrogen-doped single-crystal diamond surfaces have shown thermionic emission with a work function of ≈2 eV.[261] The value is higher than anticipated, and has been attributed to the deep donor level for nitrogen (1.7 eV) and the presence of upward band bending. Studies of thermionic emission from polycrystalline n- and p-doped diamond have shown exceedingly low work functions of 1.4 and 0.9 eV, respectively.[262] It has been speculated that the band-bending is mitigated by the high doping density and the presence of grain boundaries. A key research challenge/opportunity here is:

19. Devices: Negative-electron-affinity and/or ultra-low-work-function surfaces for robust, high-electron-emission efficiency cold cathodes and/or electron collector surfaces.

### 4.4. Deep-UV Optoelectronics

As history has repeatedly shown, the principal applications of new materials are often not technologies that they replace, but technologies that they create. In that sense, deep-ultraviolet (DUV) photonic applications are a primary raison d'etre for UWBG materials and will potentially drive many advances.

Optical sources that emit in the deep UV have a wide range of applications, both commercial and military. One set of applications requires bulk "broadband" photons—lots of photons, without the need for single-wavelength operation or narrow linewidths. Another set of applications requires somewhat fewer but "narrowband" photons, more precisely tailored and coherent so as to enable, for example: Raman spectroscopies; non-line-of-sight communication; or resonant interaction with specific atomic absorption lines of interest to sensing and quantum information processing schemes (Section 4.5).

In this Section 4.4, we discuss first broadband photon devices and applications; second, narrowband photon devices and applications; and third, opportunities and challenges associated with the most mature deep UV material system, AlGaN.

#### *4.4.1. Broadband Photon Emitters and Detectors*

Applications for broadband photons include air/water/surface/food purification-disinfection, materials and polymer processing/curing, medical/biomedical diagnostics and treatment, and scientific instrumentation.

Traditional sources in the UV include mercury lamps, gas lasers (e.g., excimer) and solid-state (e.g., frequency-multiplied Nd:YAG) lasers. Generally, these commercial sources are of limited applicability due to poor SWaP characteristics (e.g., they are bulky, heavy, expensive, and inefficient, require high-voltage operation, and have limited lifetime). Moreover, the use of mercury leads to significant environmental pollution issues.

In contrast, optoelectronic devices based on UWBG semiconductors would have excellent SWaP characteristics. And, among the UWBG semiconductors, perhaps the best suited is AlN/AlGaN, which is chemically and physically robust, has a direct bandgap over its entire alloy composition, and has the potential for high-temperature operation. The challenge for the UWBG semiconductors is to achieve, in the UV-B (315–280 nm) and UV-C (280–200 nm) spectral bands, performance and efficiencies similar to those that have been demonstrated in the visible range with the narrower bandgap InGaN material system. **Figure 18** shows the reported external quantum efficiencies (EQEs) for LEDs at wavelengths from the violet into the deep UV. The data show that EQE can be quite high (>25%) at wavelengths >370 nm, with InGaN active layers, but that it drops off steadily for wavelengths <360 nm, with AlGaN active layers, and drops off precipitously at wavelengths below 250 nm. The notable exception is for LEDs near 270 nm with 10% EQE, where significant investment has been made to address germicidal applications such as water purification and fluorescence detection of biomolecules.

Ultimately, power efficiency, commonly referred to as wall-plug efficiency (WPE), in the range of 10% is likely necessary, combined with useful output power and competitive cost, to enable economical industrial-scale applications of UV LEDs. (Note that EQE tracks the efficiency for converting injected electrons into emitted photons while WPE records the conversion of electrical power into optical output power and includes series resistance losses; thus WPE ≤ EQE.)

Finally, we note that solar-blind UV-C photodetectors are also of interest for various applications in commercial gas furnaces, as well as military non-line-of-sight, short-distance, secure communications and several other threat-detection systems. While AlGaN UV photodetectors are commercially available, AlGaN-based avalanche photodiodes (APDs) are still in an early stage of development. Of the available UWBG semiconductors, $Al_xGa_{1-x}N$ is perhaps best suited for fabricating UV-C light

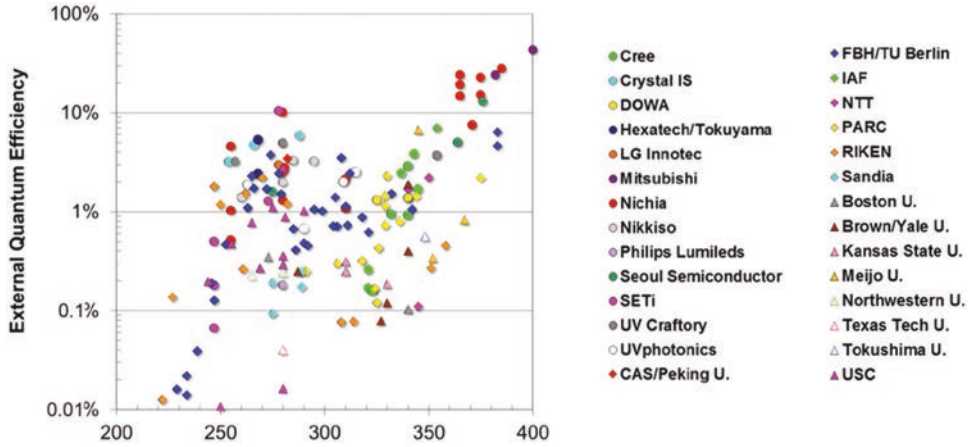


**Figure 18.** Reported external quantum efficiencies for AlGaN, InAlGaN, and InGaN quantum-well LEDs emitting in the UV spectral range.[263]

emitters and detectors, due to its chemical/physical robustness, potential for high temperature operation, ability to form heterostructures, and a direct bandgap over the entire alloy composition range.

#### *4.4.2. Narrowband Photons: Chemical Sensing and Quantum Information*

The dominant applications for which narrowband deep-UV photons are desirable are chemical sensing and quantum information. For chemical sensing, a deep-UV laser source would be highly desirable to enable point-of-need identification of bio-chemicals by Raman spectroscopy, which requires select wavelengths (<240 nm), high power, and high beam quality in a compact, rugged system. For quantum information, as discussed below in Section 4.5, narrowband laser photons enable the interrogation of quantum systems with very narrow transitions.

Two features are important for these applications.

The first feature is the emission of much shorter wavelengths than are currently possible. Attempts to realize electrically-pumped pn-junction diode lasers in the deep UV have been frustrated by materials, physics and device challenges similar to those faced by deep-UV LEDs: these are discussed below. To date, the shortest wavelength that has been achieved in an AlGaN-based diode laser is 336 nm.[264]

The second feature is, in some cases, ultra-narrow linewidths. These would require single-longitudinal-mode operation, and thus low-loss narrowband distributed Bragg reflectors (DBRs) for vertical-cavity devices or distributed feedback (DFB) gratings for horizontal (edge-emitting) devices. Fabrication of these will be challenging. The required pitch for a half-wavelength grating fabricated in AlN ($n$ = 2.32) at a wavelength of 275 nm, for example, is only 60 nm.

#### *4.4.3. AlGaN Materials, Physics and Device Challenges*

The materials, physics and device challenges associated with deep-UV LEDs and/or lasers are non-trivial. Because AlGaN semiconductors are the most mature of the UWBG semiconductors for these applications, we discuss them in some detail here. AlGaN semiconductors are far more challenging than their lower-bandgap InGaN and other counterparts used in visible/IR optoelectronics, though, in four key ways.

First, p-type dopants in AlGaN, typically Mg acceptors, present a number of difficulties. As has been discussed in Section 2.5, Mg acceptors in AlGaN are very deep, with ionization energies well over 150 meV, thus making p-doping, especially of high Al-content (x > 0.4) $Al_xGa_{1-x}N$, fairly difficult. Also, because of high UV optical absorption of p-AlGaN, light extraction and external quantum efficiency are decreased. Furthermore, because p-type doping concentrations are limited, cladding layers must be relatively thin to minimize series resistance, but then the optical confinement necessary for efficient laser diodes is poor. Therefore, the well-developed device designs commonly used for IR-visible lasers cannot be used. This has spurred interest in alternative semiconductor laser configurations, in particular approaches that can circumvent the need for p-doped AlGaN layers. For example, an alternative approach to edge-emitting laser diodes for deep-UV emission is the use of a vertical external cavity surface emitting laser with an AlGaN gain chip that is pumped with a high-energy electron beam; this architecture bypasses the p-doping issue and can realize high beam quality (spectrally and spatially).[41]

Second, in high-Al-content (x > 0.4) and highly-ionic $Al_xGa_{1-x}N$ materials, spontaneous and piezo-polarization fields are very high. This leads to a number of deleterious consequences, including a spatial separation in the electron and hole wave functions that decreases the electron-hole recombination rate.[265]

Third, electrically conducting and optically transparent substrates for the UWBG III-N materials are relatively immature. As discussed in Section 2.3, some progress has been made with $Ga_2O_3$ substrates.[122] Bulk AlN substrates, however, despite their insulating nature, are also a good potential technical choice, due to their high crystalline perfection for epitaxial growth. However, as discussed in Section 2.1, they are still in the developmental stage.

Fourth, for vertical light-emitting devices, a phenomenon called TE/TM polarization switching becomes important.

This phenomenon is due to a materials aspect of AlGaN that is not true of InGaN: GaN and AlN feature a different sign in their crystal field splitting. Whereas it is negative for AlN, it is positive for GaN, so the ordering of the valence bands differs between AlN and GaN. Thus, light generated within a GaN layer is predominantly TE polarized with an electric field vector E perpendicular to the c-direction, while light generated within an AlN layer is predominantly TM polarized with E parallel to the c-direction. For ternary AlGaN materials as used in UV light emitters, a transition from TE to TM polarization occurs as the Al concentration increases.[266] Since TM-polarized light cannot be extracted parallel to the c-direction (the most commonly used growth direction for III-N materials), the performance of vertically-emitting UV LEDs degrades as Al content increases and wavelength decreases. Vertically-emitting lasers would be similarly affected. Moreover, since TM-polarized light is generally not as tightly confined as TE-polarized light, TM optical modes interact more strongly with, and experience slightly higher optical absorption by, the p-type confinement layers in laser heterostructures. Thus, the performance of edge-emitting UV laser diodes would also be expected to experience performance degradation with TM optical modes.

Mitigating the issues listed above will not only lead to more efficient UV-C emitters and detectors, it will also improve UWBG RF and power electronic devices. Non-conventional doping schemes such as 3D superlattice doping and polarization-assisted doping can potentially be used to significantly increase the p-doping concentration in high-Al-content $Al_xGa_{1-x}N$ layers.[267] The issue of light extraction and hole transport might also be addressable through the use of interband tunnel junctions.[206] New device designs and material deposition approaches to manage the strain and polarization in UWBG heterostructures are also being explored with some initial success. To overcome the bulk AlN substrate issue, new approaches are needed to create thick and low-defect-density free-standing AlN substrates to replace inferior but readily available UV-C transparent substrates such as sapphire. These can also provide a very useful platform for systematic research.

Taken together, an overarching Research Opportunity/Challenge for UWBG optical emitters is:

20. Devices: LEDs with >10% wall-plug efficiency at wavelengths <260 nm; and compact laser sources in the UV-C and UV-B bands with power efficiency >10% and high beam quality.

### 4.5. Quantum Information

Quantum information science is a rapidly evolving global field of investigation with the potential to impact multiple technological areas, including: position determination, navigation and timing; tunnel detection; encryption code-breaking; secure communications; advanced simulation and high-speed computation; and magnetic anomaly detection.[268] UWBG semiconductors have potential roles in quantum information science in two substantial ways: as transparent hosts for dopants and defects with electronic/spin states suitable for quantum information processing; and as a photonic platform for quantum processors either based on linear optical quantum computation (LOQC) in which photons serve as the qubits, or for state manipulation in systems based on trapped-ion qubits.

#### *4.5.1. Host for Quantum States*

A first potential role for UWBG semiconductors is as the host for electronic/spin states sufficiently decoupled from the lattice to be long-lived and whose transitions are extremely sharp, yet able to be externally interrogated. Prototypical systems are the nitrogen-vacancy (N-V) or silicon-vacancy (Si-V) centers in diamond, which display long spin relaxation times and can be interrogated optically. These systems were among the first to be considered for quantum information, and continue to be an active area of research,[269] with new developments emerging, including the possibility of incorporating these centers into diamond devices where a gate bias controls the charge state of the center and affects its quantum characteristics.[115,270]

Note that here the challenges are very different from those mentioned in Section 2.5. There, the purpose of doping or defect incorporation is to create free carriers, and the depth of the defect levels in the UWBG semiconductors makes this challenging. In contrast, here one is intentionally interested in dopant and defect states that are deep in the bandgap and sufficiently decoupled from the host UWBG lattice so as to sustain long lifetimes, and thus minimize inhomogeneous broadening of their quantum states.

Also note that, while cubic (or at least covalent) materials are considered to be desirable because higher symmetry leads to better performance in nanodevices with respect to more light in the zero-phonon line, recent theoretical work on wurtzite AlN suggests that point-defect complexes could act as qubits and that manipulation of its piezoelectric properties through biaxial or uniaxial strain could enable nitrogen-vacancy centers as potential qubits.[271,272] Moreover, rare-earth ions (Nd) doped into AlN may also be a candidate for quantum memories. In this case, it is critical to control inhomogeneous broadening of the dominant rare-earth dopant optical transition, which can be aided by substitutional doping using plasma-assisted MBE, for which it has been shown that the vast majority of Nd dopants (>95%) take the majority site.[273]

Other possibilities for UWBG-semiconductor-based quantum information systems could involve valley-polarized electrons (i.e. "valleytronics") or superconductivity, both of which have been reported in diamond. The long electron lifetime for indirect-bandgap diamond, and the different effective mass for the different k-space propagation directions, can support changing the concentration of electrons in the six conduction band valleys.[274] With heavy B-doping, metallic conductivity can be achieved, and superconductivity has been established at temperatures near 11 K. There may be other structures that can achieve a superconducting state involving the diamond valence band electrons, as well.

#### *4.5.2. Photonic Platform for Interrogation of Quantum States*

A second potential role for UWBG semiconductors is as a photonic platform for the generation, manipulation, and

**Table 5.** Material and device parameters of interest for linear-optical quantum-computing (LOQC) architectures.

| Parameter | Reported/Demonstrated | | | Required Value |
|---|---|---|---|---|
| | Value | Wavelength [nm] | Material | |
| Optical Loss | 8 dB $cm^{-1}$[277] | 640 | $AlN/SiO_2$ | ≈2 dB $cm^{-1}$ |
| Linear Electro-Optic Coefficient | 0.7 pm $V^{-1}$[278] | 628 | $AlN/SiO_2$ | ≈1 pm $V^{-1}$ |
| Single-Photon Emission Efficiency | 72%[279] | 920 | GaAs/InAs | 99% |
| Maximum Quantum Emitter Count Rate | $4 \times 10^6$[280] | 625 | h-BN | – |
| Photodetector Detection Efficiency | 93%[281] | 1500 | WSi superconductor | 99% |
| Isotope Purity | 99.99%[282] | – | Diamond | 99.99% |

interrogation of quantum states. Indeed, all of the necessary photonic building blocks could potentially be based on UWBG semiconductors, and in particular on AlN/AlGaN: narrow-linewidth lasers, high single-photon-detection efficiency avalanche photodiodes, waveguides for photonic integrated circuits, and nonlinear optical media for wavelength conversion to spectral regions more suitable for low-loss transmission of photon-based quantum information (i.e., the 1300–1600 nm telecom band).

**Tables 5** and **6** contain the reported and desired values of a number of material and device parameters that are relevant to linear-optical and trapped-ion quantum-computing architectures. In LOQC systems,[275] the quantum information is represented by the states of single photons, and these states are manipulated by linear optical elements (e.g., beam splitters, phase shifters, and mirrors). In trapped-ion quantum processors, the quantum information is contained in the states of the ions,[276] and these states are typically initiated and read out by exciting each ion with lasers at a number of different wavelengths. We note that photon-based quantum information systems depend strongly on the transition wavelengths of the atoms or defect states used in these systems. Also note that the parameters shown in Tables 5 and 6 are representative of the values currently thought to be needed, but will certainly evolve in the future.

The tantalizing research opportunity/challenge here would be an integrated photonic platform containing all the building blocks necessary for the generation, manipulation, and interrogation of quantum states:

21. Devices: A photonic integrated circuit incorporating all the building blocks (e.g., UWBG lasers, AlN waveguides, AlGaN/SiC detectors) necessary for a single-chip quantum information processing system (based on trapped ions, neutral atoms, photons, or defect centers).

A first building block would be the narrow-linewidth (≈MHz to as small as <10 Hz) lasers necessary for manipulation of quantum systems such as trapped ions, as well as many other applications in atomic, molecular, and optical (AMO) physics, including laser cooling, optical trapping, atomic clocks, etc. These lasers need to be single-longitudinal-, single-transverse-mode with a range of powers from mWs (optical cycling through dipole transitions for laser cooling and fluorescence detection, as well as photoionization) to watts (Raman transitions for coherent gate operations involving multiple qubit gates). Some of the required lasers for trapped ions are in the ultraviolet—thus the importance of UWBG semiconductors, though frequency-multiplied optically pumped semiconductor lasers (OPSLs) are starting to find use here.[288] A potential candidate for the required lasers would be UWBG vertical-external-cavity surface-emitting lasers (VECSELs) with the power (watts) and narrow linewidths necessary to address the relevant transitions in ions.[288]

A second building block would be single-photon-counting detectors with high quantum efficiency (>70%) and concomitant high single-photon detection efficiency (>40%), required to work in conjunction with these lasers for both the optical cycling fluorescence measurements and the Bell state measurements required to verify entanglement of trapped ions. While previous work suggests that SiC may be capable of this performance in the UWBG 260–280 nm range,[289] hybrid(Al)GaN/SiC detectors that extend the high quantum efficiency of SiC to shorter wavelengths through mitigation of surface effects,[290] and to longer wavelengths through separate absorption and multiplication structures,[291] will likely also play a role.

**Table 6.** Material and device parameters of interest for trapped-ion quantum-computing architectures.

| Parameter | Reported/Demonstrated | | | Required Value |
|---|---|---|---|---|
| | Value | Wavelength [nm] | Material | |
| Single-mode Waveguide Optical Loss [dB $cm^{-1}$] | <0.2, 20[a]; 30[a] | 633–1092, 405; 405 | SiN; GaN | <1 at 370–1100 nm |
| Linear E-O Coefficient ($r_{13}$) [pm $V^{-1}$] | 1,[283] 10[284] | 633 | GaN, $LiNbO_3$ (bulk) | 10[b] at 400, 700 nm |
| Photodetector Detection Efficiency [%] | 30,[285] 93[281] | 422, 1550 | Si SPAD, WSi SNSPD | >90% at 422 nm |
| Waveguide Power Handling [dBm] | 33[286] | 1560 | SiN | 30–50 @ 400, 700 nm |
| Optical Amplifier Gain [dB] | 20–28[287] | 405 | GaN | 20–30, for monolithically integrated devices |

[a]Measurements at MIT Lincoln Laboratory, unpublished; [b]Assumes a 200 μm long modulator and desired $V_\pi = 10$ V.

A third building block would be optical waveguides having (i) low loss from UV to near-infrared (NIR) wavelengths, and (ii) large nonlinear optical properties to enable frequency conversion from the ultraviolet to the visible/NIR necessary to enable long-distance entanglement of quantum systems based on a trapped-ion platform (currently the most mature), in which state manipulation normally occurs in the UV. AlN is promising here, since it is both optically transparent and has relatively large nonlinear optical coefficients.[292] Combined with its potential for lasers and detectors, AlN may someday enable photonic integrated circuit platforms for quantum information processing, including those involving trapped ions.[293]

### 4.6. Extreme Environment

Extreme environment is another broad class of applications in which UWBG semiconductors can excel. Here, we discuss two broad sub-classes of these applications, in which the environments are extreme either because of the presence of radiation where radiation-hard electronics are necessary, or because of high temperature/pressure or corrosive chemistry where extreme environment sensors and electronics are necessary.

#### *4.6.1. Radiation-Hard Electronics*

Cross-cutting many of the technologies and applications already discussed, one great advantage WBG and UWBG technologies possess over silicon technologies is robustness in radiation environments. Applications requiring high-voltage, high-current, radiation-tolerant power devices include electronic thrust control actuators of rockets and missiles (as opposed to hydraulic control), and solar electric propulsion (SEP) of spacecraft. The SEP system envisioned by NASA would enable human exploration missions outside of earth's orbit, and requires functional power devices with high blocking voltages, high current capability, and high tolerance for radiation effects.[294] WBG and UWBG materials are also robust for high temperature operation, another advantage for space applications.

To date, almost all available commercial GaN power devices are not sufficiently rated for the high-voltage power conversion envisioned by NASA.[295] SiC MOSFETs meet the voltage requirement, but are susceptible to destructive events due to protons and heavy ions in space at a fraction of the maximum rated electrical voltage.[296] In fact, UWBG devices will be required in any application where both radiation hardness and high temperature operation are needed, because of the radiation vulnerability of SiC devices. A new generation of UWBG devices could be a critical enabling technology for the next generation of rockets, missiles, and spacecraft.

There are two main reasons for the radiation hardness of UWBG semiconductor technologies. First is their wider energy gap ($E_G$): this requires higher energy photons or ions transiting the material to achieve ionization of electrons and holes in the semiconductor. Second and just as important is the ability in some UWBG semiconductors to form heterostructures using two layers of materials with different bandgaps to create a region with a two-dimensional electron gas (2DEG), thereby forming a channel in a high electron mobility transistor (HEMT); the channel electron density in such structures is relatively insensitive to the impurity doping level, and hence is insensitive to deep levels due to radiation-induced displacement damage effects.

There are four basic kinds of semiconductor radiation effects, and, as illustrated in **Figure 19**, the heterostructure-based HEMT has an advantage over a silicon or silicon carbide MOSFET for each kind of radiation effect.

- *Total ionizing dose*: TID causes the accumulation of charge in a gate or field oxide resulting from photons or particles passing through the oxide, leading to shifts in threshold voltage or leakage current. RF HEMTs (though not necessarily

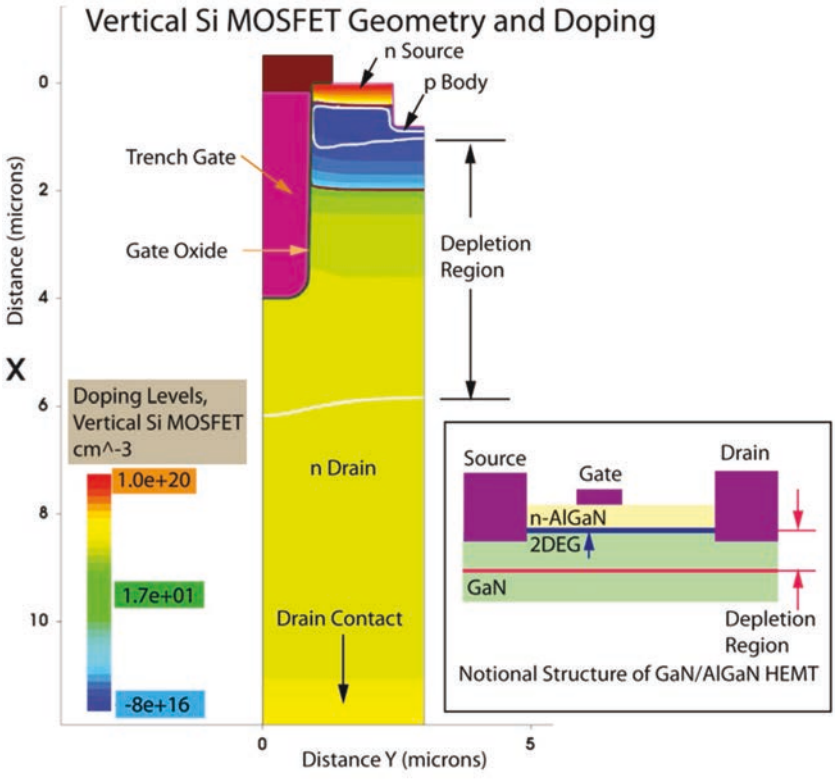


**Figure 19.** A trench-gate vertical silicon MOSFET (left) and a notional GaN HEMT (right), both biased in the off state with 100 V bias on the drain, approximately drawn to scale. Figure based on a Synopsys Sentaurus TCAD Simulation.[297,300]

power-switching HEMTs) typically have a Schottky metal gate, which eliminates most of the TID parameter shifts seen in MOSFETs.

- *Single event effects*: SEEs are caused by energetic ions passing through the semiconductor, depositing energy and creating electron-hole pairs (EHPs). The EHPs separate and drift or diffuse under the influence of an electric field or a concentration gradient, respectively. A HEMT typically has a much smaller depletion region (of order 1 micron for a drain voltage of 100 V) than Si or SiC MOSFETs for the same applied voltage (on the order of 5 microns for 100 V; see Figure 19). Consequently, less deposited charge is collected in the drain of the HEMT than in the drain of the MOSFET[297] for the same energy ion and transistor bias voltage.
- Similarly, *dose-rate* radiation effects sensitive to the entire volume of a device can be important. Since the HEMT has a smaller depletion region volume than the MOSFET, less charge is collected and the HEMT photocurrent is smaller, producing less disruption to the transistor behavior.
- The last radiation effect is *displacement damage*, in which particles such as neutrons or protons displace the semiconductor atoms from the crystalline lattice, creating traps and recombination sites in the device, or even new isotopes through fission of the original atoms in the lattice. The atom displacement increases scattering of charge carriers and reduces carrier mobility from the pre-irradiated state. Both SiC MOSFETs and GaN HEMTs have been shown to tolerate neutron or proton radiation to very high fluences,[298,299] much higher than Si MOSFETs.

Finally, there are two destructive effects that occur in Si MOSFETs that do not occur in HEMTs. *Single-event burnout* (SEB) occurs when the charge from an energetic ion creates sustained conduction of the parasitic bipolar transistor inherent in Si MOSFET design (this is an npn bipolar for an n-channel MOSFET; see Figure 19). The bipolar conduction can cause sufficient current to flow such that the device undergoes thermal damage or destruction. *Single-event gate rupture* (SEGR) occurs when charge build-up near the gate causes a breakdown in the gate oxide, resulting in gate current and the loss of electrostatic control of the Si MOSFET.

All of the above advantages of HEMTs apply to both the narrow- (InGaAs) and wide-bandgap (GaN) devices. However, the UWBG materials should improve the immunity of HEMT transistors to radiation significantly further due to their higher critical fields, which should result in smaller devices, thereby reducing the volume for collecting radiation-induced charge due to ions or photons in either single-event or dose-rate environments. Thus, we envision the following research opportunity/challenge:

22. Devices: UWBG power devices that exhibit essentially no performance degradation and no destructive single-event effects in radiation environments.

#### 4.6.2. Extreme-Environment Sensors/Electronics

Sensors efficiently gather data on the surrounding physical environment for enhanced safety, security and uninterrupted continuity of services, including those provided by critical infrastructure. Extreme environments include high temperature (350 °C to 1000 °C), high pressure (>1000 atmospheres), high shock (>1000 g), extreme mechanical vibration, high radiation (>100 Mrads), erosive flow, corrosive media, electrostatic discharge and electromagnetic interference. Such extreme conditions can destroy or degrade the performance of sensors, semiconductor electronics, dielectrics and interconnects, while also accelerating almost all aging and failure mechanisms that occur at room temperature, as well as introducing new ones.

As illustrated in **Figure 20**, traditional Si-based co-located sensors and electronics fall severely short in their performance under extreme conditions and fail to gather data on ambient conditions in systems such as the combustion chambers and exhaust systems of automotive or aviation engines, downhole environments in deep-well drilling, industrial processing plants, nuclear reactors, re-entry vehicles, and satellites in orbit. Sensing temperature, pressure, vibration, motion or distance at extreme temperatures, determining temperature and radioactivity in high radiation environments, measuring fluid levels and detecting gases and chemicals in high moisture and highly corrosive environments pose a number of challenges.

Unlike consumer electronic devices, which incorporate many sensors, microprocessors, and wireless chipsets, only

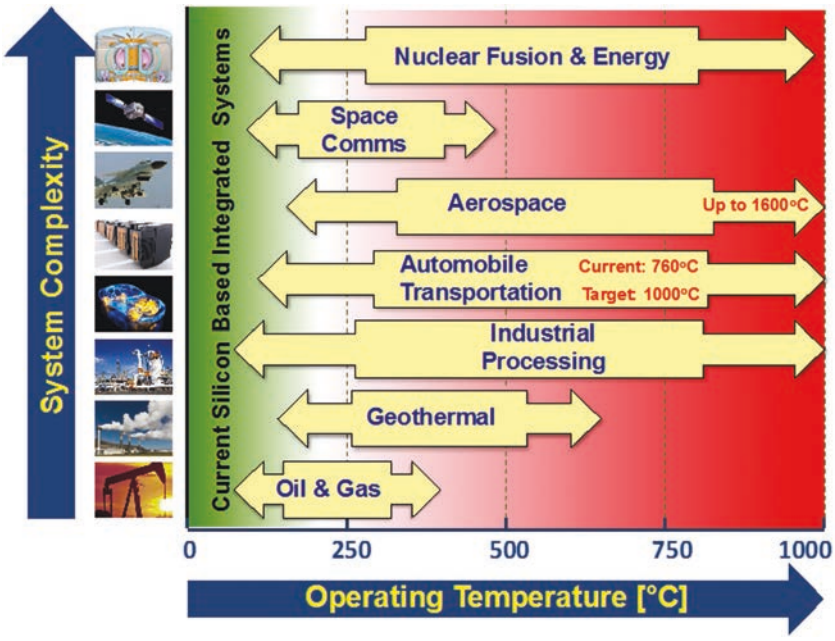


**Figure 20.** Industrial sectors in which extreme-environment sensor technologies are currently used. The technologies are organized by desired operating temperature and increasing sensing system complexity. Current silicon-based sensing systems can operate at a maximum temperature of ≈200 °C.

simple sensors are available for use in extreme environments. There are no microprocessors, wireless electronics or powering devices (batteries) suited for use at extreme temperatures (>250 °C). Today, active cooling is used in applications requiring sophisticated electronics in high temperature environments; however, active cooling is not feasible in applications where low-temperature ambient is not available (e.g., down-hole exploration or aircraft engines). In these cases, extended operation at high temperatures is required.

To extend operation to somewhat higher temperatures, silicon-on-insulator (SOI) enabled MOSFET electronics with improved off-state current have been demonstrated to operate at up to 300 °C. GaAs and its alloys, such as AlGaAs-based devices, were also demonstrated to operate beyond 300 °C, though with limited reliability.[301] Furthermore, electronics based on WBG materials such as SiC and GaN have been demonstrated to operate beyond 600 °C. However, the density of temperature-induced intrinsic carriers in these materials surpasses the concentration of dopant-induced carriers at these very high temperatures (beyond 800 °C for SiC and 1000 °C for GaN), degrading device performance.[301–305]

Thus, there is a strong incentive to develop UWBG technology for these extreme environments, perhaps able to withstand operating temperatures above 1000 °C. A first aspect of this technology is the sensors themselves, including (i) electrochemical, (ii) optical, (iii) mechanical (MEMS), and (iv) charged-particle-based sensors. These sensors might be discrete or might be integrated with other sensors for multi-component orthogonal sensing in environments that change quickly and contain a number of chemical or biological species.[306,307] A second aspect of this technology is electronics[308]—wireless data communication and power sources[306,309–315] that can be co-located with the sensors.

The challenges in building such integrated sensing/electronics systems are many. Materials-level challenges include material diffusion and intermetallic formation, and temperature-gradient-induced mechanical stress. Device-level challenges include high-performance contacts, interconnects, dielectrics, and encapsulation materials for extreme environments; controlled doping; complementary field-effect-transistors; and designs that are robust against imperfections (see e.g. Section 4.7). The hope is that new platforms based on lateral and vertical 1D,[307,316] 2D[317,318] or 3D[319] III-N structures will help in overcoming these challenges.

For example, MEMS sensors based on AlGaN can exploit the 2D electron gas (2DEG) that forms at an AlGaN/GaN heterojunction and that can act as a virtual metal electrode beneath an AlGaN MEMS resonator.[320,321] By employing recent advances in low-dimensional materials synthesis,[322] multiple analytes and physical state variables can be detected in an orthogonal fashion. Complementing electric-current-based transduction, charged particles generated by field emission and field ionization on ultra-sharp semiconductor tips or filaments can be superior transducers for fast, efficient and reliable sensing of gas, pressure, shock and vibration in extreme conditions.[323]

Beyond the integrated sensing/electronics system itself, power delivery to the system is also an important challenge. Present battery technology is limited to an operational temperature below 150 °C, and cabled-power wiring dramatically increases system weight and complexity making it impractical for many harsh environments. For these reasons, energy harvesting has emerged as a promising power source that can lead to an autonomous integrated sensing module with reduced cost.[324–326] To date, only a few energy harvesting devices for harsh environment applications have been reported using vibration[325,327] and UV.[326] AlN piezoelectric energy harvesters were demonstrated to deliver 80 μW at 300 °C.[325]

Of special interest are beta-voltaic (BV) and alpha-voltaic (AV) devices that efficiently convert radioactivity directly into electrical energy. These devices operate by the creation of electron-hole pairs in rectifying semiconductor junctions by high energy beta ($\beta$) and alpha ($\alpha$) particles, and thus generate power in a manner similar to a photovoltaic (PV) cell. When designed with UWBG materials, these power sources (with lifetimes ≈ 5 to 100 years) can offer high energy density, stability and very high durability to sensing systems in extreme environments (above 1000 °C[328]), providing a superior alternative to chemical batteries, fuel cells, super-capacitors, and radioisotope thermoelectric generators. Such sources can power wide-bandgap-based solid-state sensing electronics with capabilities for telemetry.

In this area, an overarching research opportunity/challenge is thus:

23. Devices: A new generation of extreme-environment sensors with co-located power and data processing electronics.

### 4.7. Processing, Modeling/Calibration, and Packaging

Though technically not a device or application area, here we discuss research opportunities and challenges associated with a key topic that cross-cuts all devices: how they are processed, modeled, calibrated, and ultimately packaged.

#### *4.7.1. Processing*

A number of challenges must be overcome if UWBG materials are to be effectively processed and integrated into working devices. In this subsection we discuss the most important process challenges, including doping (in particular selective area doping), Ohmic contacts, gate insulators, and integration. The overarching research opportunity/challenge is:

24. Devices: Development of an UWBG materials and device processing toolkit, including: selective area doping; low-resistance Ohmic contacts; and materials integration.

*Selective-Area Doping*: As discussed in Section 4.2, developing vertical device architectures in UWBG materials is critical to high-power electronics (HPE). In turn, such architectures depend on an effective means for lateral selective area doping. Such selective-area doping is required not only for effective edge termination, but also for the fabrication of most vertical device structures more complex than a simple pin or Schottky diode.

In the mature Si and SiC materials systems, ion implantation is used for lateral doping; indeed, the development of ion implantation for these materials was revolutionary. For compound semiconductor materials, including WBG GaN and

UWBG AlN, ion implantation is problematic, though there have been some recent promising reports for n-implantation of GaN coupled[329] with mixed reports for p-implantation (Mg) of GaN.[330] A major issue is that, after ion implantation, annealing of compound semiconductors requires second-nearest-neighbor (not just nearest-neighbor) re-ordering to heal the lattice damage caused by the implantation. This re-ordering requires relatively high annealing temperatures (relative to melting temperatures) that, at least for GaN, cause the problematic sublimation of N out of the crystal. The resulting residual defects, including localized stacking faults, can act as carrier traps,[331] effectively negating the implanted dopant. Note, though, that non-compound UWBG semiconductors such as diamond may not suffer as severely from this issue.

An alternative approach to ion implantation is etch-and-regrowth, where a region that would have been implanted is instead etched, and material of the opposite doping type is re-grown in the etched region. This approach likewise has had its share of difficulties. For example, in one instance researchers attempted to re-grow the channel on an etched current-blocking layer in a CAVET (see Figure 12), but crystalline defects formed near the top corner of the etched-out area.[217] Another example of problems with this approach is that material polarity may impact doping efficacy in regrown areas, as illustrated in **Figure 21**. Perhaps most importantly, re-grown pn junctions in GaN have thus far failed to exhibit the same electrical quality as in-situ grown junctions, as determined by junction leakage

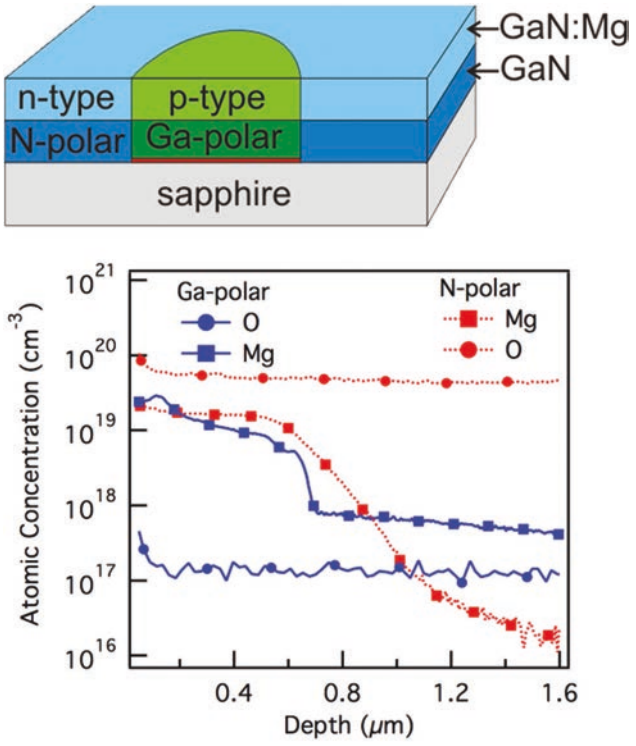


**Figure 21.** Top: Schematic of a lateral pn junction based on GaN doped with Mg. Bottom: SIMS data of O and Mg incorporation in the Ga-polar and N-polar GaN. Significantly more O is incorporated in the N-polar GaN,[332] illustrating how material polarity can affect dopant and impurity incorporation during growth. Reproduced with permission.[332] Copyright 2007, AIP Publishing.

current. Nonetheless, the demonstration of high-quality selective-area regrowth would be a major step towards realization of robust vertical devices in GaN as well as in UWBG semiconductors, in general.

Note that, in conjunction with selective-area regrowth, there are other options for doping within the regrowth areas. In polar materials such as AlGaN, compositional grading introduces a fixed polarization charge in the material, which in turn attracts free carriers from other parts of the structure (e.g., from surface states). This technique has in fact been demonstrated for AlGaN graded from 0–30% Al.[333] Another approach is to utilize a superlattice in which the polarization-induced electric fields cause ionization of the impurity dopants due to extreme band-bending.[334]

*Ohmic Contacts*: Ohmic contacts are another significant challenge for UWBG materials. In conventional semiconductors, Ohmic contacts are typically realized by metal–semiconductor junctions in which the potential barrier becomes very thin due to high doping in the semiconductor, and is thus conducive to tunneling. However, as we have seen, achieving high levels of doping in UWBG semiconductors is problematic. Further, due to the wide bandgap and lower electron affinity of UWBG materials, the Schottky barrier heights of common metals such as Pt and Ni are very high (>2 eV),[31,335] resulting in high specific contact resistivity. For AlGaN with 40–60% Al content, specific contact resistivities are typically in the $10^{-2}$ to $10^{-1}$ Ω cm$^2$ range, while by contrast Ohmic contacts to conventional WBG AlGaN/GaN HEMTs are routinely in the $10^{-6}$ Ω cm$^2$ range.[336,337] Exotic metallizations, such as vanadium, have been reported to have specific contact resistivity in the $10^{-6}$ Ω cm$^2$ range for AlGaN up to 70% Al composition, but the resistivity rapidly increases for still-higher Al compositions, peaking around 100 Ω cm$^2$ for AlN.

For the nitrides, once again compositional grading may come to the rescue; here the composition is graded from high-Al-content for the active region of the device down to low-Al-content AlGaN, or even GaN, onto which Ohmic metallization may readily be achieved. This approach has in fact achieved Ohmic contacts with specific contact resistivity in the low $10^{-6}$ Ω cm$^2$ range to devices with $Al_{0.75}Ga_{0.25}N$ channels.[338,339]

For UWBG materials for which compositional grading is not possible, metals with a low Schottky barrier height to the semiconductor of interest should be explored, and methods to achieve high doping, as outlined above, should be investigated in parallel.

*Integration*: Finally, as discussed in Section 3.3, integration of UWBG semiconductor materials will likely be important for optimization of combined thermal and electronic properties. Certainly there has been a significant effort to take advantage of the high thermal conductivity of diamond for high-power GaN HEMT RF devices. There is also a potential advantage to integrating GaN electron devices with diamond-based hole devices. This could be extended to diamond electronics and nitride optoelectronics that are monolithically integrated on the same chip. Such monolithic integration of diamond and III-N materials could potentially be enabled by using epitaxial cubic BN as an intermediary. While there is a large lattice mismatch between c-BN and AlN, the c-BN/AlN interface could exhibit chemical stability and support efficient thermal transport, and

the epitaxial c-BN/diamond interface might also effectively transfer thermal energy between the layers.

In general, vertical epitaxial heterostructures have proved crucial for compound semiconductor (including current WBG III-N) devices. Such heterostructures will almost certainly be important for UWBG devices as well, if they can be developed. It is easy to imagine these in the AlGaN/AlN system, but they could be just as important in more novel systems such as epitaxial diamond/c-BN and $Ga_2O_3/Al_2O_3$ heterostructures.

#### 4.7.2. Modeling/Calibration

Device-level technology computer-aided design (TCAD) based finite-element models (such as was used to create Figure 19) are commonly used to solve the coupled equations for carrier transport, heat transport, electrostatics (Poisson's equation), and trap occupation statistics to predict steady-state or transient spatial distributions of temperature, electric field, free carriers, and more. Such models, properly built and validated, can be used to understand how variations in device layout, doping concentration in various regions, and various other engineered parameters, determine measurable quantities such as transistor gain, switching speed, optical device efficiency, etc., as well as difficult-to-ascertain quantities such as internal electric field in a power switch, peak temperature within a power device, or the fast transient evolution of an event such as a heavy ion strike in a space application.

TCAD models are thus a critical interface between our basic scientific understanding of materials and physics, on the one hand, and the technological performance of the device, on the other. Developing UWBG TCAD will be a critical step towards informing when scientific understanding is correct (when device performance can be predicted) and towards enabling technological performance to be explored and optimized more efficiently than by trial-and-error experiment.

En route to developing UWBG TCAD, however, there are a number of challenges. These include: understanding how to best extend legacy TCAD to UWBG devices while retaining the physical validity developed for narrower-gap semiconductors; understanding how to calibrate TCAD models under the more extreme conditions experienced by UWBG devices; and understanding and incorporating new physics associated with UWBG devices.

*UWBG TCAD: Borrowing from Legacy TCAD*: TCAD is most mature for silicon devices, as silicon is both the best understood semiconductor and has been the dominant driver for such modeling since its infancy. Much can be borrowed from this legacy silicon TCAD, but there are significant challenges. Care must be taken not to borrow "default" physical mechanisms from silicon that are irrelevant for the UWBG materials in question, or that are extrapolated beyond the range (i.e., high temperatures or high electric fields) that legacy semiconducting materials support.

A first consideration for appropriate use of legacy TCAD is associated with the unphysically small theoretical intrinsic and minority-carrier concentrations in WBG/UWBG semiconductors. In conventional intrinsic semiconductors like silicon, free-electron and -hole concentrations are roughly $10^{10}$ $cm^{-3}$ at room temperature. In UWBG materials, Fermi–Dirac statistics predict they are theoretically $10^{-10}$ $cm^{-3}$ or less for intrinsic material, a concentration that has no direct physical meaning. The time-averaged carrier concentration will always be orders of magnitude greater. The physical origin of this discrepancy is that Fermi–Dirac statistics are based on the assumption that the free carriers are from the high energy tail of a thermal distribution,[340] leading to a prediction of an infinitesimal density several electron-volts from the band edge in question.

This is important because TCAD models often use free-carrier density or current(s) when solving for trap occupation statistics, steady-state potential in floating body regions or floating electrical contacts, and more. This can cause instability in the TCAD simulation's internal convergence or in the outputs, leading to long run times, or worse an incorrect understanding of the problem. Troubleshooting can include looking for unexpected sensitivity to a physically negligible source of minority carriers (such as above-bandgap photons), impact of grounding floating regions, artificially raising the ambient temperature, and unexpected sensitivity to physically negligible density of traps and/or dopants in the semiconducting materials. Naturally, it is important to solve a convergence or other model execution problem in a physically valid way.

A second consideration for legacy TCAD re-use is related to this first one. Many technologically important traps (such as are used to make material semi-insulating) are electron-volts deep in the bandgap. Classic Fermi–Dirac statistics can lead to semi-infinite times necessary to reach steady-state when modeling trap occupation at room temperature. Additionally, care must be taken when modeling, as very small modeled free-carrier current(s) can determine the occupation levels of these traps. When there are traps deep within a semi-insulating region (such as a WBG/UWBG substrate), trap occupation set through drift-diffusion carrier transport can be far different than that set through a hot-carrier transport model. Additionally, surfaces may have far more conductivity than the bulk, and defects may dominate the current flow mechanism (e.g., trap-to-trap hopping conduction).[341,342]

A third legacy consideration is associated with the much higher internal electric fields supported by UWBG materials. Breakdown by other mechanisms is likely to occur before conventional impact-ionization-driven avalanche breakdown. In GaN, noise in the gate current is often seen preceding breakdown, which typically happens in the gate dielectric.[343,344] This means in practice that other breakdown mechanisms may need to be simulated within the semiconductor, in a dielectric layer, or even in the surrounding air, for insufficiently passivated devices.

A fourth legacy consideration is the sheer range of values (in temperature, electric field, etc.) that are experienced in UWBG devices. In practice, commercial TCAD packages typically require that physical properties be fitted to parametrized polynomials, spline fits, power laws, or similar. Some TCAD packages are restrictive as to the type of function and number of fitting parameters that can be used. As a specific example, a power law fit may be possible with acceptable accuracy for thermal conductivity from 300–500 K but not 300–700 K. Thus, the quality of the fit of the physical properties to the desired function may deteriorate considerably. This is a seemingly

mundane but very easily overlooked consideration when applied over these wide physical ranges.

*UWBG TCAD: Calibration under Extreme Conditions*: All TCAD models must be calibrated through experimental determination of their materials, physics, and device parameters via specialized test structures. Calibration of UWBG TCAD models faces some additional challenges.

A first calibration challenge is the critical electric field (or equivalently the electron and hole ionization coefficients) for breakdown. Extracting this critical field from a working power device is problematic, due to the possibility of premature breakdown associated with imperfect edge terminations—a possibility made more likely by the very high voltages enabled by UWBG semiconductors. Instead, it may be necessary to use specially designed avalanche-photodetector-like structures, in which the multiplication coefficient is used to extract either the electron or hole ionization coefficient. The difficulty will be to ensure that the multiplication process is initiated by only one type of carrier.

A second calibration challenge is associated with the much smaller physical size of UWBG devices enabled by the higher electric fields they can sustain. As physical size decreases, internal gradients in voltage and temperature increase, and direct spatially resolved measurements of these become problematic. For example, the spatial resolution of any optical technique for local temperature measurement may become diffraction-limited. Thus, a technique that in a large device would be sufficient to measure a single "point" temperature might now measure a weighted average over a non-negligible volume.

A third calibration challenge is associated with determining the electronic properties of defects, both bulk and interfacial. This can be problematic even for WBG materials, and is likely to be much more so for UWBG materials. For example, defect states in UWBG materials can be very deep in the gap, leading to excessively long carrier emission times, rendering techniques based on thermal emission of carriers such as deep-level transient spectroscopy (DLTS) ineffective. This makes it necessary to use less-common techniques such as deep-level optical spectroscopy (DLOS, which uses light instead of temperature to empty very deep traps).[345] Similarly, standard techniques used to characterize the defect density at semiconductor–insulator interfaces, such as the conductance technique, may underestimate the density of traps due to long time constants; DLOS-like techniques may also be needed here.[346] In general, great care must be taken in interpreting experimental results on UWBG semiconductors, since the assumptions typically made in characterization experiments on conventional semiconductor materials (e.g., complete ionization of dopants) may very well prove to be untrue.

A fourth calibration challenge is the immaturity of synthesis and processing, leading to parameters which are less "fundamental" or intrinsic, but rather depend on materials variation or defects. Moreover, the materials can evolve (degrade) over time: physically smaller devices driven very hard imply steeper temperature gradients and higher electric fields, both of which can drive atomic diffusion, re-structuring, and even local melting.[347] There is also an opportunity here: if these material variations can be parametrized and folded into TCAD models, then subtle aspects of device performance might be used to infer and control material variations during synthesis and processing.

*UWBG TCAD: New Physics*: All TCAD models require parameterized descriptions of the important physical effects, most commonly partial differential equations that can be discretized over a mesh representing the physical structure. Some physical mechanisms will require considerable work to put into the right functional form. As an example, electron mobility is fundamentally described by physics at the atomic level. The TCAD model will typically require this to be distilled to a function of local electric field, local lattice temperature, and local dopant concentration that can be applied at any point in a meshed structure.

As discussed in Section 3, however, UWBG materials and devices will push extreme and unexplored physics regimes, and will stress our existing understanding of physics. Understanding the new physics, then distilling that physics into parameterized models is thus a particularly key research opportunity/challenge:

25. Devices: Incorporation of emerging UWBG physics into parameterized TCAD models that can then be used to validate the physics as well as to catalyze new device architectures.

A first new physics challenge is associated with multi-event effects. For example, a hot electron degradation process involving two hot electrons will scale differently than if one electron supplies the energy. This has been seen in silicon,[348] and the likelihood of multi-event effects such as this increases as the densities of hot electrons, energetic phonons, etc. increase and as the energy supplied by a single electron-hole recombination event or a carrier dropping into a deep trap increases.

A second new physics challenge is associated with multi-physics effects. As a concrete example, if an UWBG material sustains a voltage gradient of 5 MV $cm^{-1}$ in a location containing a charged defect, the defect will experience an electric field of 0.5 V $nm^{-1}$, which may alter the activation energy barrier to defect diffusion and reorganization (especially for multiply charged defects). Additionally, high fields are seen to drive electrochemical reactions.[349,350] Likewise, high temperatures and mechanical stresses, as well as gradients in these, will influence atomic processes.

A third new physics challenge is associated with non-equilibrium effects. Even basic concepts such as temperature may need revisiting. For example, GaN can sustain high enough power density that the density of optical phonons is no longer at equilibrium with the lattice temperature,[351] and this is likely to be even more pronounced for UWBG semiconductors. Where temperature is important to a modeled physical effect, the "correct" temperature can depend on the nature of the physical interaction. This will be especially critical for slow effects critical to understanding degradation and failure processes. Statistical thermodynamic assumptions underpin models of reaction kinetics, diffusion, defect formation and concentration, and more. This challenge needs work early because findings will influence other characterization and modeling efforts, including atomistic efforts usually considered the "starting points."

*4.7.3. Packaging*

In order to fully realize the potential of UWBG materials and devices, packaging technology must advance to enable envisioned high-temperature, high-voltage, and high-frequency applications. In particular, packaging technology with suitable material, thermal, and electrical properties must be developed before UWBG devices can be incorporated into high-performance systems. Many of the challenges are similar to those facing packaging researchers working with GaN and SiC devices, but with even more stringent requirements for temperature and electrical performance.

The operating temperatures of UWBG devices will surpass those that can be accommodated by conventional packaging materials, necessitating a transition to entirely new packaging materials and techniques. It is critical that all materials used in the package can withstand the increased operating temperature, and it is highly desirable that the complete package have high thermal conductivity for effective heat removal. Another critical packaging feature is the coefficient of thermal expansion (CTE) of the materials that are used to attach the die to the package, as well as to protect the device (encapsulation, molding, passivation). In particular, in pulsed power applications the wide temperature operating range makes good CTE matching critical to avoid component failures due to thermally-induced cracks in the die itself or at various interfaces. Conventional encapsulants are designed mainly for applications below 175 °C, and existing commercial high-temperature encapsulants show significant degradation in both mechanical properties (e.g., cracking) and electrical performance (e.g., dielectric strength) when operating at 250 °C.[352] New materials and encapsulation techniques must thus be explored and developed to enable such high-temperature operation.

In addition to more challenging thermal environments, UWBG devices will also require packages with improved electrical characteristics. The combination of increased voltage, power, and device switching frequency in UWBG devices leads to greatly increased switch transition speeds, where the rate of change of current ($di/dt$) and voltage ($dv/dt$) represents a formidable packaging challenge. Specifically, parasitic current loop inductances must be minimized to avoid excessive ringing during switch transitions, which can damage the device. Here, traditional wire-bond technology will likely not suffice, and more advanced die-attach methods such as wire-bond-less direct solder attachment[353] or flip-chip techniques will be required.

In high-frequency power electronics systems, the most effective way to reduce interconnect parasitics is to place switching devices and gate-drive circuitry as close to each other as possible. This is particularly important for high $dv/dt$ transitions, where the parasitic gate-drain capacitance can lead to spurious device turn-on if the parasitic gate resistance and inductance are too high. An effective method to mitigate this is through the development of integrated switching cells, where the gate drivers and one or more switching devices are placed in close proximity to reduce parasitic inductance. An example of such an integrated s witching cell, with carefully controlled impedance to minimize ringing, is shown in **Figure 22**. Here, four GaN devices, two gate drive ICs, and local decoupling capacitors were integrated onto the same substrate to achieve a high level of integration in a 2 kW inverter prototype[354] with excellent results.

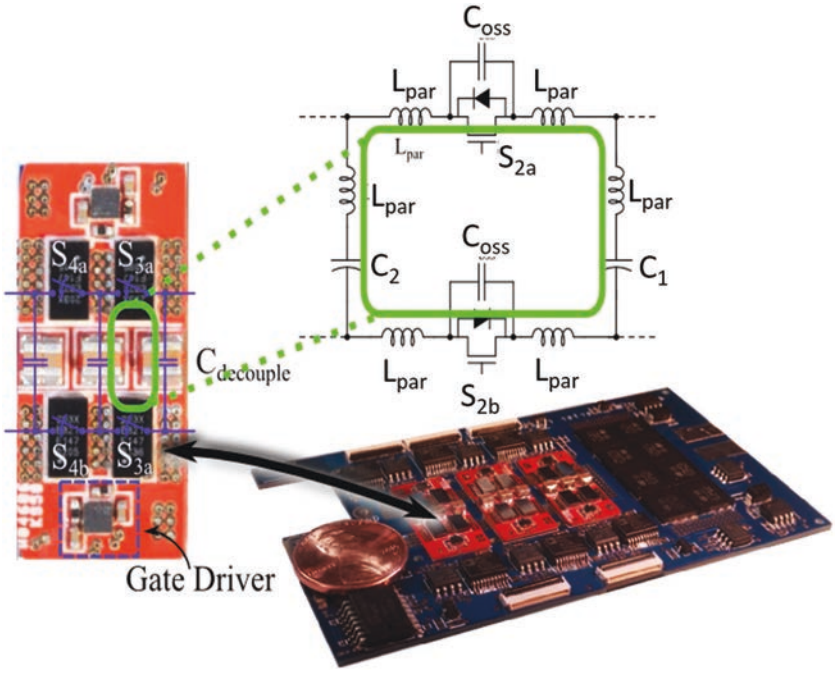


**Figure 22.** Example of an integrated switching cell used to reduce the inductive loops in the commutation of GaN devices. At the high $di/dt$ and $dv/dt$ transition transients encountered in UWBG devices, tight integration between power devices and gate drive circuitry will be critical to ensure high performance and reliability.

While integration of the gate driver, control, and sensing on the same die as the main power transistor yields the smallest parasitic interconnection, this level of integration is challenging in practice. Owing to the different material requirements of kV-scale voltage stand-off for the main power switch, and the low (typically <15 V) voltage levels of sensing and control, practical solutions to date have placed these functions on separate chips in a multi-chip module (MCM). As is the case for GaN and SiC devices, future packaging solutions will likely benefit from 3D stacked die power modules for UWBG applications, which can reduce interconnect inductance through out-of-plane connections. A key research challenge/opportunity is:

26. Devices: New packaging materials and low-inductance interconnects compatible with high-temperature, high-voltage and high-$dv/dt$ operation.

## 5. List of Research Opportunities/Challenges

1. Materials: Large (>5 cm) diameter single-crystal AlN substrates with low (<$10^4$ $cm^{-2}$) dislocation densities and negligible bowing (radius of curvature >30 m).

2. Materials: A predictive vapor-surface-film thermodynamic/kinetic framework for the atomic-scale co-evolution of morphology and composition during AlGaN heteroepitaxy.
3. Materials: A complete set of synthesis and processing tools for control of substrate diameter, defects, doping, carrier confinement, contacts, and heterostructures in diamond-based materials.
4. Materials: Novel synthesis, processing, and architectural routes for circumventing the low thermal conductivity of $Ga_2O_3$.
5. Materials: Exploration of novel UWBG materials (beyond AlN/AlGaN, diamond, and $\beta$-$Ga_2O_3$), including h-BN for 2D devices, wz-BN as an AlGaInN-alloying heterostructure-enabling material, and c-BN as a heterostructure with diamond and as a stand-alone material.
6. Materials: A first-principles theory of doping in UWBG semiconductors in conjunction with new synthesis and doping approaches (e.g., based on broken symmetries at surfaces and hetero-interfaces) that enables improved understanding and control of conventional doping methods.
7. Physics: Exploration of extreme high-field and non-equilibrium physics regimes opened up by UWBG semiconductors—regimes that will likely lead to re-evaluation of standard models for the fundamental properties of, and interactions between, the various carriers of energy (electrons, holes, phonons and photons).
8. Physics: A comprehensive understanding of the carrier and lattice dynamics underlying electron and hole transport—at low and high fields and in the breakdown regime—across the range of polar and non-polar UWBG semiconductors.
9. Physics: New theoretical descriptions and models of high-energy carrier transport and avalanche breakdown in UWBG materials, coupled with experimental verification.
10. Physics: Exploration of the physics of carrier confinement under extreme conditions (e.g., ultrathin heterostructures whose confinement requires UWBG semiconductors).
11. Physics: High-k, ultrawide-bandgap dielectrics with low-interface-state-density interfaces to UWBG semiconductors.
12. Physics: New techniques for monitoring space- and time-varying temperature profiles, and for modeling and co-designing devices for combined electrical and thermal performance.
13. Devices: Normally-off vertical power switches that combine ultra-high breakdown voltages with ultra-low on-resistance.
14. Devices: Photoconductive UWBG-semiconductor switches for pulsed-power applications.
15. Devices: New dielectric and magnetic materials and architectures that enable high-frequency ultra-compact integrated passive elements, which in turn enable system performance not limited by performance of those passive elements.
16. Devices: Thermally managed UWBG RF transistors that generate higher output powers and power densities than present Si-, III-V-, SiC-, and GaN-based devices.
17. Devices: High-voltage, low-capacitance, low-on-resistance UWBG RF switches having the ability to stand off voltages higher than those generated by UWBG power transistors.
18. Devices: Single-crystal AlGaN and AlN electromechanical RF filters with very high bandwidth and power-handling capability, small size and weight, and potential for monolithic integration with AlGaN electronics.
19. Devices: Negative-electron-affinity and/or ultra-low-work-function surfaces for robust, high electron-emission efficiency cold cathodes and/or electron collector surfaces.
20. Devices: LEDs with >10% wall-plug efficiency at wavelengths <260 nm; and compact laser sources in the UV-C and UV-B bands with power efficiency >10% and high beam quality.
21. Devices: A photonic integrated circuit incorporating all the building blocks (e.g., UWBG lasers, AlN waveguides, AlGaN/SiC detectors) necessary for a single-chip quantum information processing system (based on trapped ions, neutral atoms, photons, or defect centers).
22. Devices: UWBG power devices that exhibit essentially no performance degradation and no destructive single-event effects in radiation environments.
23. Devices: A new generation of extreme-environment sensors with co-located power and data processing electronics.
24. Devices: Development of an UWBG material and device processing toolkit, including: selective-area doping; low-resistance Ohmic contacts; and materials integration.
25. Devices: Incorporation of emerging UWBG physics into parameterized TCAD models that can then be used to validate the physics as well as to catalyze new device architectures.
26. Devices: New packaging materials and low-inductance interconnects compatible with high-temperature, high-voltage and high-d$v$/d$t$ operation.

## Acknowledgements

We acknowledge support from the National Science Foundation (NSF, Dimitris Pavlidis), the Army Research Office (ARO, Joe Qiu), the Air Force Office of Scientific Research (AFOSR, Ken Goretta), and Sandia National Laboratories (SNL, Olga Spahn). Financial and logistical support was provided by NSF (Workshop Award No. ECCS-1641056) and AFOSR. We thank the staff at the Basic Research Innovation and Collaboration Center/Virginia Tech Applied Research Corporation for hosting the workshop. We thank, at Sandia: Clare Amann for superb technical editing support, and Alyssa Kolski and Lauren Manzanares for workshop logistic support. We thank Gregg Jessen (Air Force Research Laboratory/RYDD), David Meyer (Naval Research Laboratory) and Baxter Moody (Hexatech Inc.) for help with the materials and properties tables, and B. Jayant Baliga (North Carolina State University) for helpful tips on breakdown data for SiC and GaN. Chris Van de Walle acknowledges support by NSF under grant No. DMR-1434854.

We gratefully acknowledge all of the participants of the April 24–25, 2016 workshop held in Arlington, VA: Carol Adkins, Sandia National Laboratories; Anant Agarwal, DOE EERE; Andrew Allerman, Sandia National Laboratories; Travis Anderson, Naval Research Laboratory; Andy Armstrong, Sandia National Laboratories; Enrico Bellotti, Boston University; John Belvins, Air Force Research Laboratory; Karim Boutros, STMicroelectronics; Sukwon Choi, Pennsylvania State University; Srabanti Chowdhury, University of California, Davis; Aris Christou, University of Maryland; Alyssa Kolski, Sandia National Laboratories; Marty Chumbes, Raytheon Corporation; Robert Coffie, RLC Solutions; Ramon Collazo, North Carolina State University; Sarit Dhar, Auburn University; Don Dorsey, Air Force Research Laboratory; Samir El-Ghazaly, National Science Foundation; Mark Goorsky, University of California, Los Angeles; Kenneth Goretta, Air Force Office of Scientific Research; Samuel Graham, Georgia Institute of Technology; Dan Green, DARPA/MTO; Timothy Grotjohn, Michigan State University; Eric Heller, Air Force Research Laboratory; Asegun Henry, Georgia Institute of Technology; Masataka Higashiwaki, National Institute of Information and Communications Technology; Karl Hobart, Naval Research Laboratory; Mark Hollis, MIT

 

Lincoln Laboratory; Jinwoo Hwang, Ohio State University; Debdeep Jena, Cornell University; Gregg Jessen, Air Force Research Laboratory/RYDD; Noble Johnson, PARC; Ken Jones, Army Research Laboratory/SEDD; Bob Kaplar, Sandia National Laboratories; Asif Khan, University of South Carolina; Jacob Khurgin, Johns Hopkins University; Manos Kioupakis, University of Michigan; Isik Kizilyalli, DOE ARPA-E; Andrew Koehler, Naval Research Laboratory; Fritz Kub, Naval Research Laboratory; Marcelo Kuroda, Auburn University; Jeff LaRoche, Raytheon Corporation; Jacob Leach, Kyma Technologies, Inc.; Aivars Lelis, Army Research Laboratory; Pat Lenahan, Pennsylvania State University; Lauren Manzanares, Sandia National Laboratories; Kaiser Matin, DARPA/MTO; David Meyer, Naval Research Laboratory; Umesh Mishra, University of California, Santa Barbara; Suzanne Mohney, Pennsylvania State University; Baxter Moody, Hexatech Inc.; Shin Mou, Air Force Research Laboratory; Robert Nemanich, Arizona State University; Rebecca Nikolic, Lawrence Livermore National Laboratory; Tomas Palacios, Massachusetts Institute of Technology; Dimitris Pavlidis, National Science Foundation; Lynn Petersen, Office of Naval Research; Robert Pilawa, University of Illinois, Urbana-Champaign; Matthew Porter, Naval Postgraduate School; Q Joe Qiu, Army Research Office; Siddharth Rajan, Ohio State University; Steve Ringel, Ohio State University; Ali Sayir, Air Force Office of Scientific Research; John Schlueter, National Science Foundation; Max Shatalov, Sensor Electronic Technology, Inc.; Jerry Simmons, Sandia National Laboratories; Zlatko Sitar, North Carolina State University; Jim Speck, University of California, Santa Barbara; Marko Tadjer, Naval Research Laboratory; Daren Thomson, Air Force Research Laboratory/RYDH; Randy Tompkins, Army Research Laboratory; Jeff Tsao, Sandia National Laboratories; Chris Van de Walle, University of California, Santa Barbara; Todd Weatherford, Naval Postgraduate School; Jonathan Wierer, Lehigh University; Jim Will, DOE, NNSA's National Security Campus, Kansas City; Arthur Witluski, Institute for Space & Defense Electronics-Vanderbilt; Mike Wraback, Army Research Laboratory; Hongping Zhao, Case Western Reserve University.

This work was partially supported by the Laboratory Directed Research and Development Program at Sandia National Laboratories, a multi-mission laboratory managed and operated by National Technology and Engineering Solutions of Sandia, LLC, a wholly owned subsidiary of Honeywell International, Inc., for the United States Department of Energy's National Nuclear Security Administration under Contract No. DE-NA-0003525. This material is based upon work supported by the Assistant Secretary of Defense for Research and Engineering under Air Force Contract No. FA8721-05-C-0002 and/or FA8702-15-D-0001 at MIT Lincoln Laboratory. Any opinions, findings, conclusions or recommendations expressed in this material are those of the author(s) and do not necessarily reflect the views of the Assistant Secretary of Defense for Research and Engineering.

## Conflict of Interest

The authors declare no conflict of interest.

## Keywords

aluminum nitride, boron nitride, diamond, extreme environments, gallium oxide, power electronics, ultrawide bandgaps, UV-C

Received: November 16, 2016
Revised: February 24, 2017
Published online: December 4, 2017

[1] M. Riordan, L. Hoddeson, C. Herring, *Rev. Mod. Phys.* **1999**, *71*, S336.
[2] Semiconductor market breakdown and 2016 forecasts, http://www.eetimes.com/document.asp?doc_id=1329282 (accessed: July 2017).
[3] H. Kroemer, *Rev. Mod. Phys.* **2001**, *73*, 783.
[4] H. Störmer, R. Dingle, A. Gossard, W. Wiegmann, M. Sturge, *Solid State Commun.* **1979**, *29*, 705.
[5] H. Morkoc, P. M. Solomon, *IEEE Spectrum* **1984**, *21*, 28.
[6] J. Rosenberg, M. Benlamri, P. Kirchner, J. Woodall, G. Pettit, *IEEE Electron Device Lett.* **1985**, *6*, 491.
[7] J. C. Zolper, presented at *A DARPA Perspective on the Future of Electronics*, Scottsdale AZ, **2003**.
[8] R. D. Dupuis, *IEEE J. Quantum Electron.* **1987**, *23*, 651.
[9] J. Y. Tsao, J. Han, R. H. Haitz, P. M. Pattison, *Ann. Phys.* **2015**, *527*, A53.
[10] S. Nakamura, M. R. Krames, *Proc. IEEE* **2013**, *101*, 2211.
[11] J. Brodrick, *J. Disp. Technol.* **2007**, *3*, 91.
[12] U.S. Department of Energy, Solid-State Lighting, https://energy.gov/eere/ssl/solid-state-lighting (accessed: January 2017).
[13] U.S. Department of Energy, Energy Frontier Research Centers (EFRCs), https://science.energy.gov/bes/efrc/ (accessed: January 2017).
[14] R. Haitz, J. Y. Tsao, *Phys. Status Solidi A* **2011**, *208*, 17.
[15] J. Y. Tsao, M. H. Crawford, M. E. Coltrin, A. J. Fischer, D. D. Koleske, G. S. Subramania, G. T. Wang, J. J. Wierer, R. F. Karlicek, *Adv. Opt. Mater.* **2014**, *2*, 809.
[16] M. R. Krames, O. B. Shchekin, R. Mueller-Mach, G. O. Mueller, L. Zhou, G. Harbers, M. G. Craford, *J. Disp. Technol.* **2007**, *3*, 160.
[17] M. N. Yoder, *IEEE Trans. Electron Devices* **1996**, *43*, 1633.
[18] M. A. Khan, A. Bhattarai, J. Kuznia, D. Olson, *Appl. Phys. Lett.* **1993**, *63*, 1214.
[19] ATMI Awarded $9.46 Million For GaN Research, https://compoundsemiconductor.net/article/82019-atmi-awarded-9.46-million-for-gan-research.html (accessed: July 2017).
[20] K. Chu, P. Chao, J. Windyka, *Int. J. High Speed Electron. Syst.* **2004**, *14*, 738.
[21] Market for GaN and SiC power semiconductors to top $1B in 2020, http://electroiq.com/blog/2016/03/market-for-gan-and-sic-power-semiconductors-to-top-1b-in-2020/ (accessed: July 2017).
[22] B. Baliga, *J. Appl. Phys.* **1982**, *53*, 1759.
[23] E. Johnson, *RCA Rev.* **1965**, *26*, 163.
[24] T. Chu, R. Kelm, *J. Electrochem. Soc.* **1975**, *122*, 995.
[25] R. Collazo, S. Mita, J. Xie, A. Rice, J. Tweedie, R. Dalmau, Z. Sitar, *Phys. Status Solidi C* **2011**, *8*, 2031.
[26] Q. Guo, A. Yoshida, *Jpn. J. Appl. Phys.* **1994**, *33*, 2453.
[27] F. Kaess, S. Mita, J. Xie, P. Reddy, A. Klump, L. H. Hernandez-Balderrama, S. Washiyama, A. Franke, R. Kirste, A. Hoffmann, *J. Appl. Phys.* **2016**, *120*, 105701.
[28] I. C. Kizilyalli, A. P. Edwards, H. Nie, D. Disney, D. Bour, *IEEE Trans. Electron Devices* **2013**, *60*, 3067.
[29] M. E. Levinshtein, S. L. Rumyantsev, M. S. Shur, *Properties of Advanced Semiconductor Materials: GaN, AlN, InN, BN, SiC, SiGe*, John Wiley & Sons, Hoboken, NJ **2001**.
[30] H. Morkoç, *Handbook of nitride semiconductors and devices, Materials Properties, Physics and Growth*, Vol. *1*, John Wiley & Sons, Hoboken, NJ **2009**.
[31] J. Xie, S. Mia, R. Dalmau, R. Collazo, A. Rice, J. Tweedie, Z. Sitar, *Phys. Status Solidi C* **2011**, *8*, 2407.
[32] F. Yun, M. A. Reshchikov, L. He, T. King, H. Morkoç, S. W. Novak, L. Wei, *J. Appl. Phys.* **2002**, *92*, 4837.
[33] J. Edmond, A. Abare, M. Bergman, J. Bharathan, K. L. Bunker, D. Emerson, K. Haberern, J. Ibbetson, M. Leung, P. Russel, *J. Cryst. Growth* **2004**, *272*, 242.
[34] D. Stocker, E. Schubert, K. Boutros, J. Flynn, R. Vaudo, V. Phanse, J. Redwing, *Electron. Lett.* **1998**, *34*, 373.
[35] H. Amano, A. Miyazaki, K. Iida, T. Kawashima, M. Iwaya, S. Kamiyama, I. Akasaki, R. Liu, A. Bell, F. Ponce, *Phys. Status Solidi A* **2004**, *201*, 2679.

 

[36] K. Ban, J.-i. Yamamoto, K. Takeda, K. Ide, M. Iwaya, T. Takeuchi, S. Kamiyama, I. Akasaki, H. Amano, *Appl. Phys. Express* **2011**, *4*, 052101.
[37] Z. Bryan, I. Bryan, J. Xie, S. Mita, Z. Sitar, R. Collazo, *Appl. Phys. Lett.* **2015**, *106*, 142107.
[38] M. Iwaya, S. Terao, T. Sano, S. Takanami, T. Ukai, R. Nakamura, S. Kamiyama, H. Amano, I. Akasaki, *Phys. Status Solidi A* **2001**, *188*, 117.
[39] S. Lee, D. Koleske, K. Cross, J. Floro, K. Waldrip, A. Wise, S. Mahajan, *Appl. Phys. Lett.* **2004**, *85*, 6164.
[40] M. Kneissl, Z. Yang, M. Teepe, C. Knollenberg, O. Schmidt, P. Kiesel, N. M. Johnson, S. Schujman, L. J. Schowalter, *J. Appl. Phys.* **2007**, *101*, 123103.
[41] T. Wunderer, J. E. Northrup, N. M. Johnson, in *III-Nitride Ultraviolet Emitters: Technology and Applications*, Vol. *227* (Eds.: M. Kneissl, J. Rass), Springer, Cham, Switzerland, **2016**, pp. 193–218.
[42] I. Bryan, Z. Bryan, S. Mita, A. Rice, L. Hussey, C. Shelton, J. Tweedie, J.-P. Maria, R. Collazo, Z. Sitar, *J. Cryst. Growth* **2016**, *451*, 65.
[43] I. Bryan, Z. Bryan, S. Mita, A. Rice, J. Tweedie, R. Collazo, Z. Sitar, *J. Cryst. Growth* **2016**, *438*, 819.
[44] T. Sochacki, M. Amilusik, B. Lucznik, M. Boćkowski, J. L. Weyher, G. Nowak, B. Sadovyi, G. Kamler, I. Grzegory, R. Kucharski, in *SPIE OPTO*, International Society for Optics and Photonics, Bellingham, WA **2013**, pp. 86250B-86250B-86211.
[45] H. Morkoç, *Nitride Semiconductor Devices: Fundamentals and Applications*, John Wiley & Sons, Hoboken, NJ **2013**.
[46] U. W. Pohl, *Epitaxy of Semiconductors: Introduction to Physical Principles*, Springer Science & Business Media, Berlin, **2013**.
[47] C. E. Dreyer, A. Janotti, C. G. Van de Walle, *Phys. Rev. B* **2014**, *89*, 081305.
[48] S. Mita, R. Collazo, A. Rice, R. Dalmau, Z. Sitar, *J. Appl. Phys.* **2008**, *104*, 013521.
[49] D. Takeuchi, S. Koizumi, T. Makino, H. Kato, M. Ogura, H. Ohashi, H. Okushi, S. Yamasaki, *Phys. Status Solidi A* **2013**, *210*, 1961.
[50] D. Takeuchi, H. Kawashima, D. Kuwabara, T. Makino, H. Kato, M. Ogura, H. Ohashi, H. Okushi, S. Yamasaki, S. Koizumi, in *Proceedings of the 2015 IEEE 27th International Symposium on Power Semiconductor Devices & IC's (ISPSD), May 10–14, 2015, Kowloon Shangri-La, Hong Kong*, IEEE, Piscataway, NJ **2015**, 197.
[51] C. I. Pakes, J. A. Garrido, H. Kawarada, *MRS Bull.* **2014**, *39*, 542.
[52] M. W. Doherty, N. B. Manson, P. Delaney, F. Jelezko, J. Wrachtrup, L. C. Hollenberg, *Phys. Rep.* **2013**, *528*, 1.
[53] Y. Tang, K. Shinohara, D. Regan, A. Corrion, D. Brown, J. Wong, A. Schmitz, H. Fung, S. Kim, M. Micovic, *IEEE Electron Device Lett.* **2015**, *36*, 549.
[54] S. Pearton, *GaN and ZnO-based materials and devices*, Vol. *156*, Springer Science & Business Media, Berlin, **2012**.
[55] M. Feneberg, R. A. Leute, B. Neuschl, K. Thonke, M. Bickermann, *Phys. Rev. B* **2010**, *82*, 075208.
[56] C. Janowitz, V. Scherer, M. Mohamed, A. Krapf, H. Dwelk, R. Manzke, Z. Galazka, R. Uecker, K. Irmscher, R. Fornari, *New J. Phys.* **2011**, *13*, 085014.
[57] G. Spriggs, in *Powder Metallurgy Data. Refractory, Hard and Intermetallic Materials*, Springer, Berlin, **2002**, pp. 118–139.
[58] M. Levinshtein, S. Rumyantsev, M. Shur, *Handbook Series of Semiconductor Parameters, Vol 1: Elementary Semiconductors and A3B5 Compounds Si, Ge C, GaAs, GaP, GaSb InAs, InP, InSb*, World Scientific, Singapore **1996**.
[59] A. Armstrong, A. Allerman, A. Fischer, M. King, M. van Heukelom, M. Moseley, R. Kaplar, J. Wierer, M. Crawford, J. Dickerson, *Electron. Lett.* **2016**, *52*, 1170.
[60] M. A. Hollis, R. J. Kaplar, unpublished.
[61] E. Bellotti, F. Bertazzi, *J. Appl. Phys.* **2012**, *111*, 103711.
[62] M. Higashiwaki, K. Sasaki, A. Kuramata, T. Masui, S. Yamakoshi, *Appl. Phys. Lett.* **2012**, *100*, 013504.
[63] K. Hirama, H. Sato, Y. Harada, H. Yamamoto, M. Kasu, *Jpn. J. Appl. Phys.* **2012**, *51*, 090112.
[64] H. Sato, M. Kasu, *Diamond Rel. Mater.* **2013**, *31*, 47.
[65] D. Huang, F. Yun, M. Reshchikov, D. Wang, H. Morkoc, D. Rode, L. Farina, C. Kurdak, K.-T. Tsen, S. Park, *Solid-State Electron.* **2001**, *45*, 711.
[66] V. Chin, T. Tansley, T. Osotchan, *J. Appl. Phys.* **1994**, *75*, 7365.
[67] M. Shur, B. Gelmont, M. A. Khan, *J. Electron. Mater.* **1996**, *25*, 777.
[68] Y. Taniyasu, M. Kasu, T. Makimoto, *Appl. Phys. Lett.* **2006**, *89*, 182112-1.
[69] C.-X. Wang, G.-W. Yang, T.-C. Zhang, H.-W. Liu, Y.-H. Han, J.-F. Luo, C.-X. Gao, G.-T. Zou, *Appl. Phys. Lett.* **2003**, *83*, 4854.
[70] T. Oishi, Y. Koga, K. Harada, M. Kasu, *Appl. Phys. Express* **2015**, *8*, 031101-1.
[71] Y. Kang, K. Krishnaswamy, H. Peelaers, C. G. Van de Walle, *J. Phys.: Condens. Matter* **2017**, *29*, 234001.
[72] J. Isberg, J. Hammersberg, E. Johansson, T. Wikström, D. J. Twitchen, A. J. Whitehead, S. E. Coe, G. A. Scarsbrook, *Science* **2002**, *297*, 1670.
[73] I. Akimoto, Y. Handa, K. Fukai, N. Naka, *Appl. Phys. Lett.* **2014**, *105*, 032102.
[74] Z. Hu, K. Nomoto, B. Song, M. Zhu, M. Qi, M. Pan, X. Gao, V. Protasenko, D. Jena, H. Xing, *Applied Physics Letters* **2015**, *107*, 243501–1 to 5.
[75] D. Litvinov, C. A. Taylor, R. Clarke, *Diamond Rel. Mater.* **1998**, *7*, 360.
[76] C. Verona, W. Ciccognani, S. Colangeli, E. Limiti, M. Marinelli, G. Verona-Rinati, *J. Appl. Phys.* **2016**, *120*, 025104.
[77] P. Siddiqua, W. A. Hadi, M. S. Shur, S. K. O'Leary, *J. Mater. Sci.: Mater. Electron.* **2015**, *26*, 4475.
[78] C. S. Badescu, unpublished.
[79] M. Pomorski, E. Berdermann, A. Caragheorgheopol, M. Ciobanu, M. Kiš, A. Martemiyanov, C. Nebel, P. Moritz, *Phys. Status Solidi A* **2006**, *203*, 3152.
[80] D. Ferry, *Phys. Rev. B* **1975**, *12*, 2361.
[81] K. Hirama, H. Takayanagi, S. Yamauchi, J. Yang, H. Kawarada, H. Umezawa, *Appl. Phys. Lett.* **2008**, *92*, 112107.
[82] L. Reggiani, S. Bosi, C. Canali, F. Nava, S. Kozlov, *Phys. Rev. B* **1981**, *23*, 3050.
[83] A. Barker Jr., M. Ilegems, *Phys. Rev. B* **1973**, *7*, 743.
[84] K. Karch, *Phys. Rev. B* **1998**, *57*, 7043.
[85] B. Downey, D. Katzer, N. Nepal, D. Meyer, D. Storm, V. Wheeler, M. Hardy, *Electron. Lett.* **2016**, *52*, 1263.
[86] K. Sasaki, A. Kuramata, T. Masui, E. G. Víllora, K. Shimamura, S. Yamakoshi, *Appl. Phys. Express* **2012**, *5*, 035502.
[87] P. Gielisse, S. Mitra, J. Plendl, R. Griffis, L. Mansur, R. Marshall, E. Pascoe, *Phys. Rev.* **1967**, *155*, 1039.
[88] H. Shibata, Y. Waseda, H. Ohta, K. Kiyomi, K. Shimoyama, K. Fujito, H. Nagaoka, Y. Kagamitani, R. Simura, T. Fukuda, *Mater. Trans.* **2007**, *48*, 2782.
[89] G. A. Slack, R. A. Tanzilli, R. Pohl, J. Vandersande, *J. Phys. Chem. Solids* **1987**, *48*, 641.
[90] B. J. Baliga, *Fundamentals of Power Semiconductor Devices*, Springer Science & Business Media, Berlin **2010**.
[91] Z. Guo, A. Verma, X. Wu, F. Sun, A. Hickman, T. Masui, A. Kuramata, M. Higashiwaki, D. Jena, T. Luo, *Appl. Phys. Lett.* **2015**, *106*, 111909.
[92] M. D. Santia, N. Tandon, J. Albrecht, *Appl. Phys. Lett.* **2015**, *107*, 041907.
[93] N. V. Novikov, *Dopov. Akad. Nauk Ukr. RSR, Ser. A: Fiz.-Tekh. Mat. Nauki* **1983**, *10*, 72.
[94] L. Lindsay, D. Broido, T. Reinecke, *Phys. Rev. Lett.* **2013**, *111*, 025901.

 

[95] T. R. Anthony, W. F. Banholzer, *Diamond Rel. Mater.* **1992**, *1*, 717.
[96] L. Wei, P. Kuo, R. Thomas, T. Anthony, W. Banholzer, *Phys. Rev. Lett.* **1993**, *70*, 3764.
[97] L. Gordon, J. B. Varley, J. L. Lyons, A. Janotti, C. G. Van de Walle, *Phys. Status Solidi RRL* **2015**, *9*, 462.
[98] S. N. Mohammad, *Solid-State Electron.* **2002**, *46*, 203.
[99] T. Borst, O. Weis, *Diamond Rel. Mater.* **1995**, *4*, 948.
[100] E. P. Visser, G. Bauhuis, G. Janssen, W. Vollenberg, J. van Enckevort, L. Giling, *J. Phys.: Condens. Matter* **1992**, *4*, 7365.
[101] T. Grotjohn, unpublished.
[102] Hexatech, www.hexatechinc.com (accessed: January 2017).
[103] Tamura Corporation, http://www.tamura-ss.co.jp/en/index.html (accessed: January 2017).
[104] Excellent Diamond Products, http://www.d-edp.jp/en/ (accessed: January 2017).
[105] Namiki Precision Jewel Company, www.namiki.net (accessed: January 2017).
[106] M. Schreck, M. Mayr, O. Klein, M. Fischer, S. Gsell, A. F. Sartori, B. C. Gallheber, *Phys. Status Solidi A* **2016**, *213*, 2028.
[107] Augsburg Diamond Technology GMBH, Large Size Single Crystal Diamond for High-end Applications, http://www.audiatec.de/index_EN.html (accessed: January 2017).
[108] M. Schreck, J. Asmussen, S. Shikata, J.-C. Arnault, N. Fujimori, *MRS Bull.* **2014**, *39*, 504.
[109] S. Khumpuang, F. Imura, S. Hara, *IEEE Trans. Semicond. Manuf.* **2015**, *28*, 551.
[110] S. Khumpuang, S. Hara, *IEEE Trans. Semicond. Manuf.* **2015**, *28*, 393.
[111] S. Hara, H. Maekawa, S. Ikeda, S. Nakano, *J. Jpn. Soc. Precis. Eng.* **2011**, *77*, 249.
[112] H. Kato, K. Oyama, T. Makino, M. Ogura, D. Takeuchi, S. Yamasaki, *Diamond Rel. Mater.* **2012**, *27*, 19.
[113] M. Landstrass, K. Ravi, *Appl. Phys. Lett.* **1989**, *55*, 975.
[114] T. Makino, K. Yoshino, N. Sakai, K. Uchida, S. Koizumi, H. Kato, D. Takeuchi, M. Ogura, K. Oyama, T. Matsumoto, *Appl. Phys. Lett.* **2011**, *99*, 061110.
[115] M. V. Hauf, P. Simon, N. Aslam, M. Pfender, P. Neumann, S. b. Pezzagna, J. Meijer, J. r. Wrachtrup, M. Stutzmann, F. Reinhard, *Nano Lett.* **2014**, *14*, 2359.
[116] H. Tippins, *Phys. Rev.* **1965**, *140*, A316.
[117] M. Orita, H. Ohta, M. Hirano, H. Hosono, *Appl. Phys. Lett.* **2000**, *77*, 4166.
[118] H. He, R. Orlando, M. A. Blanco, R. Pandey, E. Amzallag, I. Baraille, M. Rérat, *Phys. Rev. B* **2006**, *74*, 195123.
[119] T. Onuma, S. Saito, K. Sasaki, T. Masui, T. Yamaguchi, T. Honda, M. Higashiwaki, *Jpn. J. Appl. Phys.* **2015**, *54*, 112601.
[120] N. Ueda, H. Hosono, R. Waseda, H. Kawazoe, *Appl. Phys. Lett.* **1997**, *70*, 3561.
[121] E. G. Víllora, K. Shimamura, Y. Yoshikawa, T. Ujiie, K. Aoki, *Appl. Phys. Lett.* **2008**, *92*, 202120.
[122] K. Iizuka, Y. Morishima, A. Kuramata, Y.-J. Shen, C.-Y. Tsai, Y.-Y. Su, G. Liu, T.-C. Hsu, J. Yeh, in *SPIE OPTO*, International Society for Optics and Photonics, Bellingham, WA **2015**, pp. 93631Z-93631Z-93636.
[123] E. G. Víllora, K. Shimamura, Y. Yoshikawa, K. Aoki, N. Ichinose, *J. Cryst. Growth* **2004**, *270*, 420.
[124] Y. Tomm, P. Reiche, D. Klimm, T. Fukuda, *J. Cryst. Growth* **2000**, *220*, 510.
[125] Z. Galazka, K. Irmscher, R. Uecker, R. Bertram, M. Pietsch, A. Kwasniewski, M. Naumann, T. Schulz, R. Schewski, D. Klimm, *J. Cryst. Growth* **2014**, *404*, 184.
[126] K. Hoshikawa, E. Ohba, T. Kobayashi, J. Yanagisawa, C. Miyagawa, Y. Nakamura, *J. Cryst. Growth* **2016**, *447*, 36.
[127] H. Aida, K. Nishiguchi, H. Takeda, N. Aota, K. Sunakawa, Y. Yaguchi, *Jpn. J. Appl. Phys.* **2008**, *47*, 8506.
[128] M. Higashiwaki, K. Sasaki, H. Murakami, Y. Kumagai, A. Koukitu, A. Kuramata, T. Masui, S. Yamakoshi, *Semicond. Sci. Technol.* **2016**, *31*, 034001.
[129] A. Kuramata, K. Koshi, S. Watanabe, Y. Yamaoka, T. Masui, S. Yamakoshi, *Jpn. J. Appl. Phys.* **2016**, *55*, 1202A1202.
[130] Tamura Corporation, Standard specifications of gallium oxide substrates, https://www.tamura-ss.co.jp/file.jsp?id=13280 (accessed: January 2017).
[131] Z. Galazka, R. Uecker, D. Klimm, K. Irmscher, M. Naumann, M. Pietsch, A. Kwasniewski, R. Bertram, S. Ganschow, M. Bickermann, *ECS J. Solid State Sci. Technol.* **2017**, *6*, Q3007.
[132] J. Varley, A. Janotti, C. Franchini, C. Van de Walle, *Phys. Rev. B* **2012**, *85*, 081109.
[133] W. S. Hwang, A. Verma, H. Peelaers, V. Protasenko, S. Rouvimov, H. G. Xing, A. Seabaugh, W. Haensch, C. Van de Walle, Z. Galazka, *Appl. Phys. Lett.* **2014**, *104*, 203111.
[134] H. Peelaers, D. Steiauf, J. B. Varley, A. Janotti, C. G. Van de Walle, *Phys. Rev. B* **2015**, *92*, 085206.
[135] Z. Galazka, D. Klimm, K. Irmscher, R. Uecker, M. Pietsch, R. Bertram, M. Naumann, M. Albrecht, A. Kwasniewski, R. Schewski, *Phys Status Solidi A* **2015**, *212*, 1455.
[136] T. Endo, Y. Sato, H. Takizawa, M. Shimada, *J. Mater. Sci. Lett.* **1992**, *11*, 424.
[137] R. S. Pease, *Acta Crystallogr.* **1952**, *5*, 356.
[138] A. Herold, B. Marzluf, P. Perio, *C. R. Hebd. Seances Acad. Sci.* **1958**, *246*, 1866.
[139] J. Thomas, N. E. Weston, T. O'connor, *J. Am. Chem. Soc.* **1962**, *84*, 4619.
[140] R. Wentorf Jr., *J. Chem. Phys.* **1957**, *26*, 956.
[141] R. Wentorf Jr., *J. Chem. Phys.* **1961**, *34*, 809.
[142] C. E. Dreyer, J. L. Lyons, A. Janotti, C. G. Van de Walle, *Appl. Phys. Express* **2014**, *7*, 031001.
[143] B. P. Gunning, M. W. Moseley, D. D. Koleske, A. A. Allerman, S. R. Lee, *J. Cryst. Growth*, **2017**, *464*, 190.
[144] X. Zhang, *Thin Solid Films* **2013**, *544*, 2.
[145] Y. Yap, T. Aoyama, S. Kida, Y. Mori, T. Sasaki, *Diamond Rel. Mater.* **1999**, *8*, 382.
[146] N. Deyneka, X. Zhang, H.-G. Boyen, P. Ziemann, F. Banhart, *Diamond Rel. Mater.* **2004**, *13*, 473.
[147] S. Manorama, G. Chaudhari, V. Rao, *J. Phys. D: Appl. Phys.* **1993**, *26*, 1793.
[148] H. Saitoh, W. A. Yarbrough, *Appl. Phys. Lett.* **1991**, *58*, 2228.
[149] X. Ma, J. Yang, D. He, G. Chen, *Thin Solid Films* **1998**, *322*, 37.
[150] K. Bewilogua, J. Buth, H. Hübsch, M. Grischke, *Diamond Rel. Mater.* **1993**, *2*, 1206.
[151] C. Samantaray, R. Singh, *Int. Mater. Rev.* **2005**, *50*, 313.
[152] O. Mishima, K. Era, J. Tanaka, S. Yamaoka, *Appl. Phys. Lett.* **1988**, *53*, 962.
[153] C. Freysoldt, B. Grabowski, T. Hickel, J. Neugebauer, G. Kresse, A. Janotti, C. G. Van de Walle, *Rev. Mod. Phys.* **2014**, *86*, 253.
[154] C. G. Van de Walle, J. Neugebauer, *J. Appl. Phys.* **2004**, *95*, 3851.
[155] T. Oishi, Y. Koga, K. Harada, M. Kasu, *Appl. Phys. Express* **2015**, *8*, 031101.
[156] S. Bajaj, T.-H. Hung, F. Akyol, D. Nath, S. Rajan, *Appl. Phys. Lett.* **2014**, *105*, 263503.
[157] A. G. Baca, A. M. Armstrong, A. A. Allerman, E. A. Douglas, C. A. Sanchez, M. P. King, M. E. Coltrin, T. R. Fortune, R. J. Kaplar, *Appl. Phys. Lett.* **2016**, *109*, 033509.
[158] M. J. Tadjer, N. A. Mahadik, V. D. Wheeler, E. R. Glaser, L. Ruppalt, A. D. Koehler, K. D. Hobart, C. R. Eddy, F. J. Kub, *ECS J. Solid State Sci. Technol.* **2016**, *5*, P468.
[159] K. Irmscher, Z. Galazka, M. Pietsch, R. Uecker, R. Fornari, *J. Appl. Phys.* **2011**, *110*, 063720.
[160] M. Higashiwaki, personal communication **2016**.
[161] A. Parisini, R. Fornari, *Semicond. Sci. Technol.* **2016**, *31*, 035023.

[162] J. Varley, J. Weber, A. Janotti, C. Van de Walle, *Appl.Phys. Lett.* **2010**, *97*, 142106.
[163] A. Izumi, Y. Hirai, K. Tsutsui, N. Sokolov, *Appl. Phys.Lett.* **1995**, *67*, 2792.
[164] S. W. Kaun, F. Wu, J. S. Speck, *J. Vac. Sci. Technol., A* **2015**, *33*, 041508.
[165] M. B. Maccioni, F. Ricci, V. Fiorentini, *J. Phys. Condens. Matter* **2016**, *28*.
[166] T. Fang, R. Wang, H. Xing, S. Rajan, D. Jena, *IEEE Electonr Device Lett.* **2012**, *33*, 709.
[167] J. Khurgin, Y. J. Ding, D. Jena, *Appl. Phys. Lett.* **2007**, *91*, 252104.
[168] J. B. Khurgin, D. Jena, Y. J. Ding, *Appl. Phys. Lett.* **2008**, *93*, 032110.
[169] B. Ridley, *Semicond. Sci. Technol.* **1989**, *4*, 1142.
[170] J. Shah, A. Pinczuk, A. Gossard, W. Wiegmann, *Phys. Rev. Lett.* **1985**, *54*, 2045.
[171] K. Wang, J. Simon, N. Goel, D. Jena, *Appl. Phys. Lett.* **2006**, *88*, 22103.
[172] S. Bajaj, O. F. Shoron, P. S. Park, S. Krishnamoorthy, F. Akyol, T.-H. Hung, S. Reza, E. M. Chumbes, J. Khurgin, S. Rajan, *Appl. Phys. Lett.* **2015**, *107*, 153504.
[173] K. Matocha, T. P. Chow, R. J. Gutmann, *IEEE Trans. Electron Devices* **2005**, *52*, 6.
[174] M. Su, C. Chen, S. Rajan, *Semicond. Sci. Technol.* **2013**, *28*, 074012.
[175] T.-H. Hung, M. Esposto, S. Rajan, *Appl. Phys. Lett.* **2011**, *99*, 162104.
[176] T.-H. Hung, S. Krishnamoorthy, M. Esposto, D. N. Nath, P. S. Park, S. Rajan, *Appl. Phys. Lett.* **2013**, *102*, 072105.
[177] H. Zhou, X. Lou, N. J. Conrad, M. Si, H. Wu, S. Alghamdi, S. Guo, R. G. Gordon, D. Y. Peide, *IEEE Electron Device Lett.* **2016**, *37*, 556.
[178] E. A. Paisley, M. Brumbach, A. A. Allerman, S. Atcitty, A. G. Baca, A. M. Armstrong, R. J. Kaplar, J. F. Ihlefeld, *Appl. Phys. Lett.* **2015**, *107*, 102101.
[179] Z. Y. Al Balushi, K. Wang, R. K. Ghosh, R. A. Vilá, S. M. Eichfeld, J. D. Caldwell, X. Qin, Y.-C. Lin, P. A. DeSario, G. Stone, S. Subramanian, D. F. Paul, R. M. Wallace, S. Datta, J. M. Redwing, J. A. Robinson, *Nat Mater* **2016**, *15*, 1166.
[180] Y. Taniyasu, M. Kasu, *Appl. Phys. Lett.* **2011**, *99*, 251112.
[181] J. Verma, S. Islam, V. Protasenko, P. K. Kandaswamy, H. G. Xing, D. Jena, *Appl. Phys. Lett.* **2014**, *104*, 021105.
[182] W. Mönch, *J. Appl. Phys.* **1996**, *80*, 5076.
[183] L. Fonseca, D. Liu, J. Robertson, *Appl. Phys. Lett.* **2008**, *93*, 2905.
[184] D. König, R. Scholz, D. Zahn, G. Ebest, *J. Appl. Phys.* **2005**, *97*, 093707.
[185] J. Robertson, B. Falabretti, *J. Appl. Phys.* **2006**, *100*, 4111.
[186] G. Liu, B. R. Tuttle, S. Dhar, *Appl. Phys. Rev.* **2015**, *2*, 021307.
[187] M. Meneghini, presented at *International Reliability Physics Symposium*, Waikoloa, HI, June 1–5 **2014**.
[188] J. Shan, F. Wang, E. Knoesel, M. Bonn, T. F. Heinz, *Phys. Rev. Lett.* **2003**, *90*, 247401.
[189] Y. Zhang, J. Singh, *J. Appl. Phys.* **1999**, *85*, 587.
[190] J. Garg, N. Bonini, B. Kozinsky, N. Marzari, *Phys. Rev. Lett.* **2011**, *106*, 045901.
[191] W. Liu, A. A. Balandin, *J. Appl. Phys.* **2005**, *97*, 73710.
[192] W. Lv, A. Henry, *New J. Phys.* **2016**, *18*, 013028.
[193] D. Altman, M. Tyhach, J. McClymonds, S. Kim, S. Graham, J. Cho, K. Goodson, D. Francis, F. Faili, F. Ejeckam, in *Thermal and Thermomechanical Phenomena in Electronic Systems (ITherm), 2014 IEEE Intersociety Conference on*, IEEE, Piscataway, NJ **2014**, pp. 1199–1205.
[194] T. Batten, J. Pomeroy, M. Uren, T. Martin, M. Kuball, *J. Appl. Phys.* **2009**, *106*, 094509.
[195] S. Choi, E. R. Heller, D. Dorsey, R. Vetury, S. Graham, *IEEE Trans. Electron Devices* **2013**, *60*, 1898.
[196] S. Choi, E. R. Heller, D. Dorsey, R. Vetury, S. Graham, *IEEE Trans. Electron Devices* **2013**, *60*, 159.
[197] E. Heller, S. Choi, D. Dorsey, R. Vetury, S. Graham, *Microelectron. Reliab.* **2013**, *53*, 872.
[198] M. Kuball, J. Hayes, M. Uren, I. Martin, J. Birbeck, R. Balmer, B. Hughes, *IEEE Electron Device Lett.* **2002**, *23*, 7.
[199] M. Kuball, A. Sarua, H. Ji, M. J. Uren, R. S. Balmer, T. Martin, in *2006 IEEE MTT-S International Microwave Symposium Digest*, IEEE, Piscataway, NJ **2006**, pp. 1339–1342.
[200] S. Natarajan, Y. Habtemichael, S. Graham, *J. Heat Transfer* **2013**, *135*, 091201.
[201] A. Manoi, J. W. Pomeroy, R. Lossy, R. Pazirandeh, J. Wurfl, M. J. Uren, T. Martin, M. Kuball, *Solid-State Electron.* **2011**, *57*, 14.
[202] G. J. Riedel, J. W. Pomeroy, K. P. Hilton, J. O. Maclean, D. J. Wallis, M. J. Uren, T. Martin, M. Kuball, *IEEE Electron Device Lett.* **2008**, *29*, 416.
[203] F. Lecourt, A. Agboton, N. Ketteniss, H. Behmenburg, N. Defrance, V. Hoel, H. Kalisch, A. Vescan, M. Heuken, J.-C. De Jaeger, *IEEE Electron Device Lett.* **2013**, *34*, 978.
[204] A. J. Green, K. D. Chabak, E. R. Heller, R. C. Fitch, M. Baldini, A. Fiedler, K. Irmscher, G. Wagner, Z. Galazka, S. E. Tetlak, A. Crespo, K. Leedy, G. H. Jessen, *IEEE Electron Device Lett.* **2016**, *37*, 902.
[205] K. Ueda, M. Kasu, Y. Yamauchi, T. Makimoto, M. Schwitters, D. Twitchen, G. Scarsbrook, S. Coe, *IEEE Electron Device Lett.* **2006**, *27*, 570.
[206] Y. Zhang, S. Krishnamoorthy, J. M. Johnson, F. Akyol, A. Allerman, M. W. Moseley, A. Armstrong, J. Hwang, S. Rajan, *Appl. Phys. Lett.* **2015**, *106*, 141103.
[207] Y. Fu, M. Willander, Z.-F. Li, W. Lu, *Phys. Rev. B* **2003**, *67*, 113313.
[208] I. C. Kizilyalli, A. P. Edwards, O. Aktas, T. Prunty, D. Bour, *IEEE Trans. Electron Devices* **2015**, *62*, 414.
[209] S. Sun, J. D. Plummer, *IEEE J. Solid-State Circuits* **1980**, *15*, 562.
[210] T. E. Beechem, A. E. McDonald, E. J. Fuller, A. A. Talin, C. M. Rost, J.-P. Maria, J. T. Gaskins, P. E. Hopkins, A. A. Allerman, *J. Appl. Phys.* **2016**, *120*, 095104.
[211] M. Landstrass, M. Plano, M. Moreno, S. McWilliams, L. Pan, D. Kania, S. Han, *Diamond Rel. Mater.* **1993**, *2*, 1033.
[212] S. Sze, K. N. Kwok, *Physics of semiconductor devices 3rd Edition*, John Wiley & Sons, Hoboken, NJ **2007**.
[213] R. Raghunathan, B. Baliga, *Solid-State Electron.* **1999**, *43*, 199.
[214] T. Kimoto, J. A. Cooper, *Fundamentals of Silicon Carbide Technology: Growth, Characterization, Devices and Applications*, John Wiley & Sons, Hoboken, NJ **2014**.
[215] J. Lutz, H. Schlangenotto, U. Scheuermann, R. De Doncker, *Semiconductor Power Devices: Physics, Characteristics, Reliability.*, Springer, Berlin **2011**.
[216] M. H. Wong, K. Sasaki, A. Kuramata, S. Yamakoshi, M. Higashiwaki, *IEEE Electron Device Lett.* **2016**, *37*, 212.
[217] S. Chowdhury, M. H. Wong, B. L. Swenson, U. K. Mishra, *IEEE Electron Device Lett.* **2012**, *33*, 41.
[218] H. Nie, Q. Diduck, B. Alvarez, A. P. Edwards, B. M. Kayes, M. Zhang, G. Ye, T. Prunty, D. Bour, I. C. Kizilyalli, *IEEE Electron Device Lett.* **2014**, *35*, 939.
[219] D. Ji, S. Chowdhury, *IEEE Trans. Electron Devices* **2015**, *62*, 2571.
[220] T. Oka, T. Ina, Y. Ueno, J. Nishii, *Appl. Phys. Express* **2015**, *8*, 054101.
[221] S.-C. Shen, R. D. Dupuis, Z. Lochner, Y.-C. Lee, T.-T. Kao, Y. Zhang, H.-J. Kim, J.-H. Ryou, *Semicond. Sci. Technol.* **2013**, *28*, 074025.
[222] S. C. Glidden, H. D. Sanders, in *Power Modulator Symposium, 2006. Conference Record of the 2006 Twenty-Seventh International*, IEEE, Piscataway, NJ **2006**, pp. 314–317.
[223] M. Hinojosa, H. O'Brien, E. Van Brunt, A. Ogunniyi, C. Scozzie, in *Pulsed Power Conference (PPC), 2015 IEEE*, IEEE, Piscataway, NJ **2015**, pp. 1–5.
[224] B. J. Baliga, in *Fundamentals of Power Semiconductor Devices*, Springer, Berlin, **2008**, pp. 276–503.

 

[225] J. L. Hudgins, G. S. Simin, E. Santi, M. A. Khan, *IEEE Trans. Power Electron.* **2003**, *18*, 907.
[226] F. J. Zutavern, A. Mar, G. A. Vawter, S. F. Glover, H. P. Hjalmarson, K. H. Greives, in *2013 19th IEEE Pulsed Power Conference (PPC)*, IEEE, Piscataway, NJ **2013**, pp. 1–6.
[227] J. Leach, R. Metzger, E. Preble, K. Evans, in *SPIE OPTO*, International Society for Optics and Photonics, Bellingham, WA **2013**, pp. 86251Z-86251Z-86257.
[228] H. A. Mantooth, M. D. Glover, P. Shepherd, *IEEE J. Emerging Sel. Top. Power Electron.* **2014**, *2*, 374.
[229] P. Choi, U. Radhakrishna, C.-C. Boon, D. Antoniadis, L.-S. Peh, *IEEE Trans. Power Electron.* **2016**, *31*, 5365.
[230] C. L. Chua, D. K. Fork, K. Van Schuylenbergh, J.-P. Lu, *J. Microelectromech. Syst.* **2003**, *12*, 989.
[231] S. Prabhakaran, T. O'Donnell, C. R. Sullivan, M. Brunet, S. Roy, C. O'Mathuna, *J. Magn. Magn. Mater.* **2005**, *290*, 1343.
[232] U. K. Mishra, L. Shen, T. E. Kazior, Y.-F. Wu, *Proc. IEEE* **2008**, *96*, 287.
[233] A. Bar-Cohen, K. Bloschock, *Advanced thermal management technologies for defense electronics.,* Proc. SPI Defense, Security and Sensing Conference, Baltimore, MD, April, **2012**.
[234] A. Bar-Cohen, J. J. Maurer, J. G. Felbinger, *DARPA's Intra/Interchip (ICECool) Program, Online Digest of the CS ManTech International Conference on Compound Semiconductor Manufacturing Technology* (New Orleans, May 13–16, 2013) **2013**.
[235] K. D. Chabak, J. K. Gillespie, V. Miller, A. Crespo, J. Roussos, M. Trejo, D. E. Walker Jr., G. D. Via, G. H. Jessen, J. Wasserbauer, *IEEE Electron Device Lett.* **2010**, *31*, 99.
[236] M. J. Tadjer, T. J. Anderson, K. D. Hobart, T. I. Feygelson, J. D. Caldwell, C. R. Eddy Jr., F. J. Kub, J. E. Butler, B. Pate, J. Melngailis, *IEEE Electron Device Lett.* **2012**, *33*, 23.
[237] P.-C. Chao, K. Chu, C. Creamer, J. Diaz, T. Yurovchak, M. Shur, R. Kallaher, C. McGray, G. D. Via, J. D. Blevins, *IEEE Trans. Electron Devices* **2015**, *62*, 3658.
[238] R. Ruby, in *Proc. Sixth Intl Symp. on Acoustic Devices for Future Mobile Communication Systems,* Chiba University, Japan, November 24–25, 2015, **2015**, pp. 13–17.
[239] G. F. R. Aigner, A. Tajic, A. Volatier, F. Dumont, P. Stokes, M. AlJoumayly, in *Proc. Sixth Intl Symp. on Acoustic Devices for Future Mobile Communication Systems,* Chiba University, Japan, November 24–25, 2015, **2015**, pp. 7–12.
[240] K. Lakin, in *Ultrasonics Symposium, 1999. Proceedings. 1999 IEEE*, Vol. *2*, IEEE, Piscataway, NJ **1999**, pp. 895–906.
[241] J. D. Larson, R. Ruby, P. Bradley, Y. Oshmyansky, in *Ultrasonics Symposium, 1999. Proceedings. 1999 IEEE*, Vol. *2*, IEEE, Piscataway, NJ **1999**, pp. 887–890.
[242] H. Loebl, C. Metzmacher, D. Peligrad, R. Mauczok, M. Klee, W. Brand, R. Milsorn, P. Lok, R. Van Straten, A. Tuinhout, in *Ultrasonics Symposium, 2002. Proceedings. 2002 IEEE*, Vol. *1*, IEEE, Piscataway, NJ **2002**, pp. 919–923.
[243] T. Nishihara, T. Yokoyama, T. Miyashita, Y. Satoh, in *Ultrasonics Symposium, 2002. Proceedings. 2002 IEEE*, Vol. *1*, IEEE, Piscataway, NJ **2002**, pp. 969–972.
[244] I. Poole, LTE Frequency Bands & Spectrum Allocations, http://www.radio-electronics.com/info/cellulartelecomms/lte-long-term-evolution/lte-frequency-spectrum.php (accessed: September 2016).
[245] M. Moreira, J. Bjurström, I. Katardjev, V. Yantchev, *Vacuum* **2011**, *86*, 23.
[246] R. Matloub, A. Artieda, C. Sandu, E. Milyutin, P. Muralt, *Appl. Phys. Lett.* **2011**, *99*, 092903.
[247] Y. I. T. Yokoyama, T. Nishihara, J. Tsutsumi, in *Proc. Sixth Intl Symp. on Acoustic Devices for Future Mobile Communication Systems,* Chiba University, Japan, November 24–25, 2015, **2015**, pp. 24–31.
[248] K. Mutamba, D. Neculoiu, A. Muller, G. Konstantinidis, D. Vasilache, C. Sydlo, A. Kostopoulos, A. Adikimenakis, A. Georgakilas, H. L. Hartnagel, in *2006 Asia-Pacific Microwave Conference*, IEEE, Piscataway, NJ **2006**, pp. 1757–1760.
[249] A. Muller, D. Neculoiu, G. Konstantinidis, A. Stavrinidis, D. Vasilache, A. Cismaru, M. Danila, M. Dragoman, G. Deligeorgis, K. Tsagaraki, *IEEE Electron Device Lett.* **2009**, *30*, 799.
[250] M. Rais-Zadeh, V. J. Gokhale, A. Ansari, M. Faucher, D. Théron, Y. Cordier, L. Buchaillot, *J. Microelectromech. Sys.* **2014**, *23*, 1252.
[251] Y. Aota, Y. Sakyu, S. Tanifuji, H. Oguma, S. Kameda, H. Nakase, T. Takagi, K. Tsubouchi, in *2006 IEEE Ultrasonics Symposium*, IEEE, Piscataway, NJ **2006**, pp. 337–340.
[252] J. B. Shealy, J. B. Shealy, P. Patel, M. D. Hodge, R. Vetury, J. R. Shealy, in *2016 IEEE Radio and Wireless Symposium (RWS)*, IEEE, Piscataway, NJ **2016**, pp. 16–19.
[253] J. B. Shealy, M. D. Hodge, P. Patel, R. Vetury, A. Y. Feldman, S. R. Gibb, M. D. Boomgarden, M. P. Lewis, J. B. Shealy, J. R. Shealy, in *IEEE Radio Frequency Integrated Circuits Symposium*, IEEE, Piscataway, NJ **2016**, pp. 103–106.
[254] C. M. Armstrong, in *Vacuum Electronics Conference (IVEC), 2013 IEEE 14th International*, IEEE, Piscataway, NJ **2013**, pp. 1–3.
[255] D. Takeuchi, H. Kato, G. Ri, T. Yamada, P. Vinod, D. Hwang, C. Nebel, H. Okushi, S. Yamasaki, *Appl. Phys. Lett.* **2005**, *86*, 2103.
[256] F. Himpsel, J. Knapp, J. VanVechten, D. Eastman, *Phys. Rev. B* **1979**, *20*, 624.
[257] J. van der Weide, Z. Zhang, P. Baumann, M. Wensell, J. Bernholc, R. Nemanich, *Phys. Rev. B* **1994**, *50*, 5803.
[258] M. Geis, N. Efremow, J. Woodhouse, M. McAleese, M. Marchywka, D. Socker, J. Hochedez, *IEEE Electron Device Lett.* **1991**, *12*, 456.
[259] M. Powers, M. Benjamin, L. Porter, R. Nemanich, R. Davis, J. Cuomo, G. Doll, S. J. Harris, *Appl. Phys. Lett.* **1995**, *67*, 3912.
[260] M. Benjamin, C. Wang, R. Davis, R. Nemanich, *Appl. Phys. Lett.* **1994**, *64*, 3288.
[261] M. Kataoka, C. Zhu, F. A. Koeck, R. J. Nemanich, *Diamond Rel. Mater.* **2010**, *19*, 110.
[262] F. A. Koeck, R. J. Nemanich, A. Lazea, K. Haenen, *Diamond Rel. Mater.* **2009**, *18*, 789.
[263] M. Kneissl, Curriculum Vitae, http://www.ifkp.tu.berlin.de/?id=agkneissl (accessed: January 2017).
[264] H. Yoshida, Y. Yamashita, M. Kuwabara, H. Kan, *Appl. Phys. Lett.* **2008**, *93*, 241106.
[265] C. Ren, *Mater. Sci. Technol.* **2016**, *32*, 418.
[266] J. Northrup, C. Chua, Z. Yang, T. Wunderer, M. Kneissl, N. Johnson, T. Kolbe, *Appl. Phys. Lett.* **2012**, *100*, 021101.
[267] J. Simon, V. Protasenko, C. Lian, H. Xing, D. Jena, *Science* **2010**, *327*, 60.
[268] *Advancing Quantum Information Science: National Challenges and Opportunities*, National Science and Technology Council, Washington, D.C. **2016**.
[269] R. Schirhagl, K. Chang, M. Loretz, C. L. Degen, *Ann. Rev. Phys. Chem.* **2014**, *65*, 83.
[270] A. Sipahigil, R. Evans, D. Sukachev, M. Burek, J. Borregaard, M. Bhaskar, C. Nguyen, J. Pacheco, H. Atikian, C. Meuwly, *Science* **2016**, *354*, 847.
[271] H. Seo, M. Govoni, G. Galli, *Sci. Rep.* **2016**, *6*, 20803.
[272] J. Varley, A. Janotti, C. Van de Walle, *Phys. Rev. B* **2016**, *93*, 161201.
[273] G. D. Metcalfe, E. D. Readinger, R. Enck, H. Shen, M. Wraback, N. T. Woodward, J. Poplawsky, V. Dierolf, *Opt. Mater. Express* **2011**, *1*, 78.
[274] J. Isberg, M. Gabrysch, J. Hammersberg, S. Majdi, K. K. Kovi, D. J. Twitchen, *Nat. Mater.* **2013**, *12*, 760.
[275] P. Kok, W. J. Munro, K. Nemoto, T. C. Ralph, J. P. Dowling, G. J. Milburn, *Rev. Mod. Phys.* **2007**, *79*, 135.
[276] R. Blatt, D. Wineland, *Nature* **2008**, *453*, 1008.
[277] M. Stegmaier, J. Ebert, J. Meckbach, K. Ilin, M. Siegel, W. Pernice, *Appl. Phys. Lett.* **2014**, *104*, 091108.

 

[278] P. Gräupner, J. Pommier, A. Cachard, J. Coutaz, *J. Appl. Phys.* **1992**, *71*, 4136.
[279] J. Claudon, J. Bleuse, N. S. Malik, M. Bazin, P. Jaffrennou, N. Gregersen, C. Sauvan, P. Lalanne, J.-M. Gérard, *Nat. Photonics* **2010**, *4*, 174.
[280] T. T. Tran, K. Bray, M. J. Ford, M. Toth, I. Aharonovich, *Nat. Nanotechnol.* **2016**, *11*, 37.
[281] F. Marsili, V. B. Verma, J. A. Stern, S. Harrington, A. E. Lita, T. Gerrits, I. Vayshenker, B. Baek, M. D. Shaw, R. P. Mirin, *Nat. Photonics* **2013**, *7*, 210.
[282] M. Markham, J. Dodson, G. Scarsbrook, D. Twitchen, G. Balasubramanian, F. Jelezko, J. Wrachtrup, *Diamond Rel. Mater.* **2011**, *20*, 134.
[283] M. Cuniot-Ponsard, I. Saraswati, S.-M. Ko, M. Halbwax, Y. Cho, E. Dogheche, *Appl. Phys. Lett.* **2014**, *104*, 101908.
[284] J. D. Zook, D. Chen, G. N. Otto, *Appl. Phys. Lett.* **1967**, *11*, 159.
[285] R. M. Field, J. Lary, J. Cohn, L. Paninski, K. L. Shepard, *Appl. Phys. Lett.* **2010**, *97*, 211111.
[286] C. J. Krückel, P. A. Andrekson, D. T. Spencer, J. F. Bauters, M. J. Heck, J. E. Bowers, *Opt. Lett.* **2015**, *40*, 875.
[287] R. Koda, H. Watanabe, S. Kono, in *Some Advanced Functionalities of Optical Amplifiers* (Ed.: S. K. Garai), InTech, Rijeka, Croatia **2015**.
[288] S. Burd, D. Leibfried, A. Wilson, D. Wineland, in *SPIE LASE*, International Society for Optics and Photonics, Bellingham, WA **2015**, pp. 93490P-93490P-93498.
[289] X. Bai, X. Guo, D. C. Mcintosh, H.-D. Liu, J. C. Campbell, *IEEE J. Quantum Electron.* **2007**, *43*, 1159.
[290] A. V. Sampath, Y. Chen, Q. Zhou, R. W. Enck, G. A. Garrett, B. L. Vanmil, R. B. Chung, M. L. Reed, H. Shen, J. C. Campbell, in *Materials Science Forum*, Vol. *858*, Trans Tech Publications, Zurich, Switzerland **2016**, pp. 1206–1209.
[291] A. Sampath, Q. Zhou, R. Enck, D. McIntosh, H. Shen, J. Campbell, M. Wraback, *Appl. Phys. Lett.* **2012**, *101*, 093506.
[292] Y. Fujii, S. Yoshida, S. Misawa, S. Maekawa, T. Sakudo, *Appl. Phys. Lett.* **1977**, *31*, 815.
[293] C. Xiong, W. H. Pernice, X. Sun, C. Schuck, K. Y. Fong, H. X. Tang, *New J. Phys.* **2012**, *14*, 095014.
[294] D. J. Hoffman, T. W. Kerslake, J. S. Hojnicki, D. H. Manzella, R. D. Falck, H. A. Cikanek III, M. D. Klem, J. M. Free, *NASA Technical Memorandum NASA/TM-2011-217281*, NASA, Hampton, VA **2011**, *IAC-11-D2*, pp. 1–16.
[295] T. W. Kerslake, K. M. Bury, J. S. Hojinicki, A. M. Sajdak, R. J. Scheiddegger, Solar Electric Propulsion (SEP) Tug Power System Considerations, **2011**.
[296] J.-M. Lauenstein, M. C. Casey, K. A. LaBel, S. Ikpe, A. D. Topper, E. P. Wilcox, H. Kim, A. M. Phan, Single-Event Effects in Silicon Carbide Power Devices, *NEPP Electronics Technology Workshop,* Greenbelt, MD, June 23–26, 2015, **2015**, pp. 1–15.
[297] K.-H. Cho, Y.-H. Choi, J. Lim, M.-K. Han, *IEEE Trans. Electron Devices* **2009**, *56*, 365.
[298] A. Akturk, J. McGarrity, S. Potbhare, N. Goldsman, *IEEE Trans. Nucl. Sci.* **2012**, *59*, 3258.
[299] N. E. Ives, J. Chen, A. F. Witulski, R. D. Schrimpf, D. M. Fleetwood, R. W. Bruce, M. W. McCurdy, E. X. Zhang, L. W. Massengill, *IEEE Trans. Nucl. Sci.* **2015**, *62*, 2417.
[300] Synopsis Incorporated, Synopsys TCAD Tools, http://www.synopsys.com (accessed: July 2017).
[301] P. G. Neudeck, R. S. Okojie, L.-Y. Chen, *Proc. IEEE* **2002**, *90*, 1065.
[302] V. Bougrov, M. E. Levinshtein, S. L. Rumyantsev, A. Zubrilov, in *Properties of Advanced Semiconductor Materials: GaN, AlN, InN, BN, SiC, SiGe* (Eds.: M. E. Levinshtein, S. L. Rumyantsev, M. S. Shur), John Wiley & Sons, Hoboken, NJ **2001**, pp. 1–30.
[303] Y. Goldberg, M. E. Levinshtein, S. L. Rumyantsev, in *Properties of Advanced Semiconductor Materials: GaN, AlN, InN, BN, SiC, SiGe* (Eds.: M. E. Levinshtein, S. L. Rumyantsev, M. S. Shur), John Wiley & Sons, Hoboken, NJ **2001**, pp. 93–148.
[304] M. Ruff, H. Mitlehner, R. Helbig, *IEEE Trans. Electron Devices* **1994**, *41*, 1040.
[305] J. Zolper, *Solid-State Electron.* **1998**, *42*, 2153.
[306] B. P. Luther, S. D. Wolter, S. E. Mohney, *Sens. Actuators, B* **1999**, *56*, 164.
[307] R. B. Sadeghian, M. S. Islam, *Nat. Mater.* **2011**, *10*, 135.
[308] D. Maier, M. Alomari, N. Grandjean, J. F. Carlin, M. A. Diforte-Poisson, C. Dua, S. Delage, E. Kohn, *IEEE Electron Device Lett.* **2012**, *33*, 985.
[309] S. Shelton, M. L. Chan, H. Park, D. Horsley, B. Boser, I. Izyumin, R. Przybyla, T. Frey, M. Judy, K. Nunan, F. Sammoura, K. Yang, in *Ultrasonics Symposium (IUS), 2009 IEEE International*, IEEE, Piscataway, NJ **2009**, pp. 402–405.
[310] R. J. Przybyla, S. E. Shelton, A. Guedes, I. I. Izyumin, M. H. Kline, D. A. Horsley, B. E. Boser, *IEEE Sens. J.* **2011**, *11*, 2690.
[311] Y. Lu, A. Heidari, S. Shelton, A. Guedes, D. A. Horsley, in *2014 IEEE 27th International Conference on Micro Electro Mechanical Systems (MEMS)*, IEEE, Piscataway, NJ **2014**, pp. 745–748.
[312] Y. Lu, S. Shelton, D. Horsley, presented at *Solid State Sensor, Actuator, and Microsystem Workshop*, Hilton Head, SC, **2014**.
[313] R. J. Przybyla, H.-Y. Tang, S. E. Shelton, D. A. Horsley, B. E. Boser, in *Solid-State Circuits Conference Digest of Technical Papers (ISSCC), 2014 IEEE International*, IEEE, Piscataway, NJ **2014**, pp. 210–211.
[314] K. Yamamoto, F. Goericke, A. Guedes, G. Jaramillo, T. Hada, A. P. Pisano, D. Horsley, *Appl. Phys. Lett.* **2014**, *104*, 111111.
[315] R. J. Nikolic, A. M. Conway, R. Radev, Q. Shao, L. Voss, T. F. Wang, J. R. Brewer, C. L. Cheung, L. Fabris, C. L. Britton, M. N. Ericson, *Proc. SPIE* **2010**, *7805*, 780500.
[316] H. Karaagac, M. S. Islam, *Adv. Funct. Mater.* **2014**, *24*, 2224.
[317] H. Karaagac, V. J. Logeeswaran, M. S. Islam, *Phys. Status Solidi A* **2013**, *210*, 1377.
[318] H. N. Mark Triplett, M. Ombaba, V. J. Logeeswarren, M. Yee, K. G. Polat, J. Y. Oh, T. Fuyuki, F. Léonard, M. Saif Islam, *Nano Res.* **2014**, *7*, 998.
[319] J. Y. Oh, J. T. Park, H. J. Jang, W. J. Cho, M. S. Islam, *Adv. Mater.* **2014**, *26*, 1929.
[320] K. Brueckner, F. Niebelschuetz, K. Tonisch, C. Foerster, V. Cimalla, R. Stephan, J. Pezoldt, T. Stauden, O. Ambacher, M. A. Hein, *Phys. Status Solidi A* **2011**, *208*, 357.
[321] F. Niebelschutz, V. Cimalla, K. Tonisch, C. Haupt, K. Bruckner, R. Stephan, M. Hein, O. Ambacher, *Phys. Status Solidi C* **2008**, *5*, 1914.
[322] T. W. Yeh, Y. T. Lin, B. Ahn, L. S. Stewart, P. D. Dapkus, S. R. Nutt, *Appl. Phys. Lett.* **2012**, *100*, 033119.
[323] S. A. Wright, Y. B. Gianchandani, *J. Microelectromech. Sys.* **2009**, *18*, 736.
[324] S. P. Beeby, M. J. Tudor, N. M. White, *Meas. Sci. Technol.* **2006**, *17*, R175.
[325] S. Barker, K. V. Vassilevski, N. G. Wright, A. B. Horsfall, *Proceedings of the IEEE Sensors 2010 Conference,* Waikoloa, HI, November 1–4, **2010**, 300.
[326] S. Barker, B. Miao, D. Brennan, K. V. Vassilevski, N. G. Wright, A. B. Horsfall, *Mater. Sci. Forum* **2010**, *645–648*, 1093.
[327] Y. J. Lai, W. C. Li, C. M. Lin, V. V. Felmetsger, A. P. Pisano, *Online Digest of 2013 Transducers and Eurosensors XXVII*, Barcelona, Spain, June 16–20, **2012**.
[328] C. Honsberg, W. A. Doolittle, M. Allen, C. Wang, *Online Digest of Photovoltaic Specialists Conference,* Lake Buena Vista, FL, January 3–7, 2005, **2005**.
[329] T. J. Anderson, J. D. Greenlee, B. Feigelson, J. K. Hite, K. D. Hobart, F. J. Kub, *ECS Trans.* **2015**, *69*, 99.
[330] T. Anderson, B. Feigelson, F. Kub, M. Tadjer, K. Hobart, M. Mastro, J. Hite, C. Eddy, *Electron. Lett.* **2014**, *50*, 197.

 

[331] I. Batyrev, W. Sarney, T. Zheleva, C. Nguyen, B. Rice, K. Jones, *Phys. Status Solidi A* **2011**, *208*, 1566.
[332] R. Collazo, S. Mita, A. Rice, R. Dalmau, Z. Sitar, *Appl. Phys. Lett.* **2007**, *91*, 212103.
[333] D. Jena, S. Heikman, D. Green, D. Buttari, R. Coffie, H. Xing, S. Keller, S. DenBaars, J. S. Speck, U. K. Mishra, *Appl. Phys. Lett.* **2002**, *81*, 4395.
[334] P. Kozodoy, Y. P. Smorchkova, M. Hansen, H. Xing, S. P. DenBaars, U. K. Mishra, A. Saxler, R. Perrin, W. Mitchel, *Appl. Phys. Lett.* **1999**, *75*, 2444.
[335] J.-Y. Duboz, N. Grandjean, F. Omnes, M. Mosca, J.-L. Reverchon, *Appl. Phys. Lett.* **2005**, *86*, 063511.
[336] N. Yafune, S. Hashimoto, K. Akita, Y. Yamamoto, H. Tokuda, M. Kuzuhara, *Electron. Lett.* **2014**, *50*, 211.
[337] T. Nanjo, M. Takeuchi, M. Suita, T. Oishi, Y. Abe, Y. Tokuda, Y. Aoyagi, *Appl. Phys. Lett.* **2008**, *92*, 263502.
[338] P. S. Park, S. Krishnamoorthy, S. Bajaj, D. N. Nath, S. Rajan, *IEEE Electron Device Lett.* **2015**, *36*, 226.
[339] S. Bajaj, F. Akyol, S. Krishnamoorthy, Y. Zhang, S. Rajan, *Appl. Phys. Lett.* **2016**, *109*, 133508.
[340] F. Reif, *Fundamentals of Statistical and Thermal Physics*, McGraw-Hill, New York, NY **1965**.
[341] J. Kotani, M. Tajima, S. Kasai, T. Hashizume, *Appl. Phys. Lett.* **2007**, *91*, 093501.
[342] W. Tan, M. Uren, P. Houston, R. Green, R. Balmer, T. Martin, *IEEE Electron Device Lett.* **2006**, *27*, 1.
[343] I. Rossetto, F. Hurkx, J. Šonský, J. A. Croon, G. Meneghesso, E. Zanoni, *IEEE Trans. Electron Devices* **2015**, *62*, 2549.
[344] M. Ťapajna, O. Hilt, E. Bahat-Treidel, J. Würfl, J. Kuzmik, *IEEE Electron Device Lett.* **2016**, *37*, 385.
[345] A. Chantre, G. Vincent, D. Bois, *Phys. Rev. B* **1981**, *23*, 5335.
[346] C. M. Jackson, A. R. Arehart, E. Cinkilic, B. McSkimming, J. S. Speck, S. A. Ringel, *J. Appl. Phys.* **2013**, *113*, 204505.
[347] M. Kuball, M. Ťapajna, R. J. Simms, M. Faqir, U. K. Mishra, *Microelectron. Reliab.* **2011**, *51*, 195.
[348] S. Tyaginov, I. Starkov, H. Enichlmair, C. Jungemann, J. M. Park, E. Seebacher, R. Orio, H. Ceric, T. Grasser, *Microelectron. Reliab.* **2011**, *51*, 1525.
[349] F. Gao, S. C. Tan, J. A. del Alamo, C. V. Thompson, T. Palacios, *IEEE Trans. Electron Devices* **2014**, *61*, 437.
[350] H. Sun, M. M. Bajo, M. J. Uren, M. Kuball, *Microelectron. Reliab.* **2014**, *54*, 2650.
[351] A. P. Christensen, *Ph.D. Thesis*, Georgia Institute of Technology **2009**.
[352] Y. Yao, Z. Chen, G.-Q. Lu, D. Boroyevich, K. D. Ngo, in *Proceedings of the 60th IEEE Electrical Components and Technology Conference (ECTC)*, IEEE, Piscataway, NJ **2010**, pp. 1834–1840.
[353] H. Zhang, S. Ang, A. Mantooth, J. Balda, in *2012 IEEE Energy Conversion Congress and Exposition (ECCE)*, IEEE, Piscataway, NJ **2012**, pp. 444–450.
[354] Y. Lei, C. Barth, S. Qin, W.-c. Liu, I. Moon, A. Stillwell, D. Chou, T. Foulkes, Z. Ye, Z. Liao, in *2016 IEEE Applied Power Electronics Conference and Exposition (APEC)*, IEEE, Piscataway, NJ **2016**, pp. 1512–1519.
[355] J. Simon, V. Protasenko, C. Lian, H. Xing, D. Jena, *Science* **2010**, *327*, 60.
[356] M. Zhu, M. Qi, K. Nomoto, Z. Hu, B. Song, M. Pan, X. Gao, D. Jena, H. G. Xing, *Appl. Phys. Lett.* **2017**, *110*, 182102.
[357] N. Moser, J. McCandless, A. Crespo, K. Leedy, A. Green, A. Neal, S. Mou, E. Ahmadi, J. Speck, K. Chabak, N. Peixoto, G. Jessen, *IEEE Electron Device Letters* **2017**, *38*, 775.

 